University of Kerbala

College of Science

Department of Physics

Enhancing the Thermal Performance of Parabolic Trough Solar Collector Using Cylindrical Turbulators for Water Desalination

A Thesis

Submitted to the Council of College of Science / University of Kerbala,

in Partial Fulfillment of the Requirements for

the Ph.D. Degree in Science of Physics

Written by:

Yasser Abidnoor Jebbar

B.Sc. 2005

M.Sc. 2020

Supervised by:

Prof. Dr. Fadhil Khaddam Fuliful ***Assist. Prof. Dr. Wisam J. Khudhayer***

2025 A.D. **1446 A.H.**

بسم الله الرحمن الرحيم

قَالُوا سُبْحَانَكَ لَا عِلْمَ لَنَا إِلَّا مَا عَلَّمْتَنَا إِنَّكَ أَنتَ الْعَلِيمُ الْحَكِيمُ

صدق الله العلي العظيم

سورة البقرة الاية (32)

Supervisor Certificate

We certify that the thesis entitled "***Enhancing the Thermal Performance of Parabolic Trough Solar Collector Using Cylindrical Turbulators for Water Desalination***" was prepared under our supervision by (***Yasser Abidnoor Jebbar***) at the College of Science / University of Kerbala in a partial fulfillment of the requirements for the Ph.D. Degree of Science in Physics.

Signature:

Name: Dr. Fadhil Khaddam Fuliful
Title: Professor
Date: / /2025

Signature:

Name: Dr. Wisam J. Khudhayer
Title: Assistance Professor
Date: 8 / 4 / 2025

In view of the available recommendations, I forward this thesis for debate by the examining committee.

Signature:

Name: **Dr. Mohammed Abdulhussain AL-Kaabi**
Title: Assistant Professor
Head of Physics Department, College of Science, University of Kerbala
Date: / /2025

Examination Committee Certification

We certify that we have read this thesis, entitled "***Enhancing the Thermal Performance of Parabolic Trough Solar Collector Using Cylindrical Turbulators for Water Desalination***" and as an examining committee, examined the student "**Yasser Abidnoor Jebbar**" onits contents and that in our opinion it is adequate for the partial fulfillment of the requirements for the degree of Ph.D. of Science in Physics.

Signature: A.M.Abdl
Name: **Dr. Ahmed Mehmood Abdul-Lettif**
Title: Professor
Address: University of Kerbala, College of Science, Department of Physics.
Date: / /2025
(Chairman)

Signature:
Name: **Dr. Mohammed Hamid Husein**
Title: Professor
Address: University of Kerbala, College of Education for Pure Sciences, Department of Physics.
Date: / /2025
(Member)

Signature: Ali J. Mahdi
Name: **Dr. Ali Jafer Mahdi**
Title: Professor
Address: Al-Zahraa University for Women, College of Information Technology Engineering.
Date: / /2025
(Member)

Signature:
Name: **Dr. Mohammed A. Kadhim**
Title: Professor
Address: University of Kerbala, College of Science, Department of Physics.
Date: / /2025
(Member)

Signature:
Name: **Dr. Farhan Lafta Rashid**
Title: Assistant Professor
Address: University of Kerbala, College of Engineering.
Date: 7 / 4 /2025
(Member)

Signature:
Name: **Dr. Fadhil Khaddam Fuliful**
Title: Professor
Address: University of Kerbala, College of Science, Department of Physics.
Date: / /2025
(Member & Supervisor)

Signature: W. Em
Name: **Dr. Wisam J. Khudhayer**
Title: Assistant Professor
Address: University of Babylon, Collage of Engineering/Al-Musayab, Department of Energy and Renewable Energies Engineering.
Date: 8 / 4 /2025
(Member & Supervisor)

Signature: Hassan J. Jawad
Name: **Dr. Hassan Jameel Jawad AL-Fatlawy**
Title: Professor
Address: **Dean of the College of Science, University of Kerbala**
Date: / /2025

Dedication

To all the hands that are raised to pray to reach my goal

To all the hearts that rejoiced to my success

To all the pure souls who supported and helped me

my

father

wife

children

Mustafa

Murtaza

Yasmeen

brothers

sister

friends

Presented the results my studies

ACKNOWLEDGEMENTS

Praise and thanks be to Allah always and forever for His help, blessing, and everything during the preparation for this work. I want to extend my sincere thanks and deep gratitude to my supervisors, ***Prof. Dr. Fadhil Khaddam Fuliful***, and ***Assist. Prof. Dr. Wisam J. Khudhayer***.

Special thanks are to the Head of the Physics Department, ***Assist. Prof. Dr. Mohammed Abdulhussain AL-Kaabi***, the Staff of the Department of Physics, and ***Prof. Dr. Hassan Jameel Jawad AL-Fatlawy*** the Dean of the College of Science, University of Kerbala for their assistance.

Finally, I would like to thank my parents and all my family for their support and encouragement in my life.

Yasser Abidnoor Jebbar

2025

ABSTRACT

Water is necessary for human survival; individuals consume (10-30 L) of clean water daily for drinking, cooking, and other household activities. Contaminated water is not only unsanitary but also dangerous to one's health. The main aim of this study is to investigate this problem and improve freshwater productivity by developing a solar desalination unit (SDU) containing a solar still (SS) and a parabolic trough collector (PTC) that has a positive effect on cumulative productivity. Improving the heat transfer coefficient of the PTC is the key point of this study, which is performed by inserting a newly designed hollow cylindrical turbulators inside the parabolic trough receiver (PTR). The designed cylindrical turbulators inside a PTR are expected to improve the heat transfer coefficient and heat transfer area between a PTR and water as a heat transfer fluid (HTF) compared with other turbulators reported in the literature (twisted tape, rods, fins, etc.). The work was carried out numerically and experimentally under the climatic circumstances of Babylon city, Babil (32.77° N, 44.29° W), at the College of Engineering/Al-Musayab from 9:00 to 15:00, during selected days from October 2023 to May 2024.

Numerically, the best design for the reflector of PTC was selected using the Parabola Calculator tool 2.0 then the resulted Excel sheet introduced into the ANSYS FLUENT 20.0 R-2 to perform the simulation. The PTC and cylindrical turbulators were designed and simulated using Solidworks and computational fluid dynamics (CFD) tools, respectively. The PTC is designed with dimensions of 2.00 m in length and 1.00 m in width. The related reflector is made of lined sheets of aluminium, and the tubes are made of stainless steel used to absorb heat. They have an outer diameter of 0.051 m and a wall thickness of 0.002 m. The cylindrical turbulators are coupled axially and also radially joined to the interior of the

PTR. Eighty different internal cylindrical receivers are examined and compared with the plain tube. The lengths, thicknesses, and numbers of turbulators are tested at varied values, and all these tubes are examined under a constant inlet temperature of 300 K and mass flow rates in the range of (0.6-1.0 kg/s). The developed model is validated with experimental correlations for plain tube from the literature review. The simulation findings demonstrated that the addition of hollow cylindrical turbulators may greatly enhance the uniformity of the temperature gradient between the wall of the PTR and the water. The optimum model of the cylindrical turbulators was selected to be a length of 0.040 m, a thickness of 0.002 m, and a number of 15 turbulators. This model recoded the Nusselt number ratio of 1.79, the friction factor ratio of 1.10, and the highest performance evaluation criteria 1.73. Moreover, the outlet water temperatures of the plain tube and modified tube are increased from 300 K to 325.5 K and 339.7 K, respectively. Based on the numerical findings, the optimum model of the hollow cylindrical turbulators was considered for the experimental work.

Experimentally, the outlet water temperatures recorded 61.5°C and 57.0°C for the modified PTR (tube with novel cylindrical turbulators) and the plain tube (tube without novel cylindrical turbulators), respectively. The heat gain reaches 1053.9 W in the modified PTR and 903.3 W in the plain tube. Compared to the PTC with a plain tube, the PTC with modified PTR showed 38% enhancement in thermal efficiency. It is concluded that the experimental results are in a good agreement with the numerical results of the optimal model of cylindrical turbulators. Also, the PTC performance is evaluated by comparing the experimental and numerical outcomes: the outlet temperature, useful heat, and thermal efficiency for modified PTR and plain tube. Finally, the productivity of freshwater from the modified

SDU (MSDU) (SS+PTC contained cylindrical turbulators) improved by 89% and 15% compared to the conventional SS and SDU, respectively.

Table of contents

List of Tables

List of Figures

Nomenclature

Symbol	Definition	Unit
A	Area	m^2
AL	Altitude of the location above mean sea level	km
a	Constant	-
b	Constant	-
c	Constant	-
c_p	Specific heat capacity	J/kg.ºC
D	Distance	km
d	Diameter of PTR	m
De	Depth	m
F	PTC efficiency factor	-
f	Friction factor	-
f_L	Focal length	m
F_R	Heat removal factor	-
h	Heat transfer coefficient	W/m^2.ºC
I	Solar radiation	W/m^2
k	Thermal conductivity	W/m.ºC
L	Length of reflector	m
l	Length of cylindrical turbulator	m
m	Constant	-
$\dot{m}$	Mass flow rate	kg/s
N	Number	-
Nu	Nusselt number	-
p	Pressure	Pa
Q	Energy	W
Pr	Prandtl number	-
Re	Reynolds number	-
r	Radius	m
T	Temperature	ºC
Ti	Time	hr
t	Thickness of cylindrical turbulator	m

u	Fluid velocity	m/s
W	Width of aperture	m
w	Hour angle	degree
X	Effect loss of PTC reflector	-
x	X-axis	-
y	Y-axis	-
Greek symbol		
Δ	Ratio	-
α	Absorption	-
δ	Declination angle	degree
ε	Emittance	-
η	Efficiency	%
θ	Angle	degree
μ	Viscosity	kg/m.s
ρ	Density	kg/s
σ	Stefan-Boltzmann	$W/m^2.K^4$
τ	Reflectance	-
ϕ	Altitude angle	degree
Subscripts		
a	Air	
abs	Absorbed	
arc	Arc	
b	Beam	
bt	beam radiation on titled surface	
bu	Bulk	
c	Collector	
cond.	Conduction	
conv.	Convection	
day	Day	
f	Fluid	
i	Inlet	

inc	Incident
Loc	Location
loss	Loss
o	Outer
opt	Optical
r	Rim
rad.	Radiation
SC	Solar constant
th	Theoretical
the	Thermal
use	Useful
w	PTR's wall
z	Zenith
Abbreviations	
CFD	Computational fluid dynamic
CSC	Concentering solar collector
DSC	Dish solar collector
FC	Fixed cost
HTF	Heat transfer fluid
NCSC	Non-concentering solar collector
PEC	Performance evaluation criteria
PTC	Parabolic trough collector
PTR	Parabolic trough receiver
CSS	Conventional solar still
SC	Solar collector
SDU	Solar desalination unit
SS	Solar still
MSDU	Modified solar desalination unit
TC	Total cost
TSC	Tower solar collector
VC	Variable cost

Chapter One: Introduction

1.1 Background

Water treatment and purification are the procedures of getting rid of unfavorable chemicals, natural contaminants, as well as suspended solids from water. There are many technologies to produce freshwater, such as distillation, ion exchange, and membrane processes. Distillation is the most established desalting process that uses thermal processes for applications that are not applicable to be performed by electro dialysis reversal (EDR), for example, feed water with high salinity or where the feed water conditions would negatively affect the performance and the membrane life [1]. Many power plants produce freshwater and electrical power, such as the Umm Al Houl power plant in Qatar has a capacity of 2520 MW of electricity and 136.5 million imperial gallons of freshwater, and the Ras Al Khair power plant in Saudi Arabia has a capacity of 2400 MW. These power plants depend on non-renewable energy, so they are very costly. Therefore, the trend has shifted to producing freshwater using renewable energy, such as the Sydney station, which operates entirely using renewable energy sources (solar energy) to desalinate seawater [2].

Renewable energy is defined as energy found in nature in an unlimited state. It is constantly renewable, clean, and its use does not pollute the environment. There are many sources of renewable energy, including solar energy (which is the main source of energy on the surface of the earth), wind energy, tidal energy (resulting from the gravitational forces between the earth, the moon, and the sun), wave energy, geothermal energy, and temperature gradient energy in solar ponds [3]. The energy generated from burning agricultural and household waste is classified as renewable energy by scientists [4].

Because fossil fuels cause environmental pollution, the last two decades have witnessed a relatively large increase in the use of renewable energy compared to the use of non-renewable energy (natural gas and

coal). Therefore, it is expected that the use of renewable energy sources will increase in the coming decades, as shown in Fig. (1-1) [5].

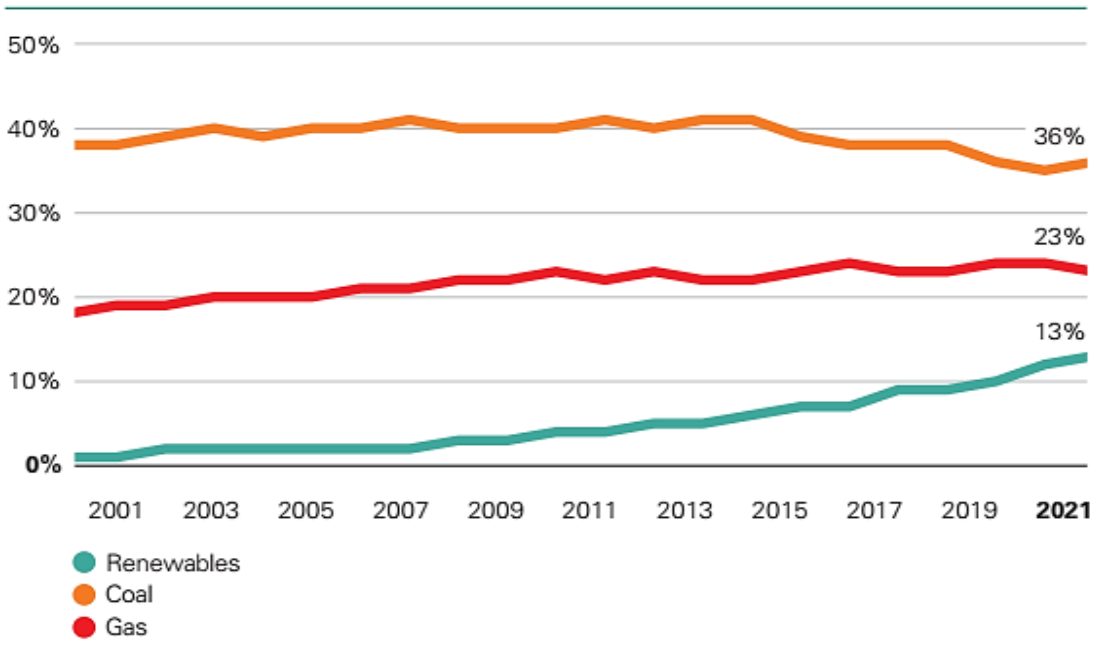

Figure (1-1): The share of renewables in global power generation continued to increase [5].

The characteristics of renewable energy sources, which primarily derive directly or indirectly from the sun, contribute to their increasing use. There are some limitations associated with using renewable energy that can be succinctly outlined as follows [6]:

1) It has a higher cost because the use of these sources requires many large areas and sized equipment, which results in a high initial cost to implement such a project.
2) Since this energy is not available regularly and varies constantly with the time of day and season, energy storage in renewable energy systems is critical.
3) Different forms of existence require the development of specific technical equipment for each energy source.

Countries with mild climates and high temperatures have several opportunities to use solar energy systems with optimal performance. One

of these countries is Iraq, which possesses the capacity to use solar radiation for approximately 4000 hours annually in strategically advantageous locations with solar energy potential [7].

Recently, the availability of clean drinking water sources has become a big problem in the world, especially in Iraq. The water desalination process consumes a lot of fossil fuels and thus has an impact on the environment and human life, in addition to the high financial cost. Thus, attention has been driven toward utilizing solar energy for water desalination.

1.2 Solar Radiation

The sun creates solar radiation through a nuclear fusion process that generates electromagnetic radiation. The solar radiation spectrum, which has a temperature of roughly 5800 K, is comparable to that of a black body in the visible short-wave component of the electromagnetic spectrum, which contains nearly half of the energy. The second half of the spectrum, which includes some ultraviolet light, is more in the near-infrared range. Because of its influence on living matter and the potential to be used for practical purposes, solar radiation is becoming more valuable. It is a never-ending source of natural energy with enormous promise for a wide range of uses, as well as other renewable energy sources, because it is abundant and readily available. [1].

It is categorized into three groups:

1) **Direct (Beam) radiation:** This is the sun's radiation that reaches the earth without being scattered.
2) **Diffuse radiation:** It is the sunlight that travels across the atmosphere and clouds.
3) **Reflected radiation:** The amount of solar radiation reflected from a surface of earth ground into the solar collector.

Position, atmospheric conditions, such as cloud cover, aerosol content, and ozone layer state; solar rotation and operation; time of day; and earth/sun distance all affect the amount of solar radiation reaching the earth's surface, as shown in Fig. (1-2) [8, 9].

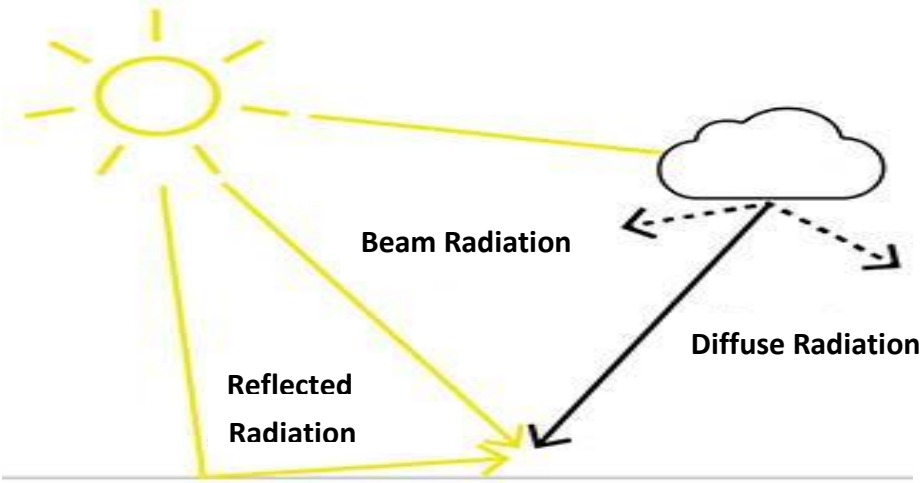

Figure (1-2): The three major solar radiation components.

1.2.1 Solar Radiation in Iraq

Theoretically, Iraq is considered at the first level (white area) of solar exposure radiation, as shown in Fig. (1-3). According to Iraq's daily averaged solar insolation contour map, almost all of Iraq has the potential to establish large-scale solar utilities. In Iraq, the annual average of energy received daily from the sun ranges between 5.0 and 6.0 kWh/m^2 as illustrated in Fig. (1-4) [10, 11].

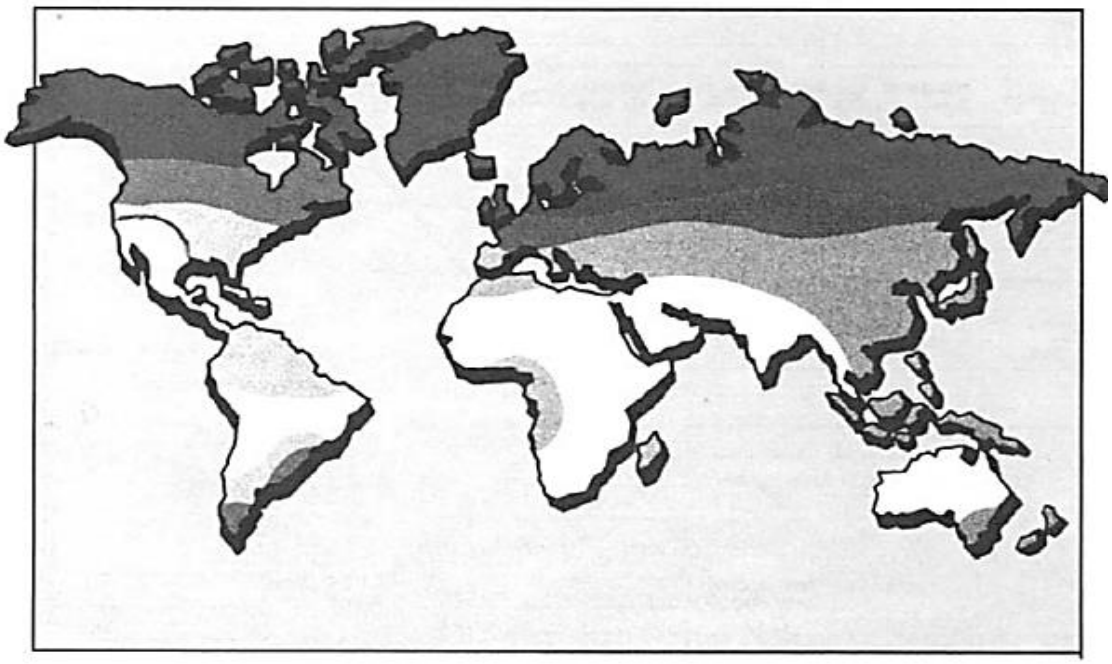

Figure (1-3): The world's solar radiation indicates that white areas have a higher potential for energy [10].

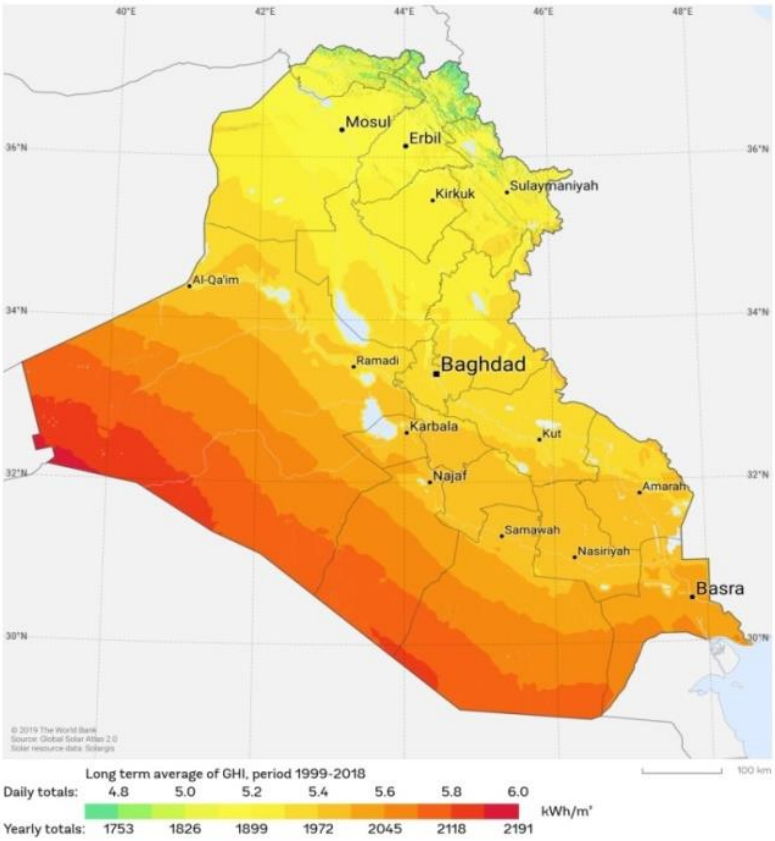

Figure (1-4): The sun's average daily radiation varies across different regions of Iraq [11].

1.2.2 Solar Energy Exposure

Usually, the duration of solar energy availability in Iraq is typically extensive, as indicated in Table (1-1).

Table (1-1): Solar exposure period in Iraq [12].

Quantity	Solar Exposure period
Sunny hours	4100 hours
Sunny day	333.6 days
Cloudy days	31.4 days

1.3 Solar Collector (SC)

Solar Collector (SC) is a special type of heat exchanger that has the ability to convert solar radiation into useful energy that can be transferred by a heat transfer fluid (HTF) (such as oil, water, or air) to be used in many applications, including electricity generation, fluid heating, and water desalination. Figure (1-5) presents the schematic of the types of SCs [3, 13].

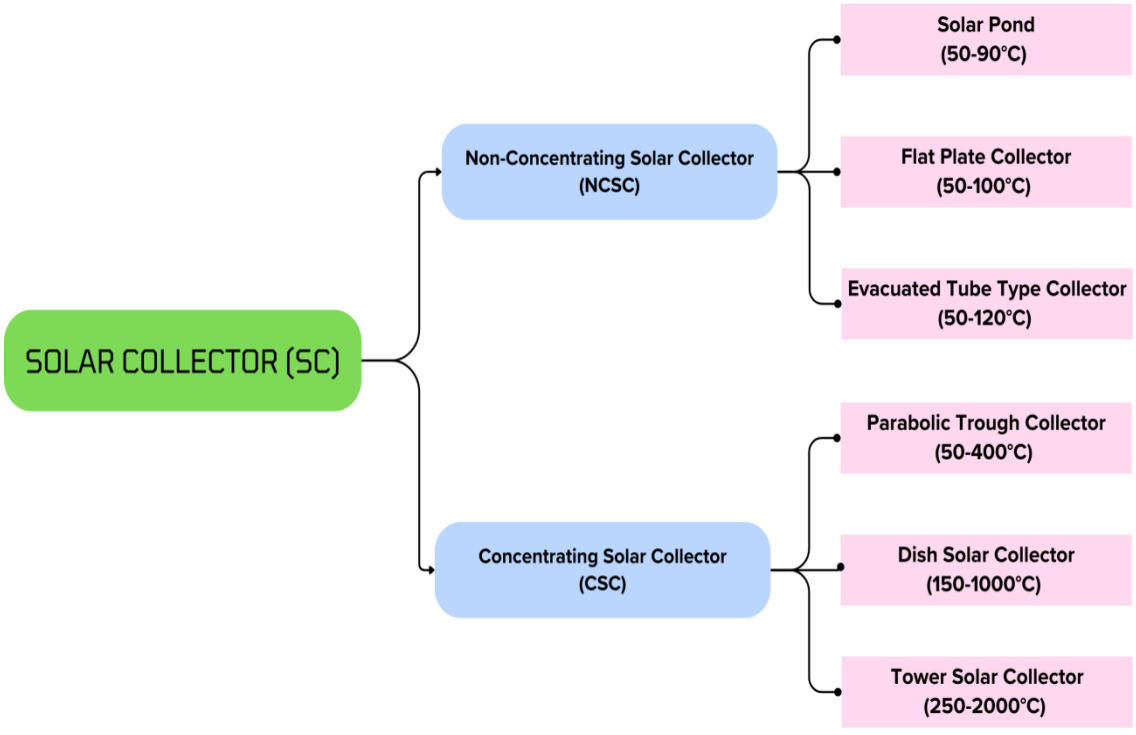

Figure (1-5): Schematic of the SC types [3, 13].

As shown in Fig. (1-5), non-concentrated solar collectors (NCSCs) are used for low-temperature (40-120ºC) applications, whereas concentrated solar collectors (CSCs) are used for medium- and high-temperature (50-2000ºC) applications. Generally, the NCSC concentrates solar radiation on a high area, matching the area of absorbed radiation, while the CSC concentrates solar radiation on a smaller area, less than the area of absorbed radiation, thereby elevating the temperature of HTF to high values. Therefore, various applications such as power production [14, 15], water desalination [16, 17], air conditioning, and other application areas [18] utilize the CSCs. The CSCs also have many geometrical designs but share some main characteristics, which can be summarized as follows:

1) **Reflector:** It reflects and concentrates solar radiation at a focal point or along a focal line using reflective surfaces (such as aluminum, stainless steel, mirrors, etc.).
2) **Absorber (Receiver):** It absorbs and transfers the reflected solar radiation into a Heat Transfer Fluid (HTF) for heating.
3) **Tracker:** It tracks the sun's movement to increase the amount of incident solar radiation on the reflector.

The CSC systems are typically divided into three categories, as indicated in Fig. (1-6) [19]:

1) **Parabolic Trough Collector (PTC):** A parabolic trough-shaped mirror reflector linearly concentrates sunlight onto the receiver tube, heating an HTF, which is then used to produce heated steam.
2) **Tower Solar Collector (TSC):** This type of collector uses numerous heliostats as central reflectors to concentrate sunlight onto a central receiver located at the top of the tower.

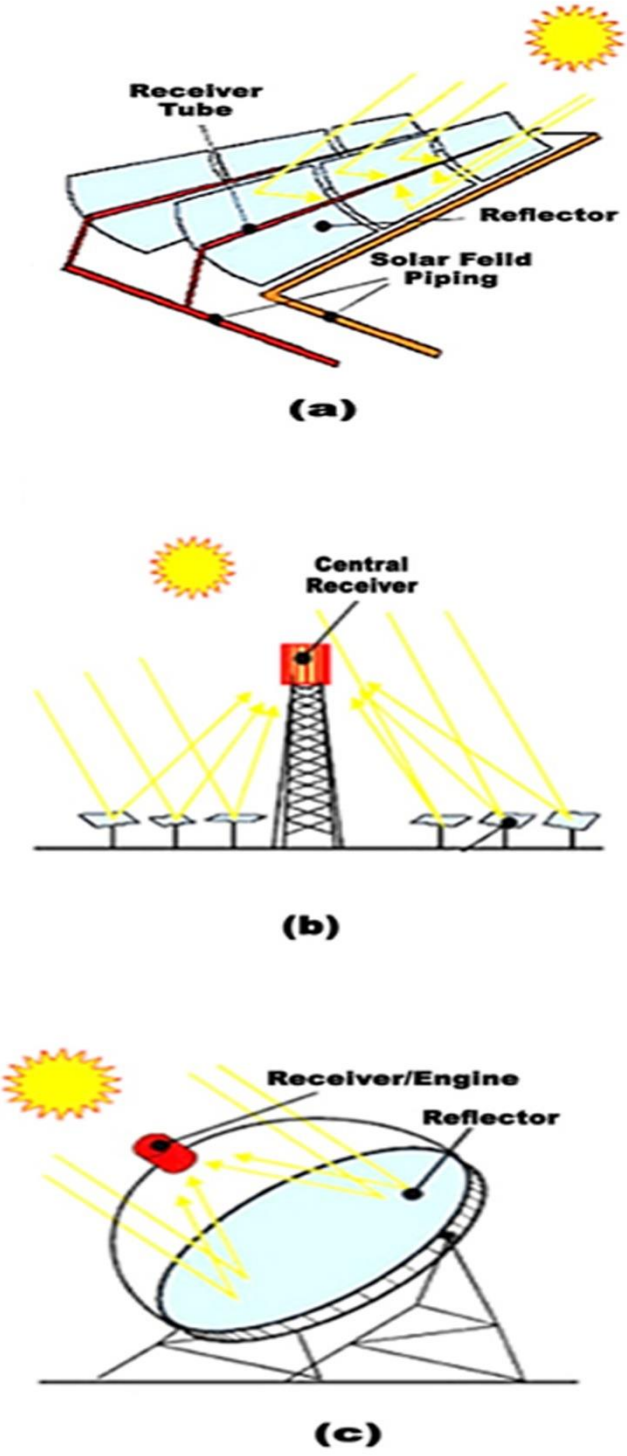

Figure (1-6): The CSC systems are: a) parabolic trough collector, b) tower solar collector, and c) dish solar collector [19].

3) **Dish Solar Collector (DSC):** A dish-shaped reflector perfectly concentrates sunlight in two dimensions and runs a small engine or turbine at the focal point of DSC.

The DSC produces low quantities of HTF depending on the size of the engine at focal point of DSC. The TSC produces HTF at a higher temperature, more than 1000ºC. Because this the PTC is becoming more popular for research because of its wide range of temperatures and reasonable cost. As a result, the PTC will be the subject of interest for this project.

The main problem in the PTC is the temperature variance of HTF behind the internal surface of the parabolic trough receiver (PTR) and the central flow of HTF. To solve this problem, turbulators will be used to distribute temperatures inside this PTR as well as increase the residence time of the HTF inside the PTR, thus harvesting more heat.

1.3.1 Technology of the PTC

Currently, the best validated solar thermal reflector technology is the PTC technology, as shown in Fig. (1-7). The solar technology uses a linear concentrator device to convert solar beam irradiance into thermal energy. PTCs utilization can be divided into two groups. The first group exclusively focuses on solar power plants. Currently, they have successfully tested and operated several commercial reflectors for this purpose. The temperatures achieved by those plants ranged from 300 to 400°C. Electric power cycles, both directly and indirectly, link the concentrating solar power plants with PTC [20]. The second group aims to provide thermal energy to applications that necessitate temperature ranges of (50-250ºC). These applications primarily involve industrial process heating, which includes tasks like cleanup, drying out, vaporization, distillation, pasteurization, sterilization, and food cooking, among others. It also encompasses applications with low-temperature heating demands and high intake rates, such as local warm water, space warming, and swimming pond warming, as well as heat-powered refrigeration and chilling [21].

Presently, the term "medium temperature reflectors" refers to reflectors operating within the temperature range (50-250°C). The solar thermal industry aims to construct reflectors suitable for use in this temperature range. To date, this temperature range has resulted in a limited number of experiences [21]. It's quite common to find commercial processes that use warm water and steam with temperatures ranging between 80 and 180ºC. Given the possible reduction in the use of typical energy resources, which led to a reduction in carbon dioxide emissions, studies on solar heating systems that can operate at these temperatures are of great relevance.

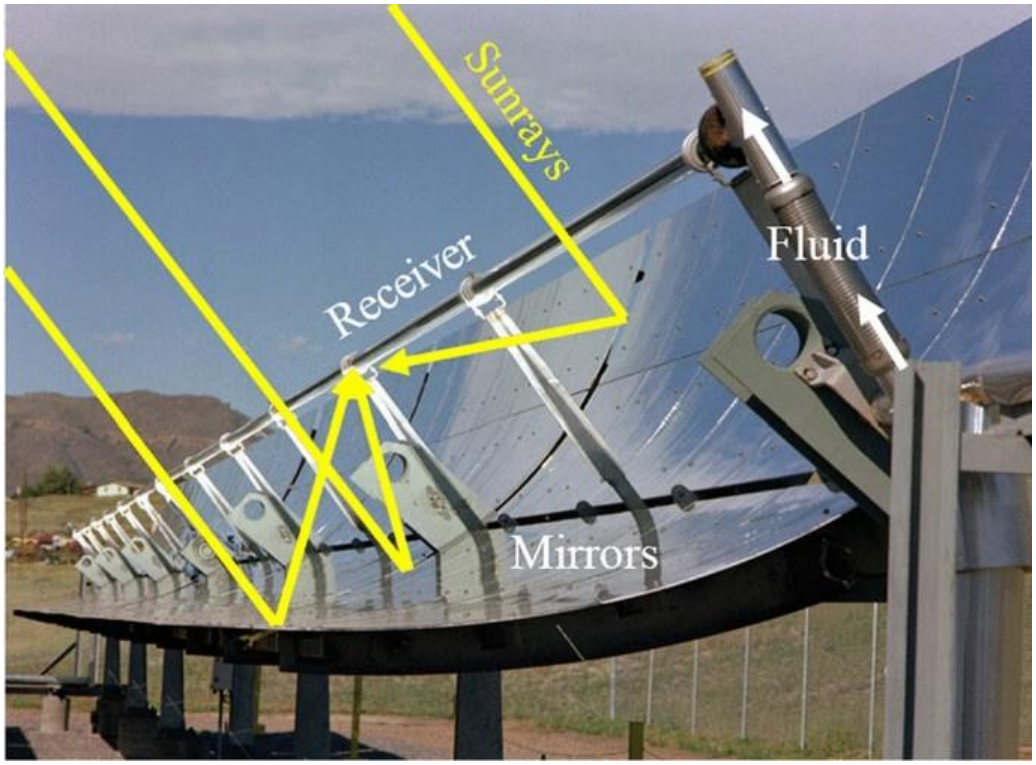

Figure (1-7): Parabolic trough collector system [22].

1.4 Applications of the PTC

The uses of PTC have multiplied, and its exploitation and conversion into thermal or electrical energy have become commonplace at present, as it can be used for building heating, water desalination, generating electrical energy, and other important uses. In this section, the various thermal

applications of PTC will be discussed. PTC heats the building by heating the fluid (either air or water) flowing through a PTR, which then travels through a closed loop of pipes positioned in the building's wall and floor or via heat exchangers situated within the building's rooms [23]. The process of water desalination involves heating the water inside a PTR, which then passes through a solar still for condensing and transforming it into freshwater suitable for drinking [24]. There are two ways to integrate PTCs with solar thermal power plants: the first method involves running a steam turbine directly from PTCs, while the second method involves heating an HTF in the solar field and using it in a heat exchanger to generate steam that powers the steam turbine [20]. The most recent example using PTCs to generate electricity is the nine commercial solar power-generating systems. The construction and installation location is Mojave Desert in California with a total capacity of 354 MW. The first plant has a capacity of 14 MW, the next six plants have an output of 30 MW, and the last two plants have a capacity of 80 MW [25]. Additionally, there are several options for integrating PTC with refrigeration systems. Solar refrigeration is used in absorption units that are powered by PTCs. The two most common fluid combinations used are lithium bromide and water (LiBr-H_2O) and ammonia and water (NH_3-H_2O). Figure (1-8) shows a schematic of a thermally driven absorption refrigeration system. The major components of the system are the absorber, generator, condenser, evaporator, heat exchanger, pumps, and expansion valves. The PTCs in the generator add heat to the refrigerant, and the condenser removes the heat from the refrigerant vapor as it exits the generator. Then, the liquid flows through an expansion valve to reduce the pressure. The evaporator adds heat from the load to the refrigerant, transforming the liquid into vapor. A weak solution absorbs the refrigerant vapour, transforming it into a strong solution. The absorber experiences heat rejection as the refrigerant vapor becomes liquid.

A liquid pump raises the liquid pressure to the condenser pressure. The generator's warm, weak solution flow preheats the strong solution in a heat exchanger. Next, it enters the generator, where a solar field provides the heat. Meanwhile, the weak solution is transferred to the absorber via the heat exchanger and expansion valve [25].

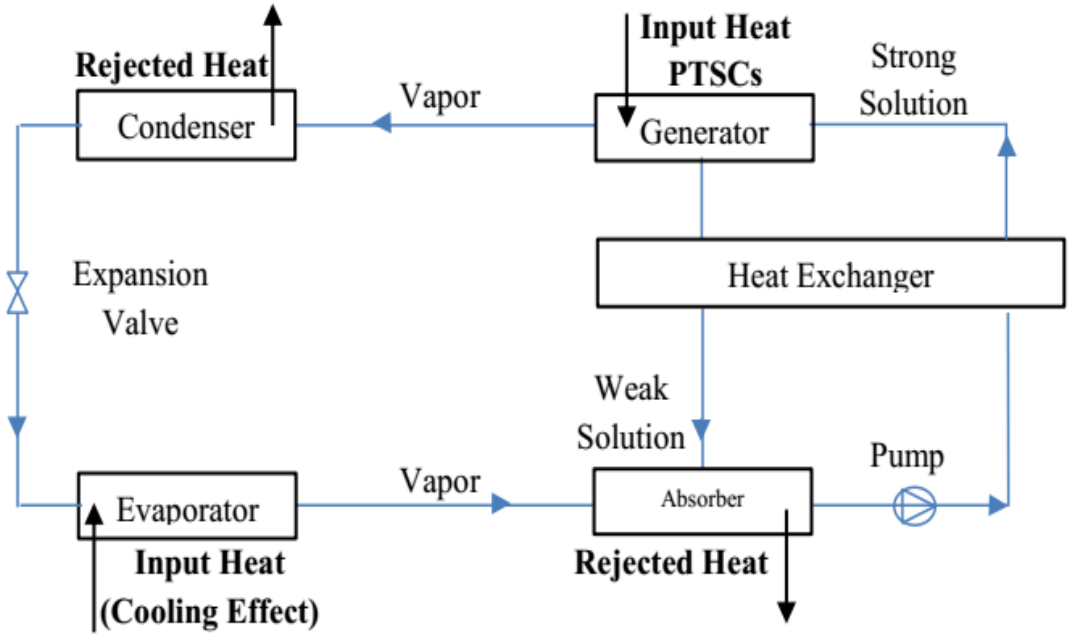

Figure (1-8): The basic principle of the absorption air conditioning system [25].

1.5 Enhancement of the Thermo-hydraulic Performance inside PTR

There are three main techniques that can be used to enhance heat transfer in tubes: active, passive, and compound (active and passive) techniques. Active techniques (such as surface vibration, suction, mechanical assistance, electric or magnetic fields, etc.) require external energy sources to enhance the thermo-hydraulic performance inside a PTR. Passive techniques involve changing a thermal system's architecture to improve its thermo-hydraulic performance without requiring external energy sources. The compound techniques mix two previous techniques (active-active, active-passive, or passive-passive) [26-28]. Figure (1-9) lists

the passive techniques which represent the main techniques to enhance thermo-hydraulic performance inside a PTR. The nanofluid technique depends on two parameters: the thermophysical properties and the concentration of nanoparticles. These parameters cause the HTF to have a higher density and viscosity (the increasing volume percent of nanofluid will improve the heat transfer of this fluid). There are limits to the addition of nanoparticles, otherwise, the entropy decreases, the flow resistance increases, the heat loss decreases and nanofluids form [29-31]. The extended surfaces technique is used to enhance heat transfer due to the larger surface area available for heat transfer, but their manufacture is hardness and cost. The turbulators technique is used to minimize heat losses from a PTR and maximize its heat transfer surface. This is done using rods, twisted tapes, rings, cylinders, and wire coils [32-35].

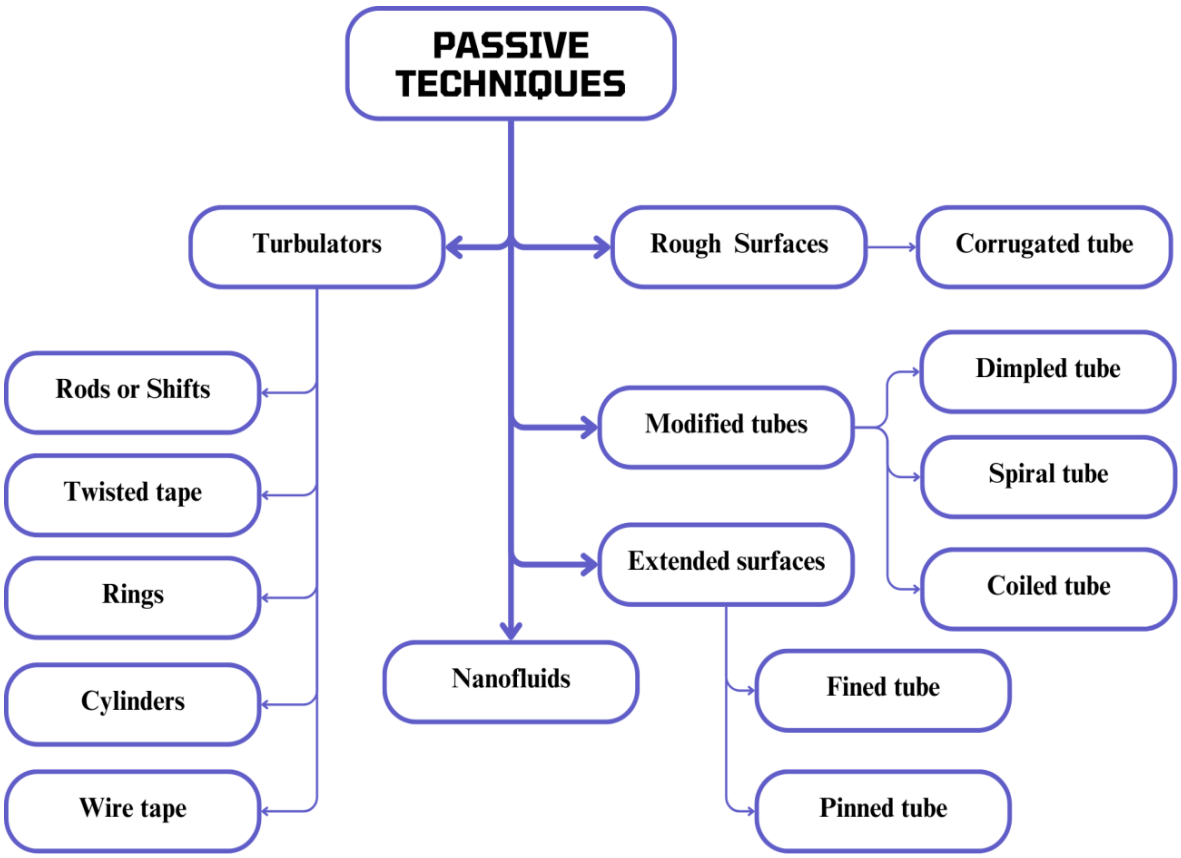

Figure (1-9): Scheme for the passive techniques of heat transfer enhancement inside tubes.

1.6 Solar Still

The evaporation and condensation processes that are part of the natural water cycle provide the basis for how solar stills (SSs) work. The glass cover (which serves as a condensing surface), the absorber plate (which serves as an evaporative surface), and the basin are the main parts of the SS. Sunlight can pass through the glass cover and land on the evaporative surface. The basin's salty water evaporates as a result of solar radiation absorption. The density shift drives the produced vapor to the condensed surface (glass). The density shift creates a buoyancy force that causes them to condense and transform into water droplets. These droplets fall to the bottom of the measuring jar and gather there [36]. Figure (1-10) shows a schematic diagram of a simple basin-type SS.

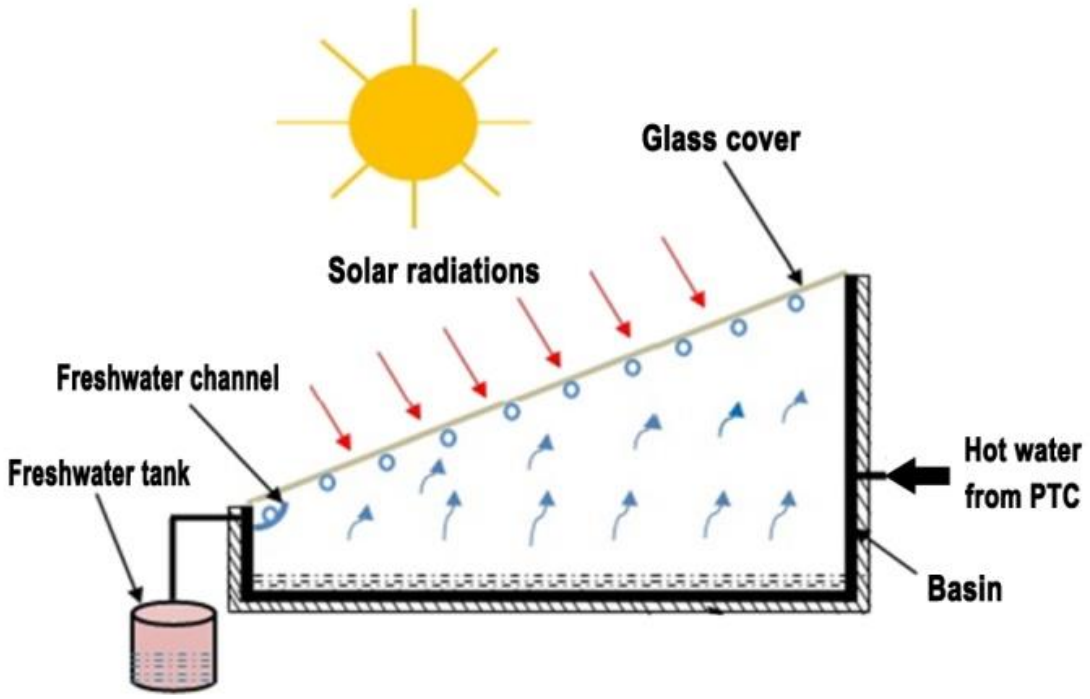

Figure (1-10): A schematic diagram of a solar still [36].

1.7 Problem statement

Salt water is the current problem that requires appropriate measures to improve the productivity of freshwater. Polluted water is not only unhealthy but also poses a threat to the individual health. Therefore, the

primary objective of this study is increasing the produced freshwater by enhancing the solar desalination unit (SDU). The enhancement of SDU is done using a PTR with a new-designed cylindrical turbulators. HTF (water) is flowing inside a PTR and then flowing into an SS to produce the freshwater. A comparison will be carried out with and without using the cylindrical turbulators and evaluate their effect on the heat transfer rate and pressure drop through a PTR.

1.8 Aim and Objectives

The aim of this study is the enhancement of heat transfer inside a PTR using cylindrical turbulators. The objectives of this study are:

1) Selecting the optimal specifications (length, thickness, and number) of cylindrical turbulators using ANSYS software.
2) Validating the present model by comparison between the experimental and numerical results.
3) Increasing the freshwater productivity from modified SDU (MSDU) using cylindrical turbulators inside a PTR of a PTC system.

1.9 Outlines of the Thesis

This study is organized as follows:

1) Chapter one provides a brief overview of solar radiation in Iraq, the SCs and their types, the PTC and some of its applications, techniques to enhance the thermal-hydraulic performance inside a PTR, and the condensing system (SS), which are all presented before describing the problem statement, aim and objectives.

2) Chapter two delves into the previous studies conducted on enhancement techniques of thermo-hydraulic performance inside a PTR.
3) Chapter three outlines the steps involved in the numerical study of the current study, which was conducted using the ANSYS Fluent 20.0 R2 software. Additionally, it presents the main equations used to calculate beam solar radiation and the thermo-hydraulic performance inside a PTR.
4) Chapter four provides a detailed description of the experimental setup of the PTC, used accessories, experimental calculations, and a summary of the present work procedure.
5) Chapter five explains and discusses of the current study's results. It includes numerical results for choosing the best length, thickness, and number of turbulators, a validation test with literature study and empirical correlations, and experimental results for the two tubes (plain tube and PTR with turbulators).
6) Chapter six elucidates the main conclusions of the current investigation and highlights some suggested recommendations for future studies.
7) Finally, references that were used in this study are listed.

Chapter Two: Literature Review

2.1 Introduction

Several experimental and numerical studies investigated the prospects of improving the thermo-hydraulic performance inside a PTR using various techniques. One of those techniques is the passive technique, which includes using nanofluids, extended surfaces, and turbulators. Due to many drawbacks of nanofluids as explained in chapter one, the effect of using extended surfaces and turbulators on a PTR performance will be presented since it minimises heat losses in a PTR and maximises its heat transfer surface. The survey focuses on the experimental and numerical studies in which various types of extended surfaces and turbulators are integrated inside a PTR.

2.2 Numerical Studies

The numerical studies simulated the PTC system with a plain tube or modified PTR by evaluating the thermal performance (Nusselt number) and hydraulic performance (friction factor) using the Fluent tool in the ANSYS software. The comparison with the plain tube case was conducted by evaluating the Nusselt number ratio, friction factor ratio, and performance evaluation criteria (PEC).

Ghadirijafarbeigloo *et al.* (2014) [37] introduced louvred twisted tape (as shown in Fig. (2-1)) to enhance the heat exchange between HTF and PTR's surface by generating turbulent swirling flow. The PTR was designed to be made from stainless steel, the turbulators were made from aluminium, and the HTF was Behran thermal oil. It was found that the highest values of the Nusselt number ratio and friction factor ratio were 3.5 and 4.1, respectively, using the louvred twisted tape with a twisted ratio of 2.67.

Chang *et al.* (2015) [32] numerically analysed the effect of varying clearance ratios and twisted ratios of a twisted tape on thermo-hydraulic

performance between a PTR (Alloy 625). It was noted there was a negative effect of these parameters on the Nusselt number ratio and friction factor ratio. The maximum values of the Nusselt number ratio and friction factor ratio reached 2.9 and 2.5, respectively, as the results revealed.

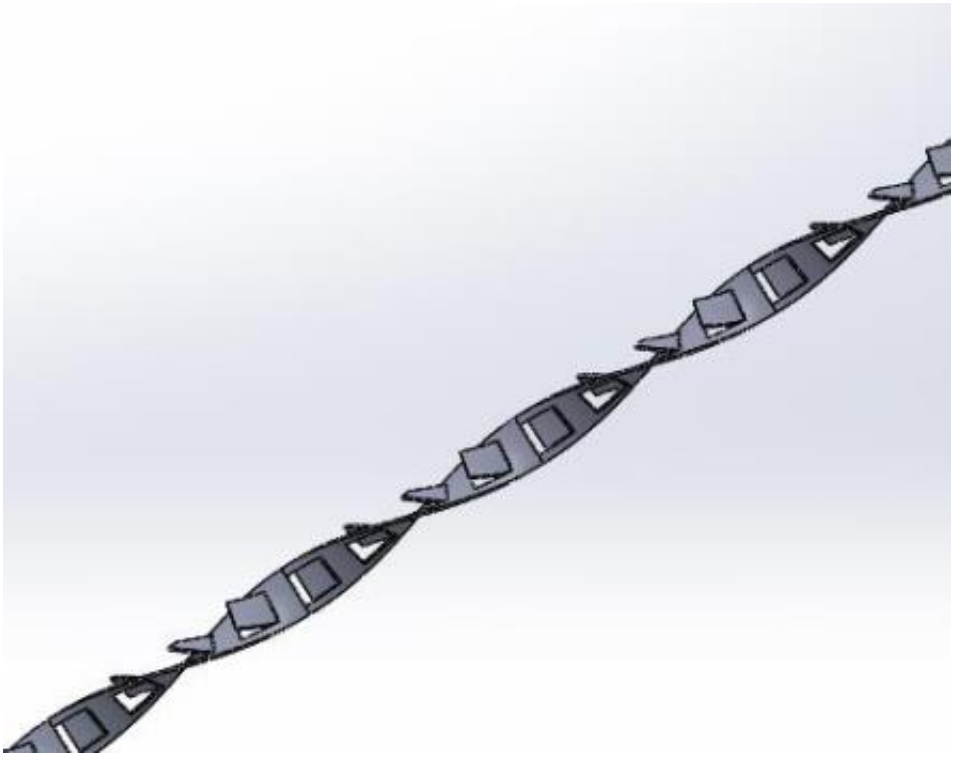

Figure (2-1): Louvred twisted tape [37].

Scientists **Zheng *et al.* (2016)** [38] enhanced the heat transfer rate and reduced the pressure drop by using porous turbulators in the upper or lower surfaces of PTR, as shown in Fig. (2-2). The researchers used different materials for porous turbulators (Cu, SiC, Al, and Fe) and noted that the good materials were Cu, SiC, and Al, whereas they advised against using Fe.

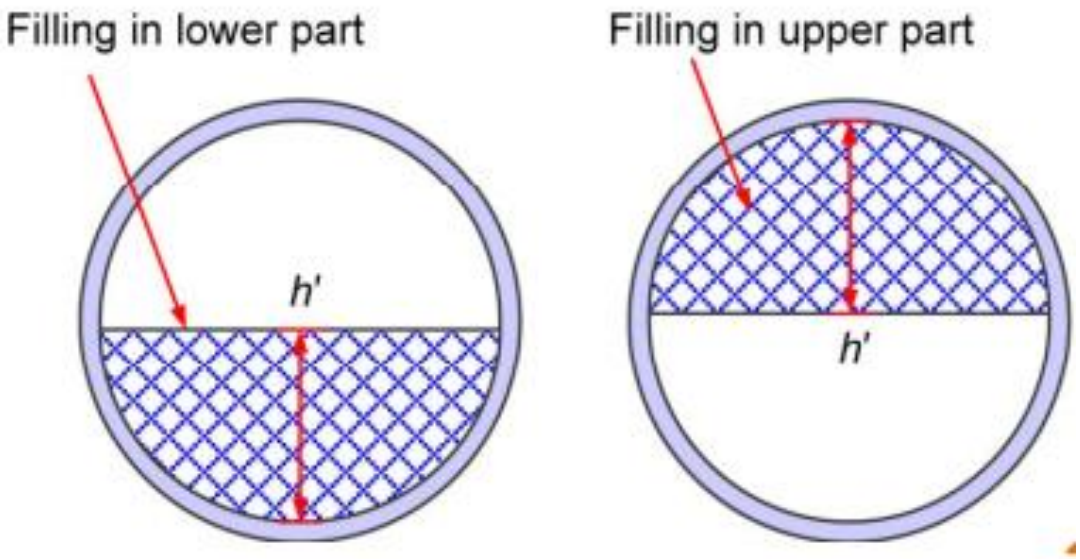

Figure (2-2): Front view of the porous turbulators [38].

Bellos *et al.* (2017) [39] studied how the geometrical parameters (length and thickness) of rectangular longitudinal fins attached by the upper and lower surfaces of PTR affected the PTC thermal efficiency. Their observations revealed that the optimal case (with a length of 10 mm and a thickness of 2 mm) had a PTC thermal efficiency of 68.8%, which is 0.82% higher than that of a plain tube. Additionally, they found that the maximum values of the Nusselt number ratio and friction factor ratio were found to be 1.65 and 2.00, respectively.

Bellos *et al.* (2018) [40] manipulated the number and position of cylindrical longitudinal rods in order to improve the PTC thermal efficiency and heat transfer rate inside a stainless steel PTR, as shown in Fig. (2-3). The CFD results showed that the PTC thermal efficiency increased as the number of rods increased, especially with the four turbulators that had positions (1-3-5-7). In this case, PTC thermal efficiency and Nusselt number improved by 0.66% and 26.9%, respectively.

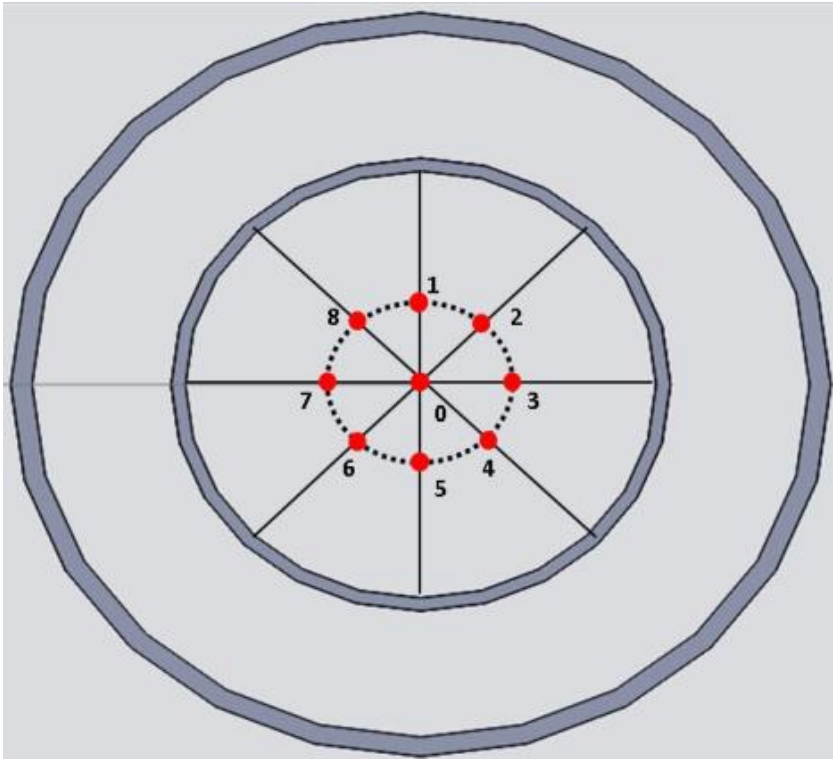

Figure (2-3): The examined locations of the flow turbulators [40].

Chang *et al.* (2018) [41] compared the effect of varying the concentric rod diameter and the eccentric rod position on the PTR's thermo-hydraulic performance. They noted that increasing the concentric rod diameter can yield the best results. Also, the Nusselt number ratio increased from 1.10 to 7.42 and the PEC from 1.12 to 3.38 as the dimensionless diameter (ratio of concentric rod diameter to the inner PTR diameter) increased from 0.1 to 0.9, as shown in Fig. (2-4).

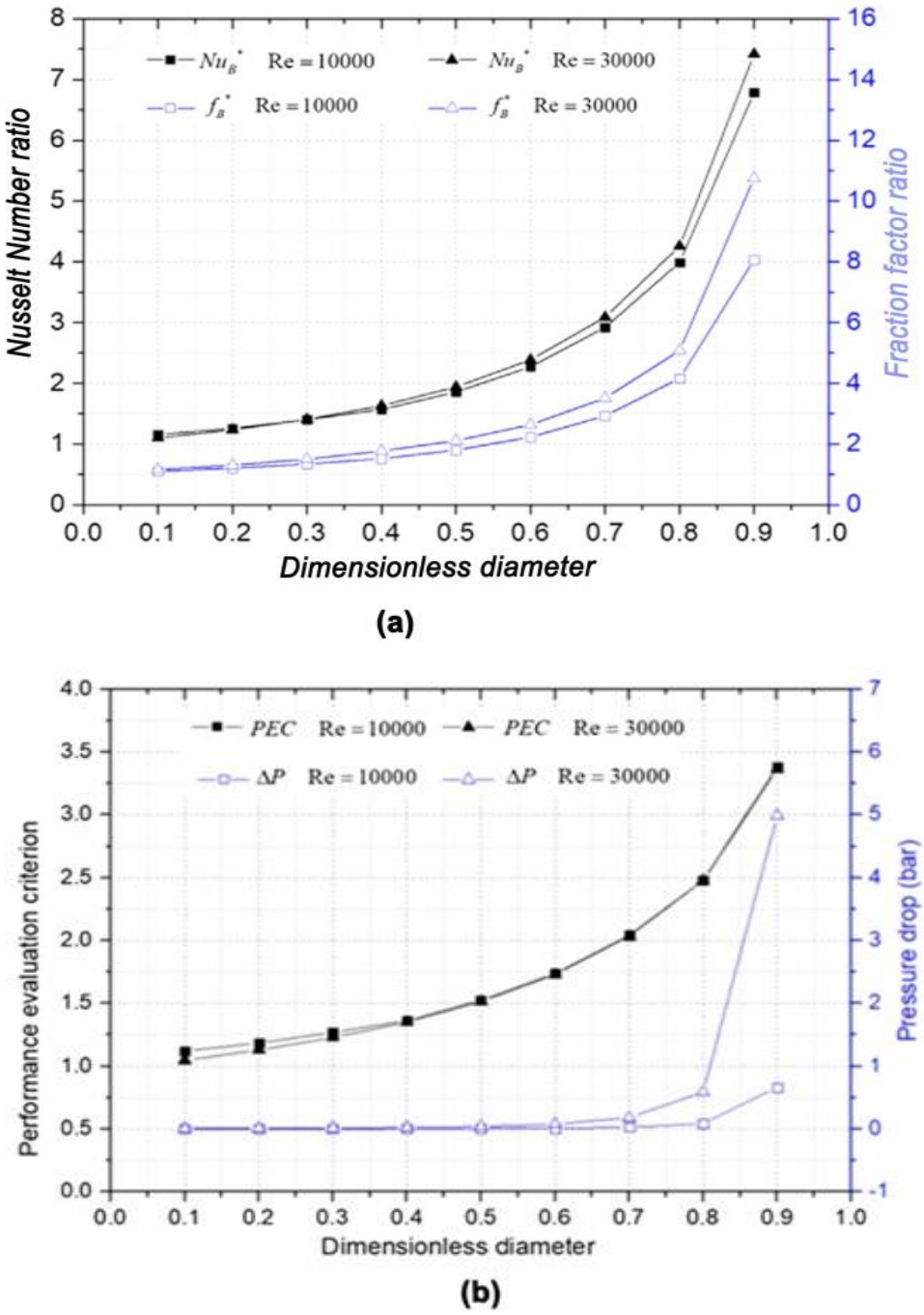

Figure (2-4): Effects of dimensionless diameter at different Reynolds number on: (a) the Nusselt number ratio and friction factor ratio, and (b) PEC and pressure drop [41].

Liu *et al.* (2019) [42] studied the effect of changing the different geometric parameters of conical strip turbulators (central angle, hollow diameter, and pitch size) on the values of the Nusselt number, friction factor, and PEC inside a stainless steel PTR. The CFD results showed both the Nusselt number and friction factor increased as the central angle

increased, while the hollow diameter and pitch size decreased. The range of enhanced Nusselt number was 45-203%, the improvement in PTC thermal efficiency was 5.04%, and the maximum value of PEC was 1.33.

Laaraba and Mebraki (2020) [43] conducted an investigation into the impact of the rectangular longitudinal fins' geometric dimensions attached to the bottom surface of copper PTR, as shown in Fig. (2-5), on the PTC thermal efficiency. The location of the fins marked the difference between this study and the previous study [39]; it was the location of the fins. The optimal case, with a length of 15 mm and a thickness of 6 mm, yielded an 8.45% maximum increase in PTC thermal efficiency, as they observed.

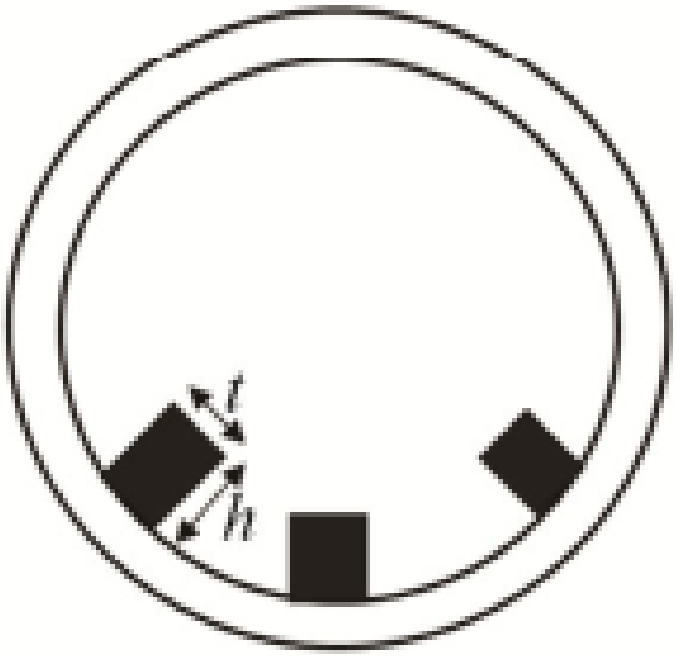

Figure (2-5): Cross-section of the PTR with fins [43].

Abbas *et al.* (2021) [34] conducted a numerical test to find the best inclined angle of twisted tape that enhances thermo-hydraulic performance inside a copper PTR. To achieve this, they varied the inclined angles with six values and used water as the HTF. Compared to the PT, the results show that the best inclined angle is 50º; at this angle, the outlet water

temperature was raised by 21%, and the maximum PEC was found to be 1.28.

Tanious and Abdel-Rehim (2021) [44] examined the behaviour of heat transfer rate and pressure drop inside an axially rotating internally finned PTR. According to CFD results, the increase in length of internal rectangular longitudinal fins and rotational speed of PTR improved the heat transfer rate and pressure drop. In the optimal case (2 mm of fin length and 10.5 of PTR rotation rate), the increases in the Nusselt number and friction factor were 110% and 81.6%, respectively.

Agagna *et al.* (2022) [45] demonstrated that spherical pins attached to the lower PTR surface improved thermal performance. They changed the pin's diameter, pin's number, angle between pins, and axial pitch size of pins. Results indicated the PEC increased as the pins number and the axial pitch size decreased. The Nusselt number and PEC were enhanced by 27.2% and 24.9%, respectively, whereas the heat losses were reduced by 9.32%.

Fatouh *et al.* (2022) [46] looked at a lot of different aspects of rectangular cross-section fins, such as their lengths, thicknesses, angles, and the rounding radii of rectangular cross-section fins that had rounding at the base of the fin. They noted that by using the optimal case of fins (which had 25 mm of length, 4 mm of thickness, 45^{o} of angle, and 4 mm of radii), the PTC thermal efficiency was enhanced by 1.36% and the PEC was recorded at 1.64.

Darbari *et al.* (2023) [47] analysed the impact of introducing porous discs with variation parameters (design shape-full, upward half, and downward half (as shown in Fig. (2-6-a)), diameter, and pitch size) inside a PTR. The CFD results showed that the full-disc configuration performed better than the half-disc alternative. Both thermal and hydraulic performances increased as the disc's diameter increased and the discs pitch

size decreased, as shown in Fig (2-6-b,c). The PEC was found to be around 1.6, and the PTC thermal efficiency was improved by around 4%.

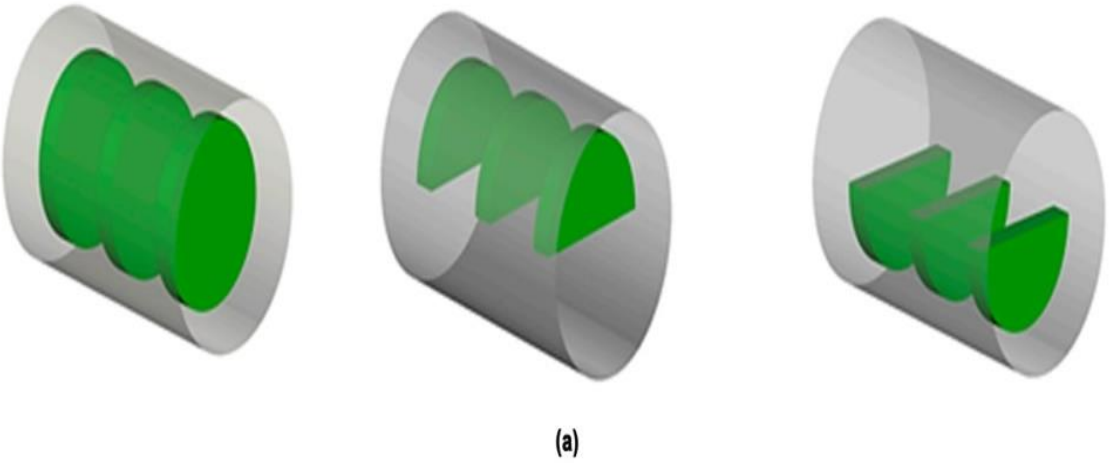

(a)

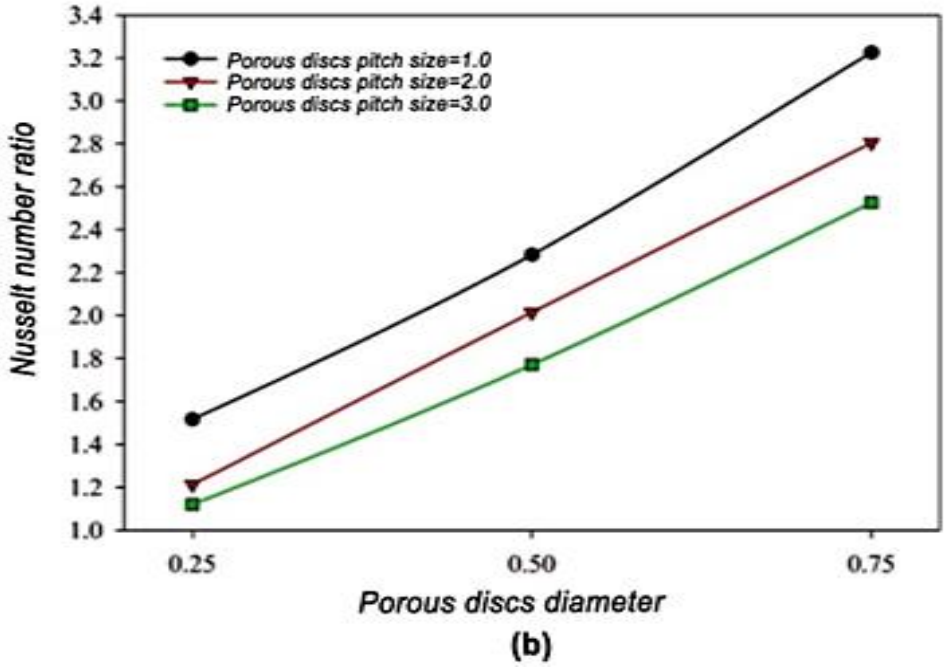

(b)

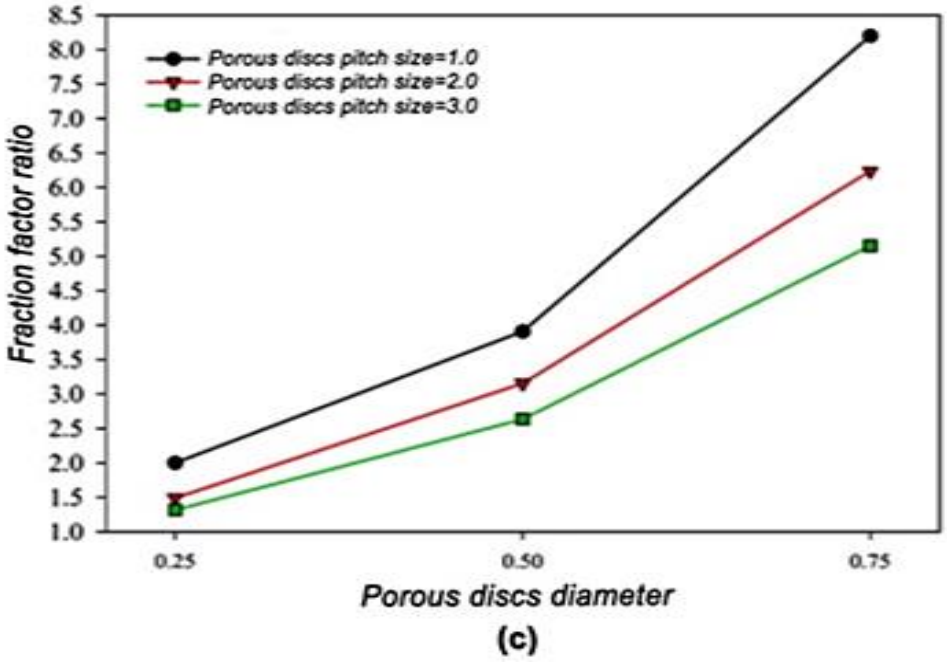

Figure (2-6): (a) The different shapes of porous discs, (b) the effect of the porous disc diameter and pitch size on the Nusselt number ratio, and (c) the effect of the porous disc diameter and pitch size on the friction factor ratio [47].

2.3 Experimental Studies

Reddy *et al.* (2015) [48] carried out (at Indian Institute of Technology Madras, Chennai, 13.07° N and 80.28° E) an experimental study for using porous discs (with different shapes and positions) inside a stainless steel PTR. Specifications of a PTC were 15 m^2 in aperture area, 65° in rim angle, 0.98 m in focal length, and single-axis tracking. The results of four days in May, from 8:00 to 15:00, demonstrated that using an alternative porous disc gave the highest value of Nusselt number, while using an unshielded tubular PTR gave the highest value of friction factor. Also, the highest range of values for PTC thermal efficiency was 63.9%-66.7%.

In order to compare the values of PTC thermal efficiency in two copper PTRs, **Kalidasan *et al.* (2016)** [49] fabricated a plain tube and a modified PTR with internal hinged blades, as shown in Fig. (2-7). The internal hinged blades had 2 mm drill holes along a straight line with a 50

mm pitch distance. PTC with a rim angle of 120° and a focal length of 0.26 m was used, which has a reflective surface made of aluminium alloy. The results showed a 14% improvement in PTC thermal efficiency with the modified PTR.

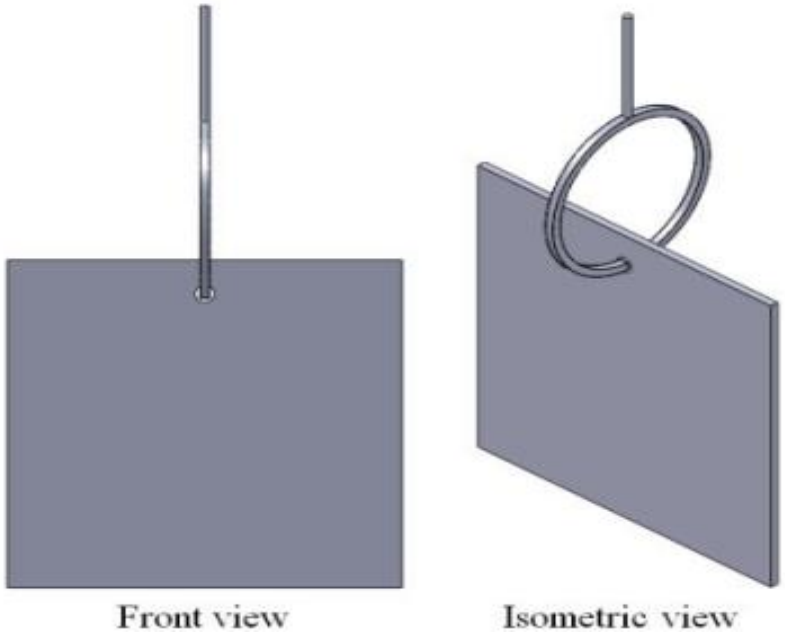

Figure (2-7): Design of blades used in [49].

Okour and Al-Odat (2018) [50] presented an experimental study of a PTC with a helical coil PTR under Irbid Jordanian (32.50° N, 35.90° E) climate conditions. According to Fig. (2-8), the specifications of a PTC were 4.06 m in length, 3.10 m in width, and 0.88 m in focal length. The study was tested over four days in December 2014, from 10:00 a.m. to 15:00 p.m. The experimental findings showed that the peak difference between the outlet and inlet water temperatures was 40.5°C, and the average PTC thermal efficiency was 64.7%.

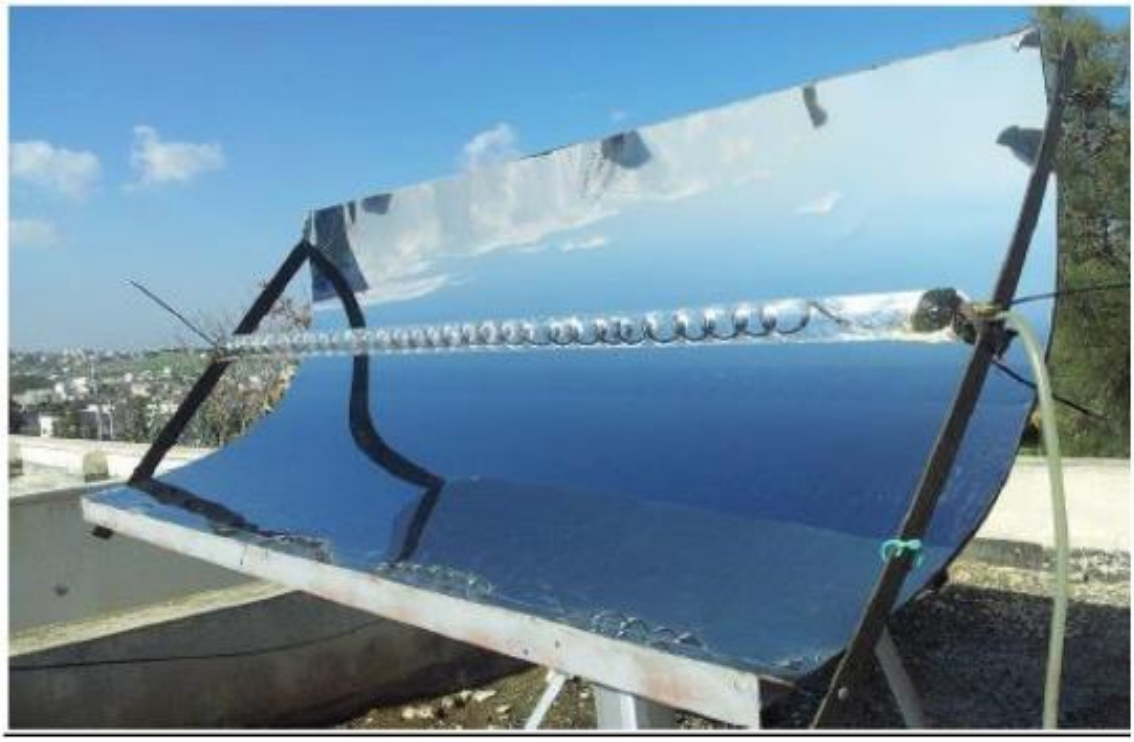

Figure (2-8): The PTC system of [50].

Kutbudeen *et al.* (2019) [51] inserted a conical strip with different twisted ratios and directions attached to a 1 mm-diameter copper rod inside a copper PTR, as shown in Fig. (2-9). The dimensions of the PTC were 2 m in length, 1 m in width, and 90° in rim angle. Stainless steel sheets made a PTC's reflector, while copper made a PTR. The experimental results showed the optimal parameters of the conical strips used were 3 of twisted ratio and backward flow of direction. In this case, the Nusselt number and friction factor were enhanced by 2.23% and 1.89%, respectively.

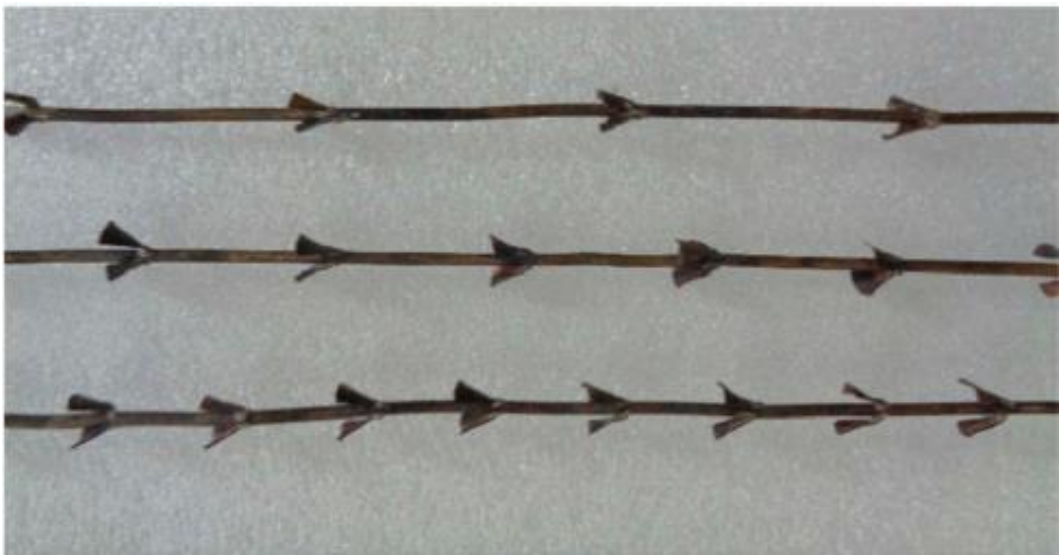

Figure (2-9): Conical strips of different twist ratios [51].

Isravel *et al.* (2020) [52] modified attached rings to conventional twisted tape to improve the heat transfer rate and pressure drop inside a PTR. They used a stainless steel reflector, a copper PTR, and aluminium twisted tape. They discovered that the improvements in PEC values were 19% when rings were attached to conventional twisted tape and 24% when rings were modified.

Naif *et al.* (2021) [53] measured the inlet and outlet water temperatures and evaluated the heat useful and PTC thermal efficiency inside a PTR with twisted tape (twisted ratio of 1.33). The PTC specifications were 1.25 m^2 in area, 0.45 m in focal length, and 90° in rim angle, as shown in Fig. (2-10). The findings showed that the use of modified PTR produced a PTC thermal efficiency of 77.8% with an enhancement of 5.4%.

Figure (2-10): The PTC system of [53].

Allam *et al.* (2022) [35] compared the thermo-hydraulic performance inside a PTR by using two types of helical shift. The first type was a fixed helical shift, while the other type rotated at speeds of 4, 11, and 21 R/min. Their results showed that as the rotation speed increased, the performance increased. The maximum PTC thermal efficiency enhancement and friction factor ratio were 46.5% and 7.7, respectively, at 21 R/min.

Thapa *et al.* (2022) [54] used perforation and winglets in four twisted tapes to improve the PEC inside a PTR. The studied parameters of modified twisted tape were the perforation ratio, twisted ratio, and depth ratio. The experimental results revealed a negative correlation between Nusselt number and friction factor and these parameters, with the highest PEC value being 2.4.

2.4 Numerical and Experimental Studies

Jaramillo *et al.* (2016) [33] performed an investigation to develop a thermodynamic model framework to analyse the PTC thermal performance with a twisted tape turbulator. They studied the effect of twisted ratios and flow rates on PTC thermal efficiency. They found that the PTC thermal efficiency increased as the twisted ratio and the flow rate decreased. In addition, the enhancement factor of PTC thermal efficiency was found to be 9.0% at twisted ratio 1 and flow rate 1 L/min.

Muter and Al-Hadithi (2021) [55] compared the experimental and theoretical results of outlet temperature, useful energy, and thermal efficiency of copper PTR with and without twisted tape. Figure (2-11) shows a PTC system of this study, which had 2 m in length and 3.48 m in width. Water is used as an HTF with a mass flow rate of 0.05 kg/s. The measurements and calculations were made under the climatic conditions in the industrial zone of Fallujah City on September 5 and 6 of 2019. In both PTRs, the results showed good agreement between experimental and theoretical results.

Ozakin (2022) [56] conducted experimental and numerical analyses to maintain the PTC efficiency using semicircular rotating turbulators inside a PTR. The thermal performance was evaluated by varying the number of turbulators at different values of Reynolds number. According to the results, the highest PTC thermal efficiency reached up to 78.2%.

Stanek *et al.* (2023) [57] examined the values of PTC thermal efficiency and PEC using twisted tape inside a PTR. The researchers selected a 33.70 mm tubular stainless steel PTR with an aperture of 1.80 m and placed it in the collector focal point. They chose the thermal oil VP-1 as the HTF. The results indicated that both PTC thermal efficiency and PEC increased as the twisted ratio decreased. The best value of PTC thermal efficiency was reached at 76.3%.

Figure (2-11): The PTC system of [55].

2.5 Summary

The following are the most important conclusions drawn from the literature review:

1) Through research, it was discovered that using turbulators inside the PTR is one of the most important ways to improve its thermo-hydraulic performance.
2) Most numerical studies used ANSYS Fluent in simulation.
3) It is clear from previous studies that there is a weakness in the number of numerical and experimental studies for the suggested turbulators in these studies. The experimental study enhances the validity of the model in the numerical study.
4) In cases that studied the heat transfer enhancement by turbulators, the flow of HTF is turbulent, i.e., the Reynolds number exceeds 3000.

5) There is a lack of data on the performance of cylindrical turbulators inserted in the PTCs. Hence, in this work, the contribution of the cylindrical turbulators inside the PTR is experimentally and numerically investigated.

Table (2-1) lists the summary of the type of study and HTF, studied parameters of turbulators, and important findings in the literature studies.

Table (2-1): Summary of the type of study and HTF, studied parameters of turbulators, and important findings in the literature studies.

Refs.	Study	Type of HTF	Studied parameters of turbulators	Findings
Ghadirijafarbeigloo *et al.* [37]	Numerical	Behran thermal oil: under *Re* (5000-25,000).	Twisted ratio: 2.67, 4.00, and 5.33.	- The highest Nusselt number ratio and friction factor ratio were 3.5 and 4.1, respectively, used the louvered twisted tape with twisted ratio of 2.67.
Chang *et al.* [32]	Numerical	Molten salt: under *Re* (7485-30,553).	- Clearance ratio: 0, 0.2, 0.5, 0.7, and 1.0. - Twisted ratio :2.5, 5.0, 12.5, 15.6, 25.0, and 41.7.	- The maximum Nusselt number ratio and friction factor ratio reached 2.9 and 2.5, respectively.
Zheng *et al.* [38]	Numerical	Water-steam: under *Re* (10,000-90,000).	Four different materials of turbulators: Cu, SiC, Al, and Fe.	- The good materials were Cu, SiC, and Al, whereas they advised against using Fe.
Bellos *et al.* [39]	Numerical	Syltherm 800.	- Length: from 5 to 20	- PTC thermal efficiency is 68.8%

			mm with a step of 5 mm. - Thickness: 2, 4, and 6 mm.	with enhancing of 0.82% compared with a plain tube. - The maximum Nusselt number ratio and friction factor ratio are 1.65 and 2.00, respectively
Bellos *et al.* [40]	Numerical	Syltherm 800: under a constant flow rate of 100 L/min.	- Number: 1, 2, 3, and 4. - Position: left, right, up, down.	- PTC thermal efficiency and Nusselt number improved by 0.66% and 26.9%, respectively.
Chang *et al.* [41]	Numerical	NO_3-KNO_3 composition (molten salt): under *Re* from 10,000 to 30,000.	- Diameter of concentric rod :from $0.1d_i$ to $0.9d_i$ with a step of $0.1d_i$. - Dimensionless eccentricity of eccentric rod: 0.4, 0.6, 0.8, -0.4, -0.6, and -0.8.	- The Nusselt number ratio increased from 1.10 to 7.42 and the PEC from 1.12 to 3.38 as the diameter of concentric rod increased from $0.1d_i$ to $0.9d_i$.
Liu *et al.* [42]	Numerical	Syltherm 800:	- Central angle: from 40º	- The enhancement in Nusselt

		under *Re* from 5000 to 791,000.	to 90º with a step of 10º. - Hollow diameter: from 20 to 50 mm with a step of 10 mm. - Pitch size: from 0.5d_i to 2.0d_i with a step of 0.5d_i.	number was 45-203% and in PTC thermal efficiency was 5.04%. - The maximum value of PEC was 1.33.
Laaraba *et al.* [43]	Numerical	Syltherm 800: under *Re* from 50,000 to 300,000.	- Length: from 5 to 20 mm with a step of 5 mm. - Thickness: from 2 to 8 mm with a step of 2 mm.	- The PTC thermal efficiency was improved by 8.45%.
Abbas *et al.* [34]	Numerical	Water: under *Re* from 2000 to 9000.	Six inclination angles: from 25º to 60º.	- The best inclined angle is 50º. - At this angle, the outlet water temperature was raised by 21% and the maximum PEC was found to be 1.28.
Tanious *et al.* [44]	Numerical	Water: with constant mass flow	- Two lengths of fin: 0.5 and 2.0 mm.	- The optimal case was 2 mm of fin length and 10.5 of PTR

		rate of 0.003 kg/s.	- Rotation rate of PTR: 1 – 21 R/min.	rotation rate. - The increases in the Nusselt number and friction factor were 110% and 81.6%, respectively
Agagna *et al.* [45]	Numerical	Jarysol oil.	- Diameter of pin: 3 - 14 mm. - Number of pin: 2, 3, and 5). - Angles between pins: 45º and 90º. - Axial pitch size: 0.03 - 0.5 m.	- The PEC increased as the number and the axial pitch size of pins decreased. - The Nusselt number and PEC were enhanced by 27.2% and 24.9%, respectively.
Fatouh *et al.* [46]	Numerical	Syltherm 800: under flow rate from 0.1 to 0.4 L/min.	- Length of fin: from 5 to 25 mm with a step of 5 mm. - Thickness of fin: 2, 4, and 6 mm.	- The PTC thermal efficiency was enhanced by 1.36%. - The PEC was recorded at 1.64.

			- Angles between fins: 45º and 90º. - Radii of the rounding fin: 0, 2, 3, and 4 mm.	
Darbari et al. [47]	Numerical	Syltherm 800: under flow rate from 0.047 to 0.233 L/min.	- Position of disc: full, upward, and downward. - Diameter of disc: 0.125d_i, 0.250d_i, and 0.375d_i. - Pitch size od disc: 0.5d_i, 1.0d_i, and 1.5d_i.	- All thermo-hydraulic performances increased as disc's diameter increased and discs pitch size decreased. - The PEC was found to be around 1.6. - The PTC thermal efficiency was improved by around 4%.
Reddy *et al.* [48]	Experimental	Water: under flow rate from 1.67 to 16.7 L/min.	Six different PTR configurations: Unshielded tubular PTR, shielded tubular PTR, bottom porous disc PTR,	- Using an alternative porous disc gave the highest value of Nusselt number, while using an unshielded tubular PTR gave the highest value of friction factor.

			U-shaped bottom porous disc PTR, inclined bottom porous disc PTR, and alternative porous disc PTR.	- The highest range of values for PTC thermal efficiency was 63.9%-66.7%.
Kalidasan *et al.* [49]	Experimental	Water.	Hinged blades had 2 mm drill holes along a straight line with pitch distance of 50 mm.	- The results showed a 14% improvement in PTC thermal efficiency with the modified PTR.
Okour *et al.* [50]	Experimental	Water: under *Re* from 100 to 6000.	Helical coil.	- The experimental findings showed that the peak difference between the outlet and inlet water temperatures was 40.5 °C. - The average PTC thermal efficiency was 64.7%.
Kutbudeen *et al.* [51]	Experimental	Water: under *Re* from 4000 to	- Twisted ratio: 2, 3, and 5.	- The experimental results showed the optimal parameters of the

		18,000.	- Direction: forward and backward.	conical strips used were 3 of twisted ratio and backward flow of direction. - Using optimal case, the Nusselt number and friction factor were enhanced by 2.23% and 1.89%, respectively.
Isravel *et al.* [52]	Experimental	Water: under *Re* from 7000 to 14,300.	Modification of rings attached twisted tape.	- The improvements in PEC values were 19% when rings were attached to conventional twisted tape and 24% when rings were modified.
Naif *et al.* [53]	Experimental	Water: under *Re* from 2000 to 4000.	- Twisted tape with 1.33 of twisted ratio.	- The use of modified PTR produced a PTC thermal efficiency of 77.8% with an enhancement of 5.4%.
Allam *et al.* [35]	Experimental	Water: with flow	- Rotated speed of helical	- The maximum PTC thermal

		rate varied from 0.5 to 2.5 L/min.	shift: 0, 4, 11, and 21 R/min.	efficiency enhancement and friction factor ratio were 46.5% and 7.7, respectively, at 21 R/min.
Thapa *et al.* [54]	Experimental	Air: under *Re* from 3000 to 21,000.	- Twisted tape: 3, 4, and 5. - Depth ratio: 0.1, 0.2, and 0.3. - Perforation ratio: 0.05, 0.15, and 0.25.	- The experimental results revealed a negative correlation between Nusselt number and friction factor and these parameters. - The highest PEC value being 2.4
Jaramillo et al. [33]	Experimental and numerical	Water: under varied flow rate from 1.0 to 6.0 L/min.	- Twisted ratio: 1, 2, 3, 4, and 5.	- The enhancement in PTC thermal efficiency was found to be 9.0% at twisted ratio 1 and flow rate 1 L/min.
Muter et al. [55]	Experimental and numerical	Water: with constant mass flow rate of 0.05 kg/s	- Twisted tape with one twisted ratio of 4.	- There was a good agreement between experimental and theoretical results.
Ozakin et al. [56]	Experimental	None.	- The number of	- The highest PTC thermal

	and numerical		turbulators: 50, 150, and 250.	efficiency reached up to 78.2%.
Stanek et al. [57]	Experimental and numerical	Thermal oil VP-1: with varied mass flow rate from 0.15 to 0.3 kg/s.	- Twisted ratio: 1, 2, and 4.	- Both PTC thermal efficiency and PEC increased as the twisted ratio decreased. - The best value of PTC thermal efficiency was reached at 76.3%.

Chapter Three: Numerical Part

3.1 Introduction

This chapter presents numerical work, including three stages: the first stage is calculating the beam solar radiation using an Excel sheet, the second stage is designing the physical dimensions of a PTC's reflector using the Parabola Calculator tool 2.0, and the third stage is employing computational fluid dynamics (CFD) to generate a three-dimensional (3D) simulation model for the design of the PTR and turbulators. Figure (3-1) shows the flow chart of the three stages.

3.2 Morphological chart

Morphology is a discipline concerned with analysing and describing the structure and configuration of an object or system. The application of this approach is recommended at the initial stages of idea generation. The study encompasses various independent parameters that are associated with the topic at hand, as well as multiple possible solutions to design for each specific function. The present study includes a morphological chart that illustrates the key design functions of the PTC and absorber tube [58]. It should be noted that the chosen parameters are independent. It is advisable to include multiple sub-solutions within the list for each design function. The process of obtaining an appropriate solution involves selecting one sub-solution from each function, combining them, and creating a comprehensive morphological chart that encompasses all fundamental concepts of solutions [58]. Table (3-1) presents the morphological chart of PTC with an absorber tube. The arrow lines depicted in the table indicate the potential solutions.

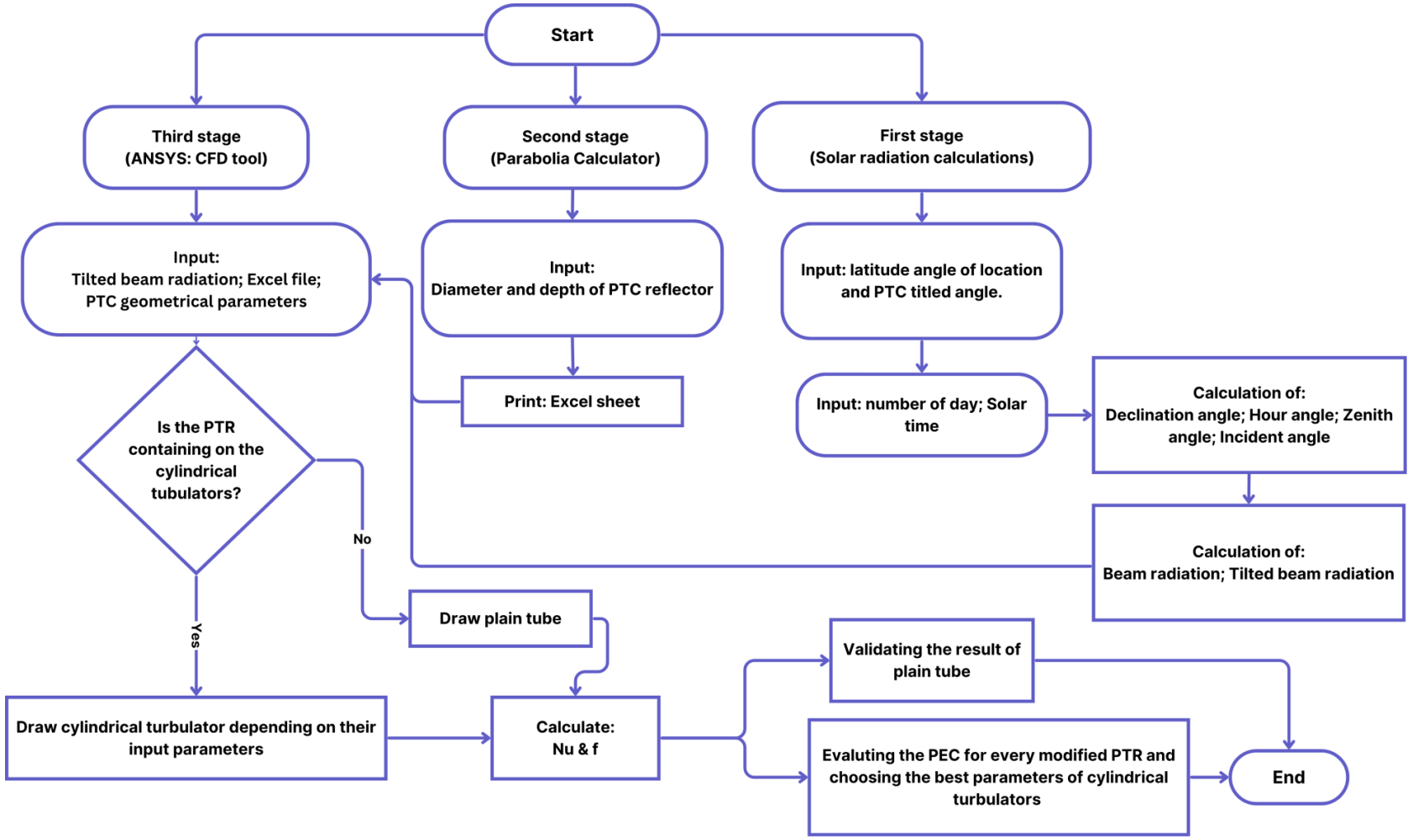

Figure (3-1): Flow chart of the numerical simulation.

Table (3-1): Morphological chart of the PTC and PTR with cylindrical turbulators.

Functions	Options		
Reflector type	1) PTC	TSC	DSC
Material of reflector	2) Aluminium	Mirror	Acrylic
Type of absorber tube	3) Straight tube	U-tube	Corrugated tube
Type of turbulators	Twisted tape	4) Cylindrical Turbulators	Coil wire
Material of PTR	Copper	5) Stainless steel	Aluminium
PTR's maintaining	Several time	Send to factory	6) Self service

The table presents the following major selection possibilities based on a thorough examination of relevant literature:

1) The morphology chart evaluates the use of PTC because of its ability to function well in a wide temperature range (50-400°C) and its resistance to harsh weather conditions like strong winds and dusty environments [59-61].
2) The aluminium is chosen for the fabrication of the reflector due to its light weight, resistance to weather conditions, ease of formation, and good reflectivity of solar radiation [25, 62].
3) When incorporating turbulators to improve heat transfer, straight tubes typically outperform U-tubes or corrugated tubes [61, 63].
4) The goal of the current study is to explore the effect of using a novel design for tabulators (cylindrical turbulators) on the PTC thermal performance and compare the results with available literature of different turbulators types such as twisted tape, coil wire, and fins [34, 39, 43, 52, 64].
5) The receiver tube ought to be constructed using a stainless steel that exhibits low emission and high absorption properties.

6) The option of self-service is selected as PTR maintenance.

3.3 The beam solar radiation

Since there was no experimental device available to measure the beam solar radiation falling on the PTC system at the work location, the study considered the theoretical calculation to estimate the solar radiation values. Solar radiation is a continuous, synchronous flow of energy in all directions outward from the sun. There are two categories of solar radiation to be calculated: extraterrestrial solar radiation and terrestrial solar radiation.

3.1.1 Extraterrestrial Solar Radiation

The extraterrestrial solar radiation (I_0) represents the solar radiation that reaches the outside of Earth's atmosphere. Several factors, including direction and distance, affect the inverse square law, which governs variation in the extraterrestrial solar radiation, as illustrated in the following equation [50, 65]:

$$I_{\mathrm{O}} = I_{sc}\left[\frac{\bar{D}_{S-E}}{D_{S-E}}\right]^2 \qquad \textbf{(3-1)}$$

where I_{sc} is defined as the energy from the sun per unit of time received on a unit area of surface perpendicular to the direction of propagation of the radiation at mean Earth-Sun distance outside the atmosphere that usually has a value of 1367 W/m^2 as shown in Fig. (3-2). The $D_{S\text{-}E}$ is the mean distance between the sun and earth (m), and the $D_{S\text{-}E}$ is the actually distance between the sun and earth (m). The $D_{S\text{-}E}$ changes with the Earth's orbital position around the sun, so it is related to the days of the year as shown in Fig. (3-3).

Typically, the extraterrestrial solar radiation is calculated from the following empirical equation [65, 66]:

$$I_0 = I_{sc}\left[1+0.033\cos(\frac{360}{365}N_{day})\right] \qquad \textbf{(3-2)}$$

where the N_{day} represents the number of days in the year ($1 \le N_{day} \le 365$).

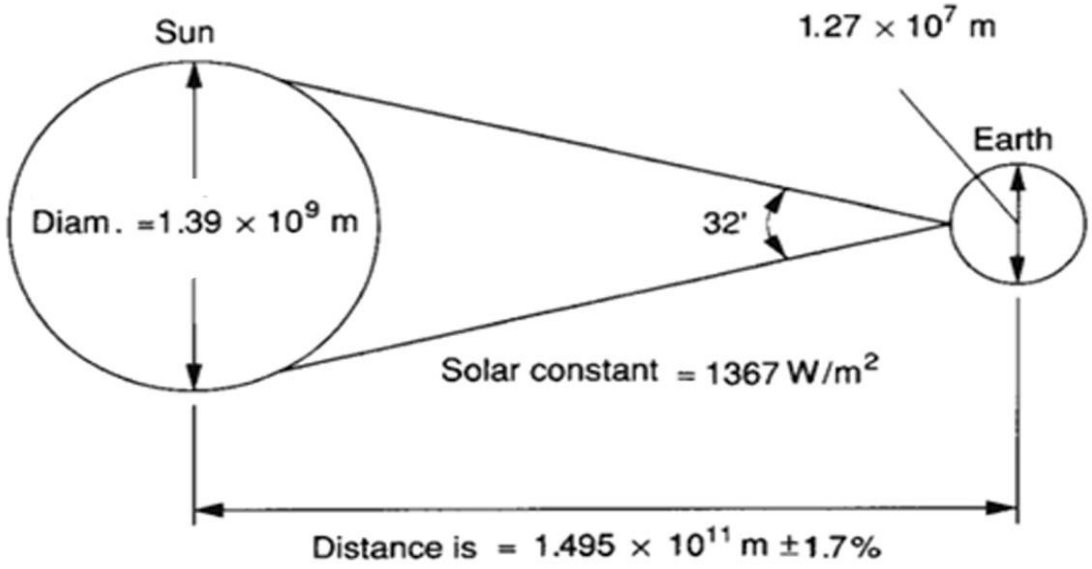

Figure (3-2): Sun-earth geometry [65].

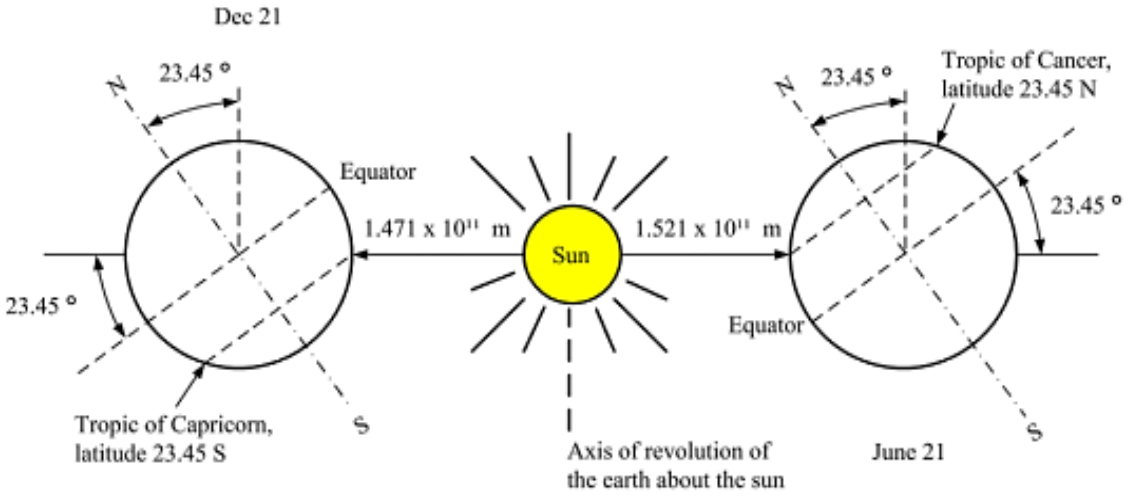

Figure (3-3): Motion of the earth around the sun [67].

3.1.2 Terrestrial Solar Radiation

The terrestrial solar radiation represents the quantity of solar energy that reaches the earth's surface. It is also called the global or total amount of

radiation incident on the earth's surface that represents the summation of beam radiation (I_b) and diffuse radiation (I_d). In this study, the beam radiation is focused because the upper and lower surfaces of PTR receive only this type of radiation [50]. The beam radiation at normal incidence can be calculated from [50, 65]:

$$I_b = I_0\left[a + b\exp(-\frac{c}{\cos\theta_z})\right] \quad \textbf{(3-3)}$$

where:

$$a = 0.94\left[0.4237 - 0.00821(6 - AL)^2\right] \quad \textbf{(3-4)}$$

$$b = 0.98\left[0.5055 + 0.00595(6.5 - AL)^2\right] \quad \textbf{(3-5)}$$

$$c = 1.02\left[0.2711 + 0.01858(2.5 - AL)^2\right] \quad \textbf{(3-6)}$$

Where AL is the altitude of the location above mean sea level (km) that can be calculated by using a GPS device (which equals 0.033 km for College of Engineering/Al-Mussaib).

The beam radiation on a titled surface (such as PTC) is related to incident angle (θ_i) and calculated from [50, 65]:

$$I_{bt} = I_b\cos(\theta_i) \quad \textbf{(3-7)}$$

3.1.3 Sun-Earth Angles

The solar-earth angles are important angles to calculate the beam radiation, which are given as follows:

3.3.1.1 Incident angle

The incident angle of beam radiation on any surface can be found from [65]:

$$\cos\theta_i = \sin\phi\sin\delta\cos\beta - \cos\phi\sin\delta\sin\beta\cos\gamma + \cos\phi\cos\delta\cos\beta\cos\omega + \sin\phi\cos\delta\sin\beta\cos\omega\cos\gamma + \cos\delta\sin\beta\sin\omega\sin\gamma \quad \textbf{(3-8)}$$

3.3.1.2 Latitude angle

It represents the angular location north or south of the equator, with the north position (-90°≤ϕ≤+90°) as shown in Fig. (3-4).

3.3.1.3 Declination Angle

The declination angle represents the angular position of the sun at solar noon (i.e., when the sun is on the local meridian) with respect to the plane of the equator, north-positive; $-23.45° \le \delta \le 23.45°$ as shown in Fig. (3-3). Cooper found the approximate equation to calculate the declination angle as follows [68]:

$$\delta = 23.45\sin(\frac{360}{365} N_{day}) \quad \textbf{(3-9)}$$

3.3.1.4 Titled angle

The titled angle (β) is the angle between the plane of the surface and the horizontal (0°≤β≤180°). If β>90° that means the surface has a downward-facing component.

3.3.1.5 Azimuth angle

The deviation of the projection on a horizontal plane of the normal to the surface from the local meridian is represented by the azimuth angle (γ). The value of this angle equals zero because the PTC system is orientated to the south. Hence, Eq. (3-8) becomes:

$$\cos\theta_i = \sin\phi\sin\delta\cos\beta - \cos\phi\sin\delta\sin\beta + \cos\phi\cos\delta\cos\beta\cos\omega + \sin\phi\cos\delta\sin\beta\cos\omega \quad \textbf{(3-10)}$$

3.3.1.6 Hour Angle

The hour angle (ω) in Eq. (3-8) represents the angular displacement of the sun east or west of the local meridian due to the rotation of the earth on its axis at 15° per hour (as shown in Fig. (3-4)); morning negative, afternoon positive. The hour angle can be calculated from [65]:

$$\omega = 15(Ti_{loc} - 12) \quad \textbf{(3-11)}$$

where Ti_{loc} represents the solar time in hours.

3.3.1.7 Zenith Angle

The zenith angle (θ_z) in Eq. (3-3) depends on many angles, such as altitude angle (ϕ), declination angle (δ), and hour angle (ω). The zenith angle can be given as [65]:

$$\cos\theta_z = \cos\phi\cos\delta\cos\omega + \sin\phi\sin\delta \qquad \textbf{(3-12)}$$

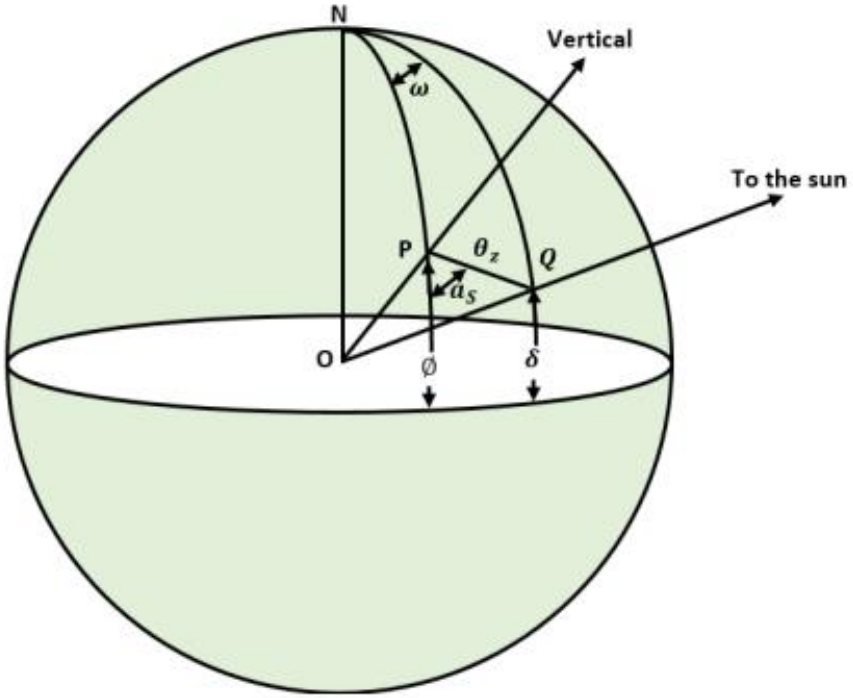

Figure (3-4): The sun-earth angles [69].

3.4 Parabola Calculator Software

A literature review indicates that the PTC provides a high concentration level of solar radiation. The precision of the PTC reflector is a crucial component that impacts a PTC's performance and efficiency compared to the PTR. The capacity to concentrate solar radiation and the resistance to wind force are important considerations in PTC's reflector design. Therefore, it is crucial to carefully examine the parabolic curve to ensure that the focal line reflects the most incoming radiation. The current study used an aluminium plate to fabricate a reflector of PTC with a length of 2 m and a width of 1 m. The equation of a parabolic curve (y) that is used by Parabola Calculator software 2.0 is given as [70-72]:

$$y = \frac{x^2}{4 f_L} \qquad \textbf{(3-13)}$$

Many researchers use the Parabola Calculator software to draw the PTC's arc. The aperture's diameter (W) and arc depth (De_{arc}) were the dimensions entered into the Parabola Calculator software. Table (3-2) lists the dimensions of the PTC reflector, which were entered into the Parabola Calculator software in order to draw this reflector as shown in Fig. (3-5).

Table (3-2): Reflector dimensions of PTC entering into Parabola Calculator software.

Item	Value	Units
Diameter of aperture	100	cm
Depth	25	cm

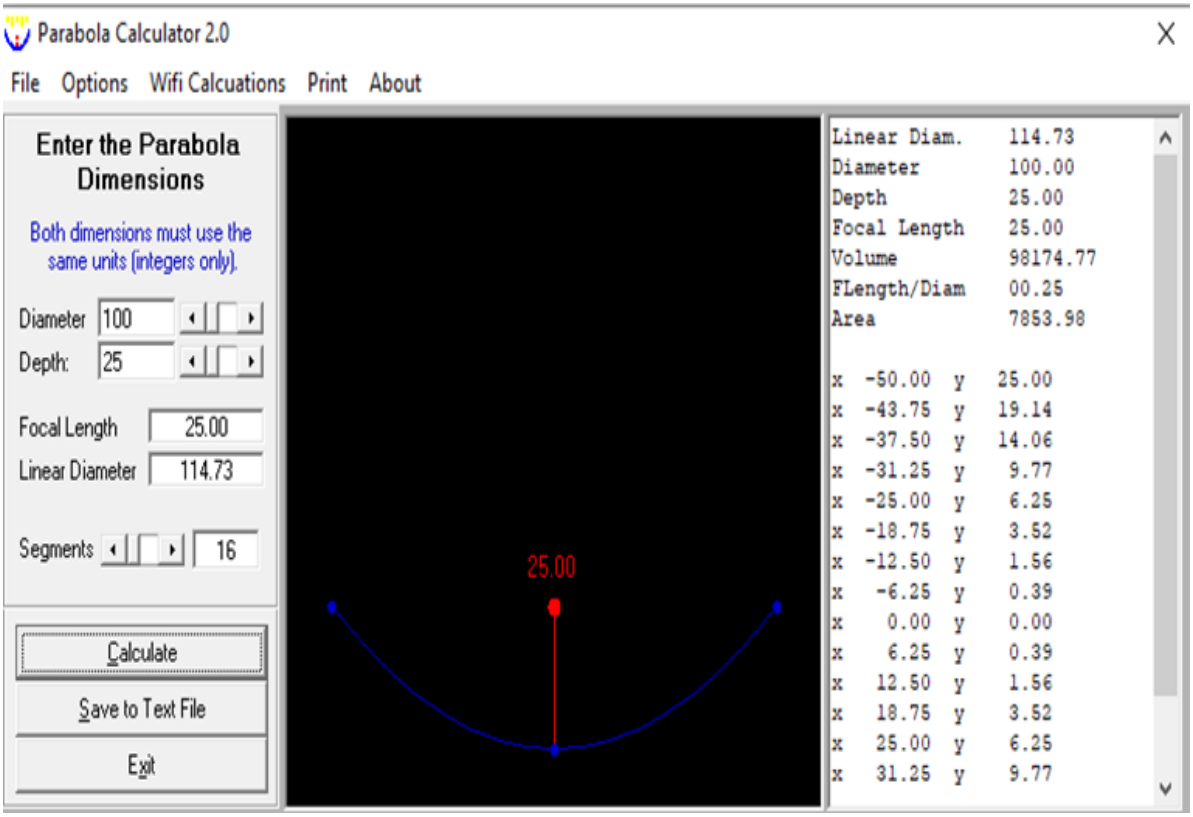

Figure (3-5): The dimensions of the PTC reflector in the Parabola Calculator software 2.0.

The output parameters from this software are the focal length (the distance from the focal point to the vertex) and linear diameter (arc length). The focal length (f_L) can be calculated from [73]:

$$f_L = \left(\frac{W}{4\sqrt{De_{arc}}} \right)^2 \quad \textbf{(3-14)}$$

The arc length (L_{arc}) is based on the rim angle (θ_r) and the focal length; it can be estimated from the following equation [74]:

$$L_{arc} = 2 f_L \left[(\sec(0.5\theta_r) \tan(0.5\theta_r)) + \ln(\sec(0.5\theta_r) \tan(0.5\theta_r)) \right] \quad \textbf{(3-15)}$$

To increase PTC efficiency, the rim angle is chosen to be 90º [13]. Hence, in this study the parabolic curve (y) (in Eq. (3-13)) will be:

$$y = 0.01x^2 \quad \textbf{(3-16)}$$

The rim angle in Eq. (3-15) corresponds to beam radiation reflected from the outer rim of the concentrator and is related to the rim radius and width aperture (W) as shown in Fig. (3-6), which can be calculated as follows [6, 65]:

$$\theta_r = \sin^{-1}\left(\frac{W}{2r_r}\right) \qquad \textbf{(3-17)}$$

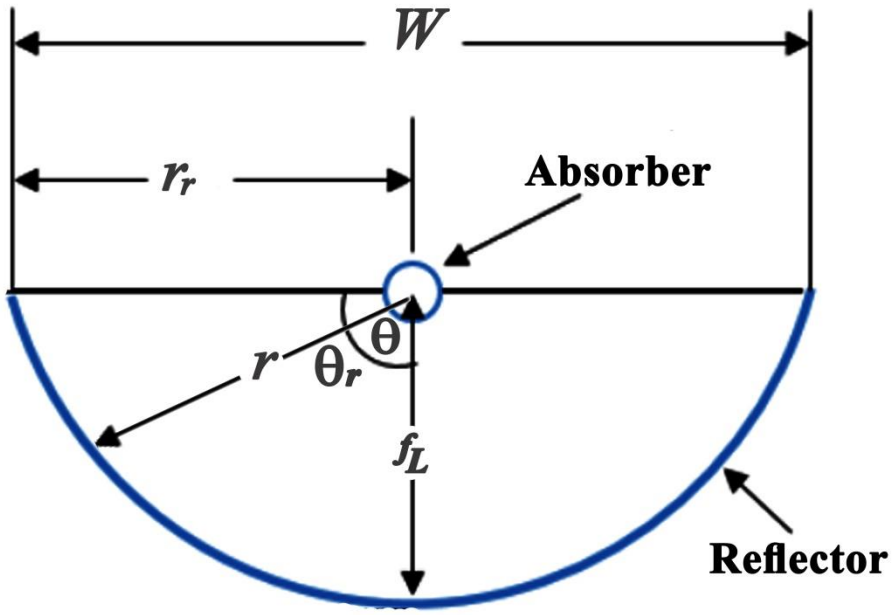

Figure (3-6): Basic design parameters of the PTC with image dimensions for a linear concentrator.

According to Fig. (3-6), the radius of a parabola at an arbitrary location is defined as mirror radius (r). The maximum value of mirror radius occurs at its outer rim and is fittingly called the rim radius (r_r) or parabolic radius. The mirror radius at any point on the parabolic reflector, may be found using the following formula [65]:

$$r = \frac{2 f_L}{1 + \cos\theta} \qquad \textbf{(3-18)}$$

where θ is the angle that changes from 0 to the rim angle between the reflection of the beam at the focus point and the collector axis; hence, the radius likewise changes from the focal length to the rim radius. For perfectly positioned specular reflectors, we can use trigonometry to determine the

diameter of the tube required to intercept the entire beam solar radiation. It is worth noting this diameter is known as [65]:

$$d_o = 2r_r \sin\theta_i \qquad \textbf{(3-19)}$$

3.5 The Numerical Study

The numerical study was performed using the ANSYS Fluent R-20 software. It should be noted that numerous literature studies, primarily focusing on PTC, have also utilised the present simulation instrument [32, 34, 39, 43, 75-77]. The ANSYS contains many analysis systems, but the related system with this study is fluid flow analysis using the Fluent solver.

3.5.1 Geometry Design Stage

The first stage in the numerical study is the geometry design stage of PTC. In this stage the output parameters (focal length and linear diameter) of the Parabola Calculator software (Excel sheet) and the characteristics of the parts specifications of the PTC (Table (3-3)) were input to draw the PTC and its PTR. Figure (3-7) shows the geometric design of the PTC after introducing these parameters.

The cylindrical turbulators with different lengths (l), thicknesses (t), and numbers (N) were inserted inside the PTR. These lengths are 10, 20, 30, 40, and 50 mm; thicknesses are 1, 2, 3, and 4 mm; and numbers are 5, 10, 15, and 20 cylindrical turbulators. Table (3-4) lists the characteristics of the parts specifications of the cylindrical turbulators that are input into the CFD tool. Figure (3-8) shows the general case of the cylindrical turbulators, and Fig. (3-9) illustrates all the examined cases of cylindrical turbulator tubes and the plain tube.

Table (3-3): Characteristics of parts specifications of the PTC (geometry design stage).

Item	Value / Type	Units
Collector length (L)	200	cm
Collector material	Aluminium	=
PTR length	200	cm
External PTR diameter (d_o)	5.1	cm
Internal PTR diameter (d_i)	4.7	cm
PTR material	Stainless steel	=

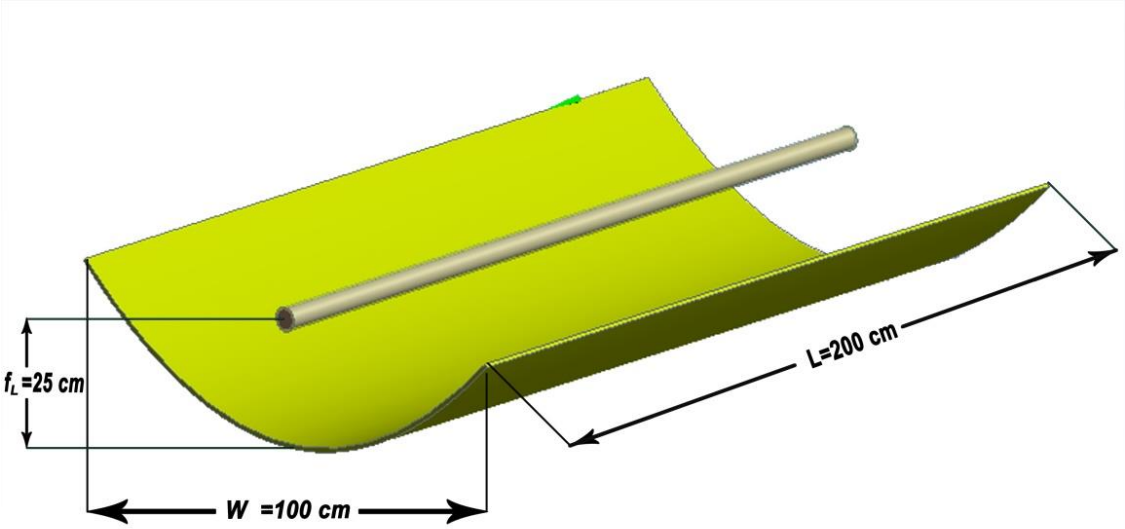

Figure (3-7): Geometry design of the PTC.

Table (3-4): Characteristics of parts specifications of the cylindrical turbulators.

Item	Value / Type	Units
Central round rod length	200	cm
Central round rod diameter	1	cm
Cylindrical turbulators diameter	4.7	cm
Cylindrical turbulators material	Stainless steel	=

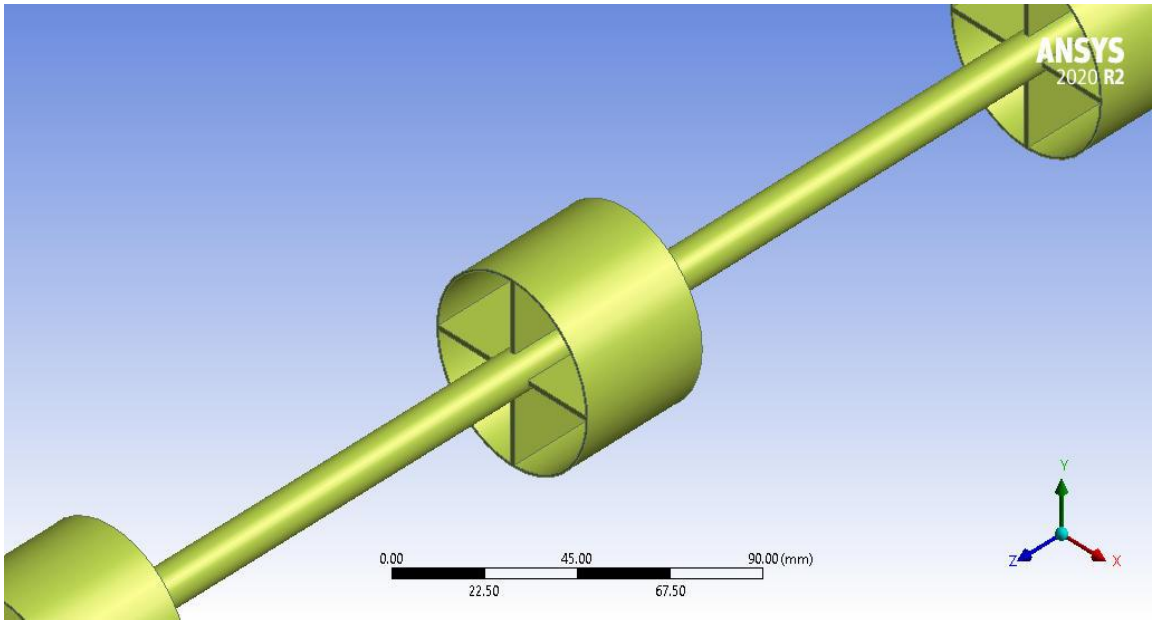

Figure (3-8): General case of the cylindrical turbulators.

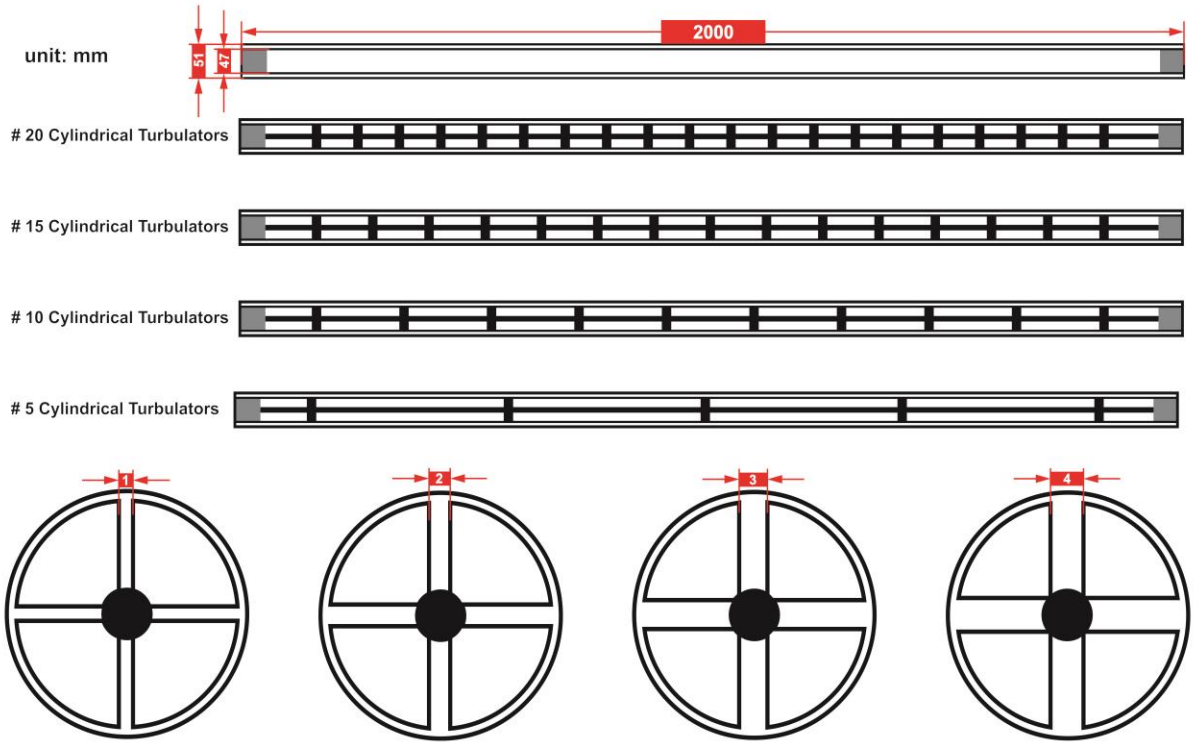

Figure (3-9): All the examined cylindrical turbulators tubes and the plain tube.

3.5.2 Mesh Stage

The mesh of the model (second stage) is the most active part of the fluid flow system; its accuracy and quality depend on the meshing technique. Once

meshing is established, the equations of fluid flow can be solved in the grid cells or in the elements created by the mesh. In this study, the plain tube and the cylindrical turbulator tubes were meshed in this stage. The hexahedral method was used to mesh the first tube (plain tube), whereas the tetrahedron method was used to mesh the other tubes because this method is more suitable for meshing complex and unstructured shapes such as cylindrical turbulators. In ANSYS, mesh quality depends on the skewness, aspect ratio, and orthogonal quality. In general, minimum orthogonal quality should be more than 0.1, and maximum skewness is recommended to be less than 0.95 (see Fig. (3-10)) [78]. However, these values varied depending on the location and number of cells, which varied according to the shapes of the models.

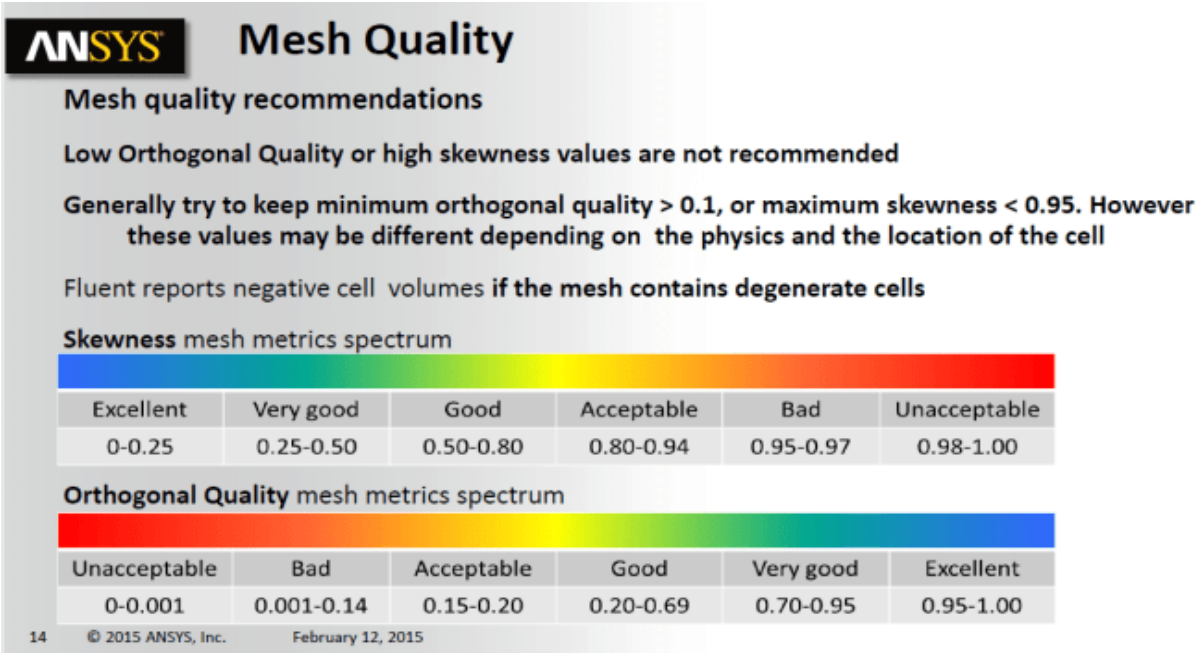

Figure (3-10): Requirements of meshing quality [78].

3.5.3 Solution Stage

Firstly, in the third stage of the fluent flow system in ANSYS Fluent (solution stage), some assumptions are applied as follows:

- The inlet temperature of HTF is selected to be 300 K.

- The beam solar radiation is selected to be 1000 W/m^2 [39, 79-81].
- The reflectance of the aluminium reflector is 83%, the absorbance of the stainless steel PTR is 96%, and the emittance of the stainless steel PTR is given by [82]:

$$\varepsilon = 0.05599 + 1.039\times10^{-4}\times T_w + 2.249\times10^{-7}\times T_w^2 \quad \textbf{(3-20)}$$

- The thermophysical properties of the HTF (water) (the density (ρ_f), the dynamic viscosity (μ_f), and the thermal conductivity (k_f)) are calculated from the average temperature of the HTF as listed in Table (3-5).
- The thermophysical material properties of the PTR (stainless steel) and the cylindrical turbulators (stainless steel) are presented in Table (3-6).

Table (3-5): Thermophysical properties of HTF [75].

Properties	Equation	Units
Density (ρ_f)	$=863+1.21T_{ave}-0.00257T_{ave}^2$	kg/m^3
Dynamic viscosity (μ_f)	$=0.0007(315/T_{ave})^{5.5}$	N.s/m^2
Thermal conductivity (k_f)	$=0.375+\left(8.84\times10^{-4}\right)T_{ave}$	W/m.ºC

Table (3-6): Thermophysical material properties of the PTR and the cylindrical turbulators [83].

Properties	Values	Units
Density (ρ_w)	8030	kg/m^3
Dynamic viscosity (μ_w)	502.48	J/kg.ºC
Thermal conductivity (k_w)	16.27	W/m.ºC

3.5.3.1 Nusselt Number

The Nusselt number is the ratio of convective to conductive heat transfer across the PTR that can be calculated as [15, 46, 76, 84]:

$$Nu = \left(\frac{d_i}{k_f} \right) h \qquad \textbf{(3-21)}$$

Where d_i is the inner diameter of the PTR (m) and h is the heat transfer coefficient between the PTR and the HTF, which can be calculated from [46, 76]:

$$h = \frac{Q_{use}}{(\overline{T}_w - T_{ave}) A_w} \qquad \textbf{(3-22)}$$

Where T_w is the average PTR temperature (ºC), which can be known by the CFD tool, and T_{ave} is the average temperature of the HTF (ºC), which can be calculated from [46]:

$$T_{ave} = \frac{(T_{fo} + T_{fi})}{2} \qquad \textbf{(3-23)}$$

The useful energy (Q_{use}) in Eq. (3-22) will be calculated from the outlet HTF temperature that is obtained from the CFD tool; hence, the useful energy is [34, 46, 76]:

$$Q_{use} = \dot{m} c_p (T_{fo} - T_{fi}) \qquad \textbf{(3-24)}$$

where $\dot{m}$ is the mass flow rate of the HTF (kg/s), c_p is the specific heat capacity of the HTF (J/kg.ºC), T_{fo} is the outlet HTF temperature (ºC), and T_{fi} is the inlet HTF temperature (ºC).

Finally, the area of the PTR wall (A_w) is given as follows [65]:

$$A_w = \pi d_o L \qquad \textbf{(3-25)}$$

3.5.3.2 Friction Factor

The friction factor can be defined in terms of the pressure drop and the HTF mass velocity and can be calculated for a fully developed flow from [14, 76, 84]:

$$f = \left(\frac{2d_i}{L\rho_f u_f^2} \right) \Delta p \qquad \textbf{(3-26)}$$

where u_f is the mean HTF velocity (m/s) and Δp is the pressure drop inside the PTR (Ps) that can be found from the CFD tool.

3.5.3.3 Reynolds Number

The flow in a PTR can be laminar or turbulent, depending on the value of the Reynolds number (*Re*). Fluid flow is streamlined and thus laminar at low velocities, but turns turbulent as the velocities are increased beyond critical values. The *Re* is defined as the ratio of inertial forces to viscous forces within a fluid that is subjected to relative internal movement due to different fluid velocities. Inside circular tubes the *Re* of water is given as [85]:

$$\mathrm{Re} = \left(\frac{4}{\pi \mu_f d_i} \right) \dot{m} \qquad \textbf{(3-27)}$$

According to the value of *Re*, the flow type can be predicted (laminar, transitional, and turbulent flow) as the following conditions [85, 86]:

$Re<2300$	laminar flow
$2300 \le Re \le 10000$	transitional flow
$Re>10000$	turbulent flow

3.5.3.4 The Heat Losses

The heat loss from PTR undergoes three distinct heat transfer processes: convection, conduction, and radiation. Convection heat transfer is heat transfer between two areas through fluid movement. The fluid properties, container geometry, and surface roughness significantly influence fluid transmission. Furthermore, the wind's velocity has a significant impact on heat transfer via convection. Thermal energy moves from a higher-temperature wall to a lower-temperature wall through a process known as conduction heat transfer. Heat loss through conduction occurs in the PTR's wall. Radiation heat transfer can occur through reflection, absorption, or transmission, resulting in the exchange of radiant energy. Figure (3-11) shows the cross-section scheme of the PTR for the heat transfer mode.

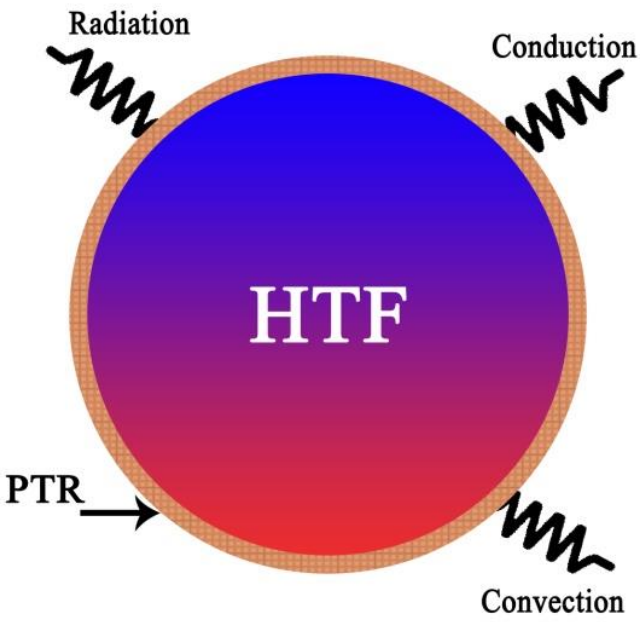

Figure (3-11): Cross-sectional scheme of heat losses from the PTR.

Theoretically, the overall heat loss from PTR to the surroundings (Q_{loss}) can be calculated from:

$$Q_{loss} = Q_{conv.} + Q_{cond.} + Q_{rad.} \quad \textbf{(3-28)}$$

3.5.3.4.1 Convection heat loss

Convection is the heat transfer between the body surface and adjacent motion fluid (gas or liquid). When the fluid motion is natural, the convection is called free (natural) convection. On the other hand, forced convection means that the fluid is forced to flow by external forces like wind, pump, or fan. In both types, the heat loss by convection can be found from [85]:

$$Q_{conv.} = h_{w-a} A_w (T_w - T_a) \quad \textbf{(3-29)}$$

where A_w is the area of PTR's surface (m^2), T_a is the ambient air temperature (^oC), and $h_{w\text{-}a}$ is the air convection heat transfer coefficient ($W/m^2.^oC$), which can be found from [85]:

$$h_{w-a} = \left(\frac{k_a}{d_o} \right) Nu_a \quad \textbf{(3-30)}$$

where k_a is the thermal conductivity of air ($W/m.^oC$) (the properties of air can be estimated from the air table (Appendix A)), and Nu_a represents the Nusselt number of air that can be calculated from [87]:

$$Nu_a = C\,\mathrm{Re}_a^m\,\mathrm{Pr}^{(1/3)} \quad \textbf{(3-31)}$$

where C and m are constants their values listed in Table (3-7).

Table (3-7): Constants for use with Eq. (3-28) [87].

Re	C	m
0.4 – 4	0.989	0.33
4 – 40	0.911	0.385
40 – 4000	0.683	0.466
4000 – 40000	0.193	0.618
40000 – 400000	0.0266	0.805

The Reynolds number of air can be estimated from [87]:

$$\mathrm{Re}_a = \left(\frac{\rho_a u_a}{\mu_a} \right) d_o \qquad \textbf{(3-32)}$$

Or

$$\mathrm{Re}_a = \left(\frac{u_a}{\upsilon_a} \right) d_o \qquad \textbf{(3-33)}$$

where ρ_a, u_a, μ_a, and υ_a are density, velocity, viscosity, and kinetic viscosity of air. These properties of air can be estimated from Appendix A based on $T_{ave,w\text{-}a}$ that is given as [87]:

$$T_{ave,w-a} = \frac{T_w + T_a}{2} \qquad \textbf{(3-34)}$$

The area of PTR's surface is [88]:

$$A_w = \pi L d_o \qquad \textbf{(3-35)}$$

3.5.3.4.2 Conduction heat loss

Conduction heat loss is the energy converted from more surfaces of similar or different substances. The conduction heat loss can be found from [85]:

$$Q_{cond} = -k_w A_w (T_{wo} - T_{wi}) \qquad \textbf{(3-36)}$$

where T_{wo} and T_{wi} are the temperatures of the outer and inner walls of the PTR, respectively.

3.5.3.4.3 Radiation heat loss

Each body emits thermal radiation when its temperature rises above absolute zero. The Stefan-Boltzmann law expresses the maximum radiation rate that a body surface can emit. Consequently, we can express the radiation heat loss as follows [85]:

$$Q_{rad} = \sigma \varepsilon_w A_w (T_w^4 - T_a^4) \quad \textbf{(3-37)}$$

where σ represents the Stefan-Boltzmann constant (its value is 5.67×10^{-8} $W/m^2.K^4$).

3.5.3.5 Performance Evaluation Criteria

Finally, a common method for determining the thermal enhancement of the flow is by comparing the heat transfer coefficient between each tube and the plain tube. However, this method fails to account for the critical pressure drops that are essential to the system's sustainability when calculating this parameter directly. So, this factor is modified in order to compare the newly designed tubes with the plain tubes under the same operating conditions. The performance evaluation criteria (PEC) is given as [57, 84]:

$$PEC = \frac{\Delta Nu}{\Delta f^{1/3}} \quad \textbf{(3-38)}$$

where ΔNu and Δf are the Nusselt number ratio and the friction factor ratio that can be calculated as [57, 84]:

$$\Delta Nu = \frac{Nu}{Nu_{plain}} \quad \textbf{(3-39)}$$

$$\Delta f = \frac{f}{f_{plain}} \quad \textbf{(3-40)}$$

where Nu_{plain} and f_{plain} are the Nusselt number and the friction factor in the plain tube case, respectively.

3.5.3.6 Validation Equations

The theoretical values for the Nusselt number (Nu_{th}) and friction factor (f_{th}) for the validation purposes of the designed model (plain tube) can be estimated from the empirical correlation of Dittus-Boelter for the Nusselt number in a smooth surface tube with the turbulent flow as follows [89]:

$$Nu_{th} = 0.023\,\mathrm{Re}^{0.8}\,\mathrm{Pr}^{0.4} \qquad \textbf{(3-41)}$$

$$f_{th} = \frac{0.184}{\mathrm{Re}^{0.2}} \qquad \textbf{(3-42)}$$

where *Pr* is the Prandtl number.

Chapter Four: Experimental Work

4.1 Introduction

The main goal of the experimental work is to investigate the thermo-hydraulic performance inside the PTR tubes with cylindrical turbulators and to compare the experimental results with the numerical results. The College of Engineering/Al-Musayab, Babylon (32.77° N, 44.29° W), hosted the experimental study. The experiments were carried out from October 2023 to May 2024 during the daytime.

The PTC model for the concentration of solar radiation has been fabricated to generate hot water. This study's experimental setup comprises locally fabricated components of a single PTC, boasting a total aperture area of 2.00 m^2. The HTF gains heat gradually as it flows through the PTR in a sequential manner. In addition, the PTC is continuously orientated directly toward the beam solar radiation to achieve maximum efficiency. The PTC system mainly consists of a support structure, reflector, PTR, cylindrical turbulators, and other accessories.

4.2 The Support Structure

The support structure for this model contains two main mechanical groups: stationary (metal support frame) and moving (manual tracking) bases.

4.2.1 The Stationary Base

The stationary structure of this model is made of a rectangular steel tube with a diameter of 6.35 cm, a length of 220 cm, and a width of 70 cm, welded together in the form of a movable pyramid frame by wheels welded from its lower end, as shown in Fig. (4-1).

Figure (4-1): The support structure of the PTC.

4.2.2 The Moving Base

The moving structure of this model consists of two parts: the base and the reflector. The base is made from square steel pipes because of its high bending and shear stress. Square steel pipes have a diameter of 2.54 cm, a height of 25 cm, and a width of 100 cm. Aluminium sheets of size 100×200 cm with 0.2 cm thickness placed longitudinally on the PTC frame were used to form the reflector of the PTC due to their light weight, resistance to weather conditions, ease of formation, and good reflectivity of solar radiation, as shown in Fig. (4-2). An aluminium sheet plate with a thickness of 0.2 cm was fixed with sixteen bolts over the structure of the PTC.

According to the dimension obtained from Eqs. (3-14) and (3-15) with a rim angle of 90°, one rib model was fabricated as a template for the other pieces. The rib width and depth calculated from these equations were 114.7 cm and 25 cm, respectively. Then, the four ribs are connected using two

straight hollow square tubes with a length of 200 cm to form the PTC structure. In order to efficiently benefit from most of the solar reflected radiation, the sun rays must be highly concentrated on the PTR.

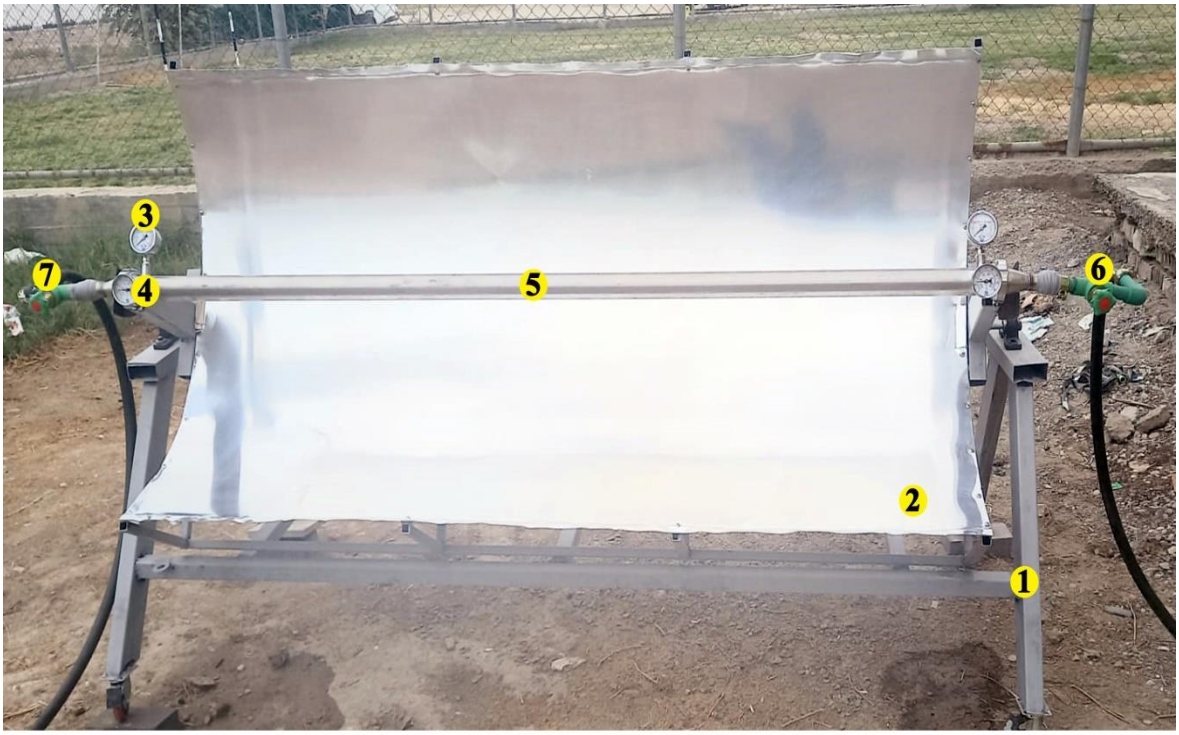

(1) Fixed frame.
(2) Reflector.
(3) Preasure gauge.
(4) Temperature gauge.
(5) PTR.
(6) & (7) Menaul valves.

Figure (4-2): The PTC system.

4.3 The PTR

Several design factors are considered prior to the material selection of the PTR to be used. The most important factors are the components of the PTR's material that must not react chemically with the water passing through it; the PTR's material must withstand the external conditions surrounding the PTC system location; and the PTR's material must withstand water temperatures that reach higher than 50°C. In addition, to ascertain the appropriate material and thickness for the tube, it is important to possess an

understanding of the maximum pressure of the system. As a result, stainless steel was used in this experiment to effectively counteract chemical reactions, survive the effects of weathering, and maintain its structural integrity at high temperatures, as seen in Fig. (4-3). The selection of the size of the PTR was based on the parameters provided in Table (3-3).

Figure (4-3): Photograph of the PTR and cylindrical turbulators.

4.4 Cylindrical Turbulators

The technical specifications for the cylindrical turbulators used in this study are given in Table (3-4). Figure (4-4) shows the process of inserting the cylindrical turbulators inside the PTR.

Figure (4-4): Cylindrical turbulators inside the PTR.

4.5 Other Accessories

4.5.1 Circulation pump

The closed cycle of the SDU uses a model (XPS25-8-180) pump with different speeds as shown in Fig. (4-5). The lowest speed is utilised with a current of 0.2 A and a power of 45 W. The system operates on a 240V/50Hz electrical connection, with a maximum flow rate of 834 L/min and a maximum head of 4 m. The maximum ambient temperature is 40ºC, which allows HTF temperatures up to 110°C, and the maximum pressure is 10 bars.

4.5.2 Working Fluid Flow Meter

The (LZM-Z) type liquid flow meter was used to calculate the amount of liquid flow (water) between the water source and the PTR. The measurement rate ranges from 0.38 to 4 L/min, as shown in Fig. (4-6).

Figure (4-5): Circulation pump.

Figure (4-6): Flow meter image.

4.5.3 Temperature Gauges

The GTS412 temperature gauges are suitable for use in numerous applications, such as boilers and heating systems, as well as machinery manufacturing. A dual-function thermowell equips them to safeguard their stem and simplify future replacements. The specifications of the GTS412 include a dial size of 63 mm, a stem length of 50 mm (a bi-metal sensor copper alloy stem), and the ability to measure temperatures up to 160°C, as shown in Fig. (4-7).

4.5.4 Pressure Gauges

The Gesa (EN 837-1) type pressure gauges were used to evaluate the pressure drop between the inlet and outlet zones of the PTR. These pressure gauges are specially designed for difficult operating conditions, such as vibrations or rapid pressure changes, and are suitable for use in systems with low viscosity (water). Their technical data include a 60 mm dial diameter, a bar range of 0 to 10 bar (0–150 Ps) as shown in Fig. (4-8).

Figure (4-7): GTS412 temperature gauge.

Figure (4-8): Gesa (EN 837-1) pressure gauge.

4.5.5 Digital Clamp Multi-meter

The digital clamp multi-meter was used to measure the variance in voltage and current in the ranges of 110-300 V and 2-400 A. The clamp multi-meter that was used in this study is ST201, as shown in Fig. (4-9).

Figure (4-9): Digital clamp multi-meter.

4.6 PTC Thermal Efficiency

There are two ways to calculate the thermal efficiency of the PTC: the first way is by dividing the useful heat from the PTC by the total incident solar radiation [15, 43, 46, 65]:

$$\eta_{the} = \frac{Q_{use}}{Q_{inc}} \quad \textbf{(4-1)}$$

The total incident solar radiation (Q_{inc}) is the product of aperture area (A_c) and the titled beam radiation (I_{bt}) [39, 46, 79]:

$$Q_{inc} = A_c I_{bt} \quad \textbf{(4-2)}$$

By substituting Eqs. (3-24) and (4-2) into Eq. (4-1) will be gated on:

$$\eta_{the} = \frac{\dot{m} c_p (T_{fo} - T_{fi})}{A_c I_{bt}} \quad \textbf{(4-3)}$$

where $\dot{m}$, c_p, T_{fo}, and T_{fi} represent mass flow rate, specific heat capacity, outlet HTF temperature, and inlet HTF temperature, respectively.

The second way to calculate the thermal efficiency of the PTC that is operated under steady-state conditions may be defined as follows according to ASHRAE Standard 93 [90]:

$$\eta_{the} = F_R \eta_{opt} - \frac{F_R U_L}{C_R}\left(\frac{T_{fi} - T_a}{I_{bt}}\right) \quad \textbf{(4-4)}$$

where F_R is the heat removal factor, η_{opt} is the optical efficiency of PTC, U_L is the thermal loss coefficient, and C_R represents the concentration ratio, which is defined as the ratio of the aperture area (A_c) to the PTR area (A_w) [57]:

$$C_R = \frac{A_c}{A_w} \quad \textbf{(4-7)}$$

The η_{opt} includes many important concentrators' optical properties (aperture reflectance (τ_c), PTR surface absorption (α_w), and End-effect loss (X_{end})) [7]:

$$\eta_{opt} = \tau_c \alpha_r K(\theta_i) X_{end} \quad \textbf{(4-8)}$$

The last term in Eq. (4-8) is typically important for long lengths of the PTR, so, in this study for shorter strings the end losses may be negligible [7].

The angle of incidence can also correlate with other losses from the collector. The effects of errors in the concentrating collector, tracking errors, and errors in the displacement of the absorber from the focus all lead to enlarged or shifted images and affect the intercept factor. The incidence angle modifier ($K(\theta_i)$), an empirical fit to experimental data for a specific collector type, can account for these errors. The incidence angle modifier for the collector is [91]:

$$K(\theta_i) = \cos\theta_i + 0.000884\theta_i - 0.00005369\theta_i^2 \quad \textbf{(4-9)}$$

The F_R in Eq. (4-4) represents the ratio of the actual useful energy gain that would result if the collector-absorbing surface had been at the local fluid temperature [92]:

$$F_R = \frac{\dot{m}c_p}{A_w U_L}\left[1 - Exp\left(-\frac{U_L F A_w}{\dot{m}c_p}\right)\right] \quad \textbf{(4-10)}$$

The PTC efficiency factor (F) can be found from [92]:

$$F = \frac{\frac{1}{U_L}}{\frac{1}{U_L} + \left(\frac{d_o}{d_i}\right)\frac{1}{h} + \left(\frac{d_o}{2k_f}\right)\ln\left(\frac{d_o}{d_i}\right)} \quad \textbf{(4-11)}$$

Finally, the U_L depends on the magnitude of conductive, radiative, and convective losses, which in turn depend on the operating temperature of the collector that is relative to the environment. It can be expressed as [92]:

$$U_L = \frac{Q_{loss}}{A_w(\bar{T}_w - T_a)} \quad \textbf{(4-12)}$$

4.7 The cost analysis

The cost-benefit analysis of the distillation unit is an important aspect, as it depends mainly on the productivity of freshwater, which depends on the intensity of incident solar radiation. As the installed location of the SDU changes, the intensity of solar radiation accordingly changes.

The total cost (TC) of any distilled unit is calculated from:

$$TC = FC + VC \quad \textbf{(4-13)}$$

where *FC* is fixed cost and *VC* is variable cost.

4.8 Experimental Setup and Procedure

The SDU is used to produce freshwater, which consists of the cold water source, the PTC device, the SS, and the water supply pipeline, as shown in Fig. (4-10). In this work, experiments were conducted on different days from October 2023 to May 2024 from 9:00 a.m. to 3:00 p.m. for all units: CSS, SDU (SS + PTC with the plain tube), and modified SDU (MSDU) (SS + PTC with the modified PTR). First, it is very important to clean the reflector of the PTC and the glass cover of the SS from any accumulated dust or dirt. Then, the PTC is tracked to capture the beam radiation and focus it on the PTR. Water is pumped from the cold water source to the PTC. The flow meter located after the pump measures the flow rate of water passing through the pipes. At the beginning of the time, one should not take readings until half an hour has passed to avoid false readings. The water was pumped into the PTR, and the water began to heat up gradually due to the concentrated solar radiation. Then the hot water coming out was transferred to the condensation system through insulated plastic pipes to avoid thermal losses.

In the first stage, the amount of freshwater productivity was recorded for every hour from the CSS, and at last daylight hours, the amount of collected freshwater was calculated. In the second stage, the PTC containing the plain tube was connected to the SS. The cold water inlet temperature and the hot water outlet temperature of the PTC system and the freshwater productivity of the SS were recorded for every daylight hour. Finally, in the third stage, novel cylindrical turbulators were introduced into the PTR to increase the heat transfer area and to reduce the heating time of the PTC system; then it was connected to the SS. Also, the cold water temperature and the hot water temperature of the PTC system and the freshwater productivity of SS were recorded hourly and daily.

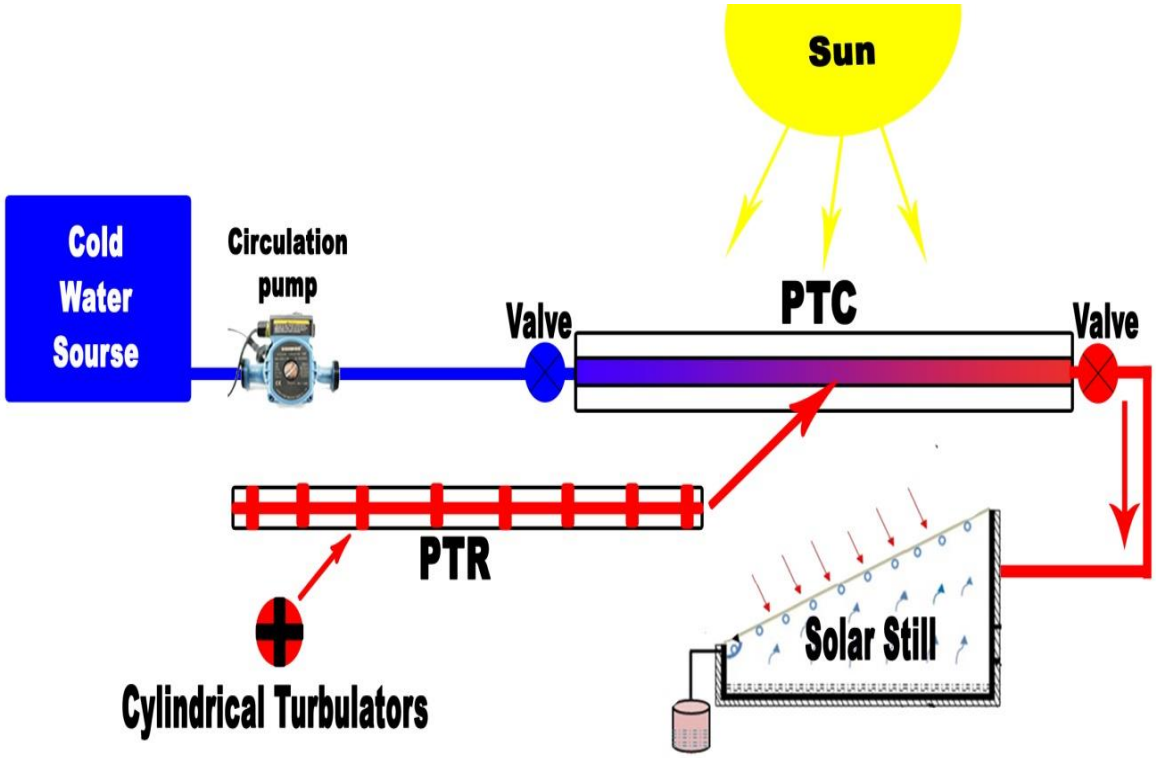

Figure (4-10): Schematic of the MSDU.

Chapter Five: Results and Discussion

5.1 Introduction

The numerical results investigated the effects of length, thickness, and number of cylindrical turbulators inside the PTR under turbulent flow on the thermo-hydraulic performance, and the temperature distribution in the plain tube and modified PTRs.

The experimental results show recorded inlet and outlet HTF temperatures in the plain tube and modified PTR during the operated hours of the PTC's system in the selected days of the year at the system's location (College of Engineering/Al-Musayab, Babylon (32.77° N, 44.29° W)). The useful heat and the PTC thermal efficiency are calculated and compared with the numerical results. In addition, a comparison between the results of the present study and previous studies is presented to show the improvement in the PEC. Finally, to demonstrate the effect of turbulators on the MSDU, the quantity of freshwater production was recorded and compared between the CSS, SDU, and MSDU.

5.2 The Numerical Results

In this work, the investigated PTC models (eighty cylindrical turbulator models and the plain tube model) were designed in SolidWorks and simulated in the CFD tools. These tools can do flow and thermal analyses all at once. It's crucial to bear in mind that numerous literature studies, primarily focusing on PTC, have utilised the current simulation tool [32, 34, 39, 43, 75-77].

5.2.1 Mesh Quality

A variety of meshes are evaluated, Tables (5-1) and (5-2) provide a detailed report of the test findings of the plain tube case and the selected cylindrical turbulator tube case (with l = 40 mm, t = 2 mm, and N = 15),

respectively. In these tests, five distinct mesh instances were looked at, the input temperature was set at 300 K, and the mass flow rate was chosen to be 0.7 kg/s. In both cases, mesh 4 was the best-selected mash because it is clear that the output fluid temperature has converged. These tables indicate that the plain tube case selected approximately 1.2 million cells, while the cylindrical turbulator tube case selected approximately 2.5 million cells. Figure (5-1) shows the meshes for the plain tube and the cylindrical turbulators PTR.

Table (5-1): GIT of the plain tube case.

Properties	Mesh 1	Mesh 2	Mesh 3	Mesh 4	Mesh 5
Million cells	0.215	0.423	0.605	1.212	1.532
T_{fo} (K)	308	316	322	325.5	325.6
Error (%)	-	2.5	1.9	1.1	0.03

Table (5-2): GIT of the selected cylindrical turbulator tube case.

Properties	Mesh 1	Mesh 2	Mesh 3	Mesh 4	Mesh 5
Million cells	0.522	1.204	1.931	2.511	3.323
T_{fo} (K)	311	321	330	339.7	339.9
Error (%)	-	3.2	2.8	2.9	0.06

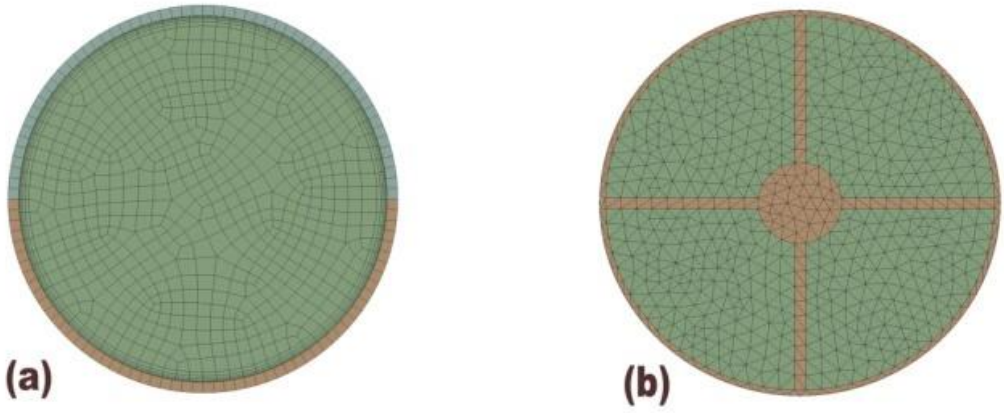

Figure (5-1): Mesh in a cross section for: a) plain tube, and b) cylindrical turbulator PTR.

In this study, succinct convergence is achieved when the scaling residuals of energy, momentum, and continuity remain constant after an estimated 216 iterations. The scaled residuals' minimum values following these iterations equal (10^{-6}), for the energy, continuity equation, and velocity quantities.

5.2.2 Validation Test

This subsection presents the accuracy of the developed model through a validation test. The validation test, as illustrated in Fig. (5-2), was compared with Sahin et al. [64]. The average variation in the Nusselt number and friction factor is -3.5% and 2.9%, respectively. The observed variances were found to be negligible; suggesting that the data obtained from the plain tube exhibits a high level of dependability. Therefore, the collected data can be used as a benchmark to evaluate the tube's performance with the inclusion of the cylindrical turbulators.

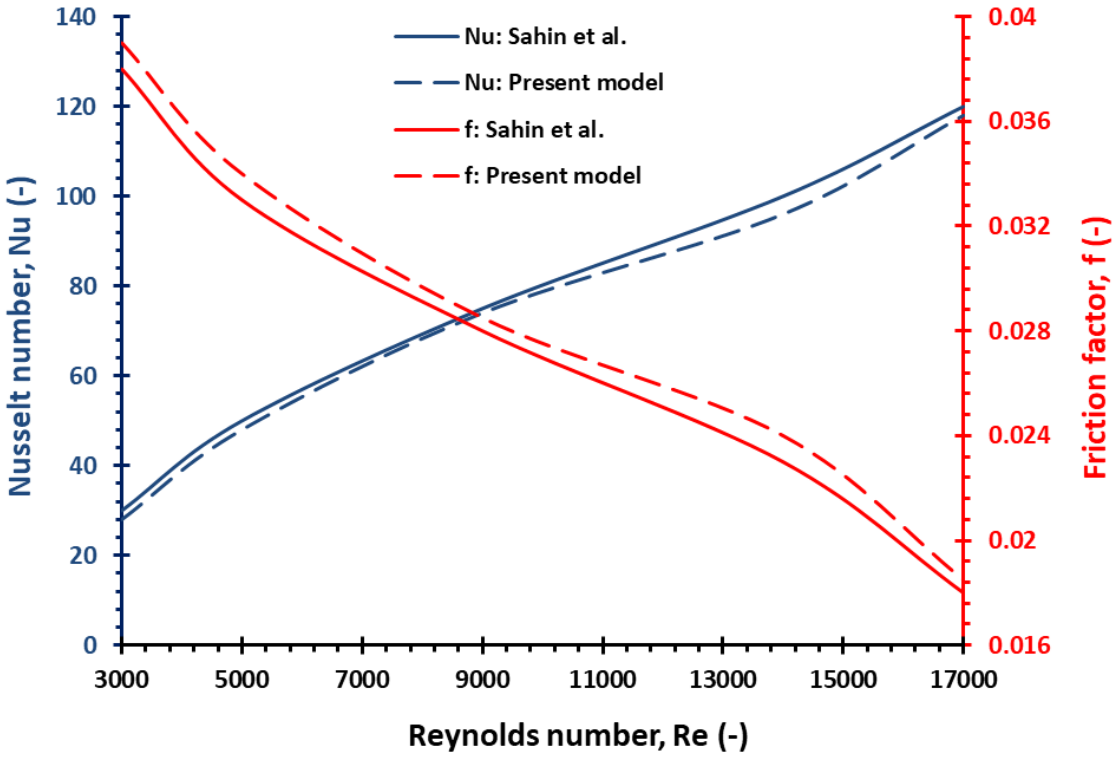

Figure (5-2): Validation of Nusselt number and friction factor for various Reynolds number with [64].

5.2.3 Effect of Cylindrical Turbulators length

To examine the impact of the cylindrical turbulator lengths, *l*, on the thermo-hydraulic performance (Nusselt number, friction factor, and PEC) inside the PTR, its values were varied from 10 mm to 50 mm with a fixed thickness (t = 2 mm) and a constant number (N = 15).

Figure (5-3) shows the variation of the Nusselt number and friction factor with mass flow rates for different cylindrical turbulator lengths with the fixed thickness (t = 2 mm) and the constant number (N = 15). According to this figure, the Nusselt number increases with the mass flow rate for all tubes (plain tube and modified PTR) due to an increase in the heat transfer coefficient (i.e., when the flow rate of the HTF increases, many eddies are formed). The Nusselt number was enhanced by 41% inside the plain tube due

to increasing the mass flow rate from 0.6 kg/s to 1.0 kg/s. At a mass flow rate of 0.6 kg/s, the Nusselt number improved by 8.10% as the cylindrical turbulator length increased from 10 mm to 50 mm, while at a mass flow rate of 1.0 kg/s, it improved by 23.3%. This is because the Nusselt number increases with cylindrical turbulator length due to increased HTF contact and turbulence (i.e., an increase in the longitudinal heat transfer area between the inner PTR surface and HTF). At the maximum mass flow rate (1.0 kg/s), the Nusselt number ratio varies from 1.48 to 1.82 by increasing the cylindrical turbulator length from 10 mm to 50 mm. On other hand, it is clear that the friction factor decreases with the mass flow rate for all tubes due to the friction factor being inversely proportional to the inlet HTF velocity, as indicated in Eq. (3-26). By increasing the mass flow rate from 0.6 kg/s to 1.0 kg/s, the friction factor inside the plain tube decreased by 67.8%, while inside the modified PTR (with 50 mm of cylindrical turbulator length) it decreased by 80.8%. Compared to the plain tube, the modified PTR has the higher friction factor due to inserting the cylindrical turbulators, which increases the pressure drop. At the mass flow rate of 1.0 kg/s, the friction factor ratio varies from 1.05 to 1.23 when increasing the cylindrical turbulator length from 10 mm to 50 mm, whereas the friction factor ratio varies from 1.05 to 1.10 when increasing the cylindrical turbulator length from 10 mm to 40 mm. The increase in lengths of cylindrical turbulators leads to increase the pressure drop.

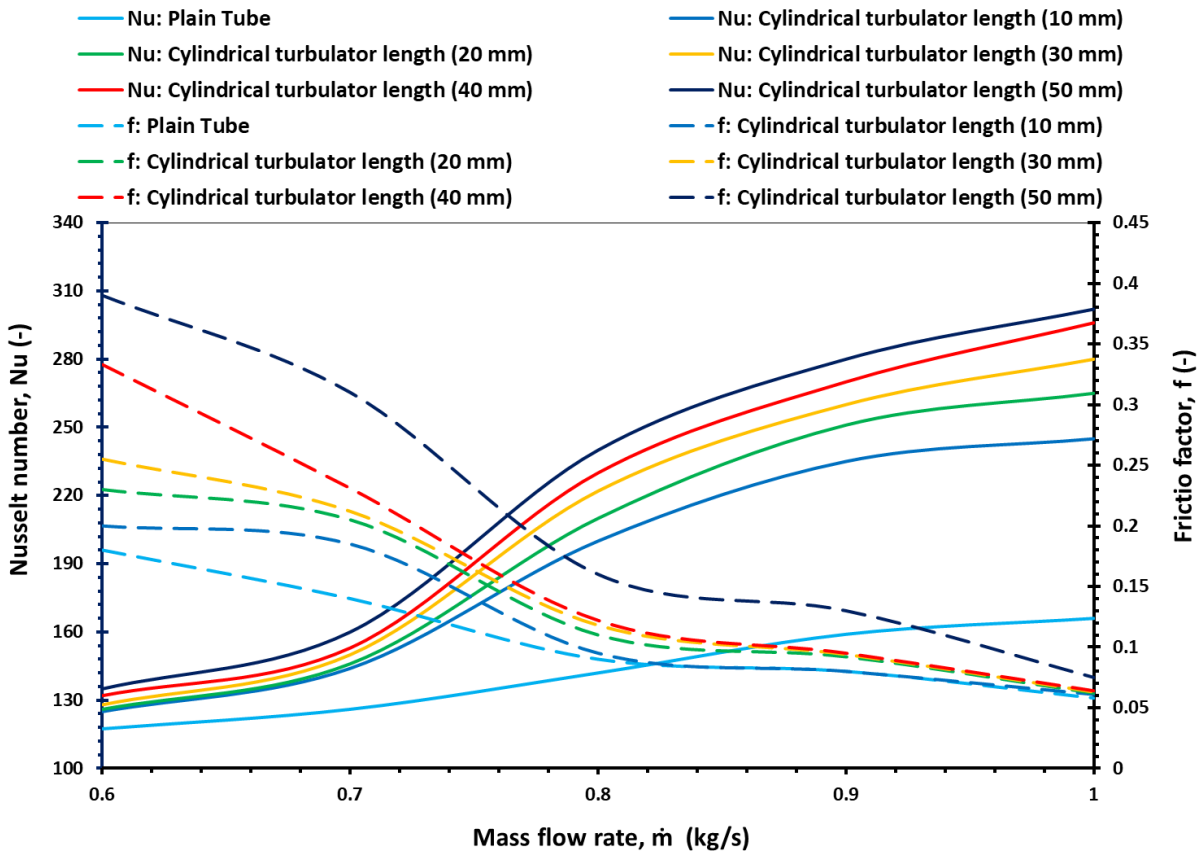

Figure (5-3): Nusselt number and friction factor with mass flow rates for different cylindrical turbulator lengths with the fixed thickness (t = 2 mm) and the constant number (N = 15).

Figure (5-4) shows the variation of the PEC with mass flow rates for different cylindrical turbulator lengths with the fixed thickness (t = 2 mm) and the constant number (N = 15). It is clearly seen from this figure that the PEC increases with mass flow rate for all tubes due to the increase in Nusselt number value. At the mass flow rate of 0.6 kg/s, the range of PEC value is 0.92-1.02, but after the mass flow rate of 0.7 kg/s the values of PECs in all modified PTRs is higher than one. Additionally, the PEC reaches 1.73 using a length of 40 mm and 1.70 using a length of 50 mm due to increasing the friction factor. Hence, the optimal length of cylindrical turbulator is 40 mm.

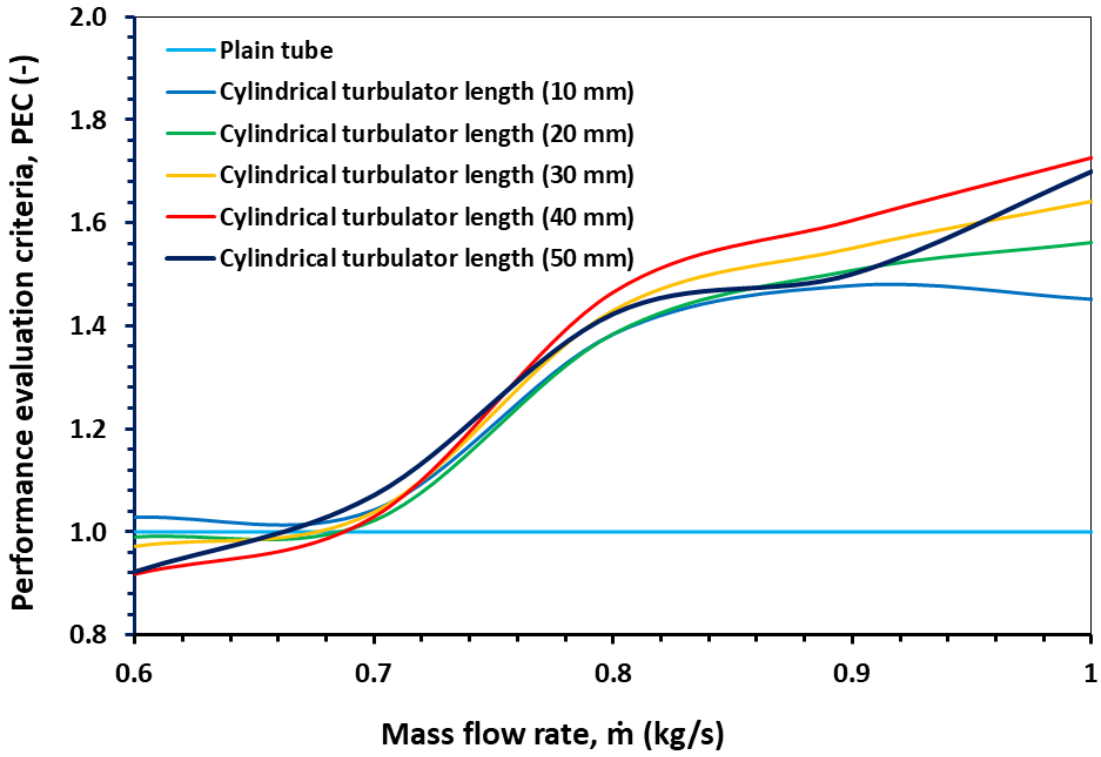

Figure (5-4): PEC with mass flow rates for different cylindrical turbulator lengths with the fixed thickness (t = 2 mm) and the constant number (N = 15).

5.2.4 Effect of Cylindrical Turbulators Thickness

In order to investigate the impact of the thickness (t) of the cylindrical turbulator on the thermo-hydraulic performance inside the PTR, its value was varied from 1 mm to 4 mm for the fixed length (l = 40 mm) and the constant number (N = 15).

Figure (5-5) shows the variation of the Nusselt number and friction factor with mass flow rates for different cylindrical turbulators thickness with the fixed length (l = 40 mm) and the constant number (N = 15). According to this figure, as mass flow rate increased the Nusselt number increased and friction factor decreases due to reason in length effect of cylindrical turbulators. It can be seen that the Nusselt number steadily rises as the cylindrical turbulators thickness increases due to the increasing cross-section

area of the cylindrical turbulators, which the HTF collected, and causes the increase in heat transfer area. At the mass flow rate of 0.6 kg/s, the Nusselt number ratio reached 1.05, 1.19, 1.21, and 1.23 for cylindrical turbulators thickness of 1, 2, 3, and 4 mm, respectively. On the other hand, the Nusselt number ratio reached 1.60, 1.78, 1.80, and 1.81 for cylindrical turbulators thickness of 1, 2, 3, and 4 mm, respectively, at a mass flow rate of 1.0 kg/s. As noted from the Nusselt number ratios, the thickness had a negligible effect on the heat transfer rate, particularly after 2 mm of cylindrical turbulator thickness.

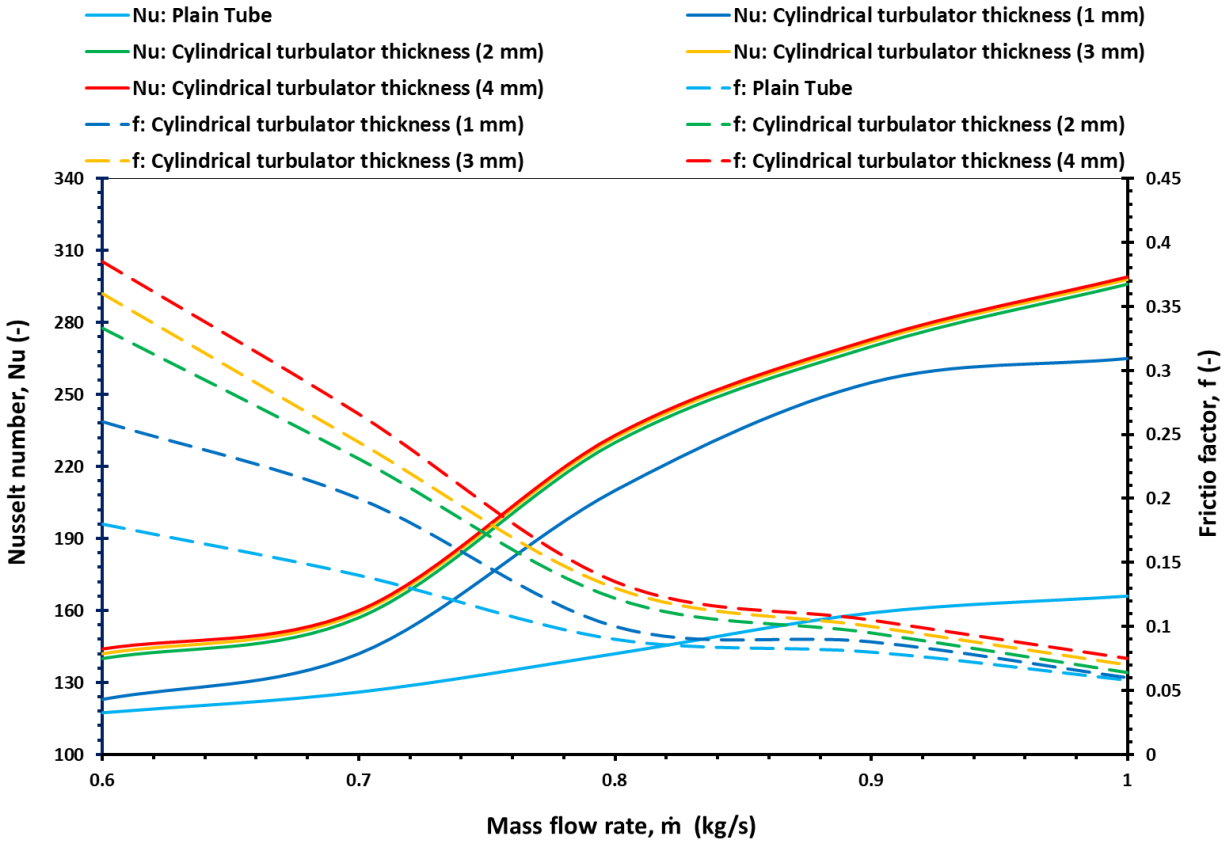

Figure (5-5): Nusselt number and friction factor with mass flow rates for different cylindrical turbulator thickness with the fixed length (*l* = 40 mm) and the constant number (*N* = 15).

Also, it was noted as the cylindrical turbulator thickness increases, the friction factor gradually increases due to the increase in the pressure drop by inserting these turbulators. At a mass flow rate of 1.0 kg/s, the friction factor ratio reached 1.03, 1.10, 1.21, and 1.29 inside the PTR using the cylindrical turbulator thickness of 1, 2, 3, and 4 mm, respectively. The increase cylindrical turbulator thickness increases the pressure drop due to inserting the cylindrical turbulators.

Figure (5-6) shows the variation of the PEC with mass flow rates for different cylindrical turbulator thicknesses with the fixed length (l = 40 mm) and the constant number (N = 15). It is observed from this figure that the PEC increases with mass flow rate for all modified PTRs due to increasing the Nusselt number values. The PEC value under mass flow rate of 0.7 kg/s is less than one. At mass flow rate of 1.0 kg/s, the PEC value using modified PTR with cylindrical turbulators thickness of 1, 2, 3, and 4 mm reaches 1.58, 1.73, 1.69, and 1.65, respectively. Hence, the optimal thickness of cylindrical turbulators is 2 mm.

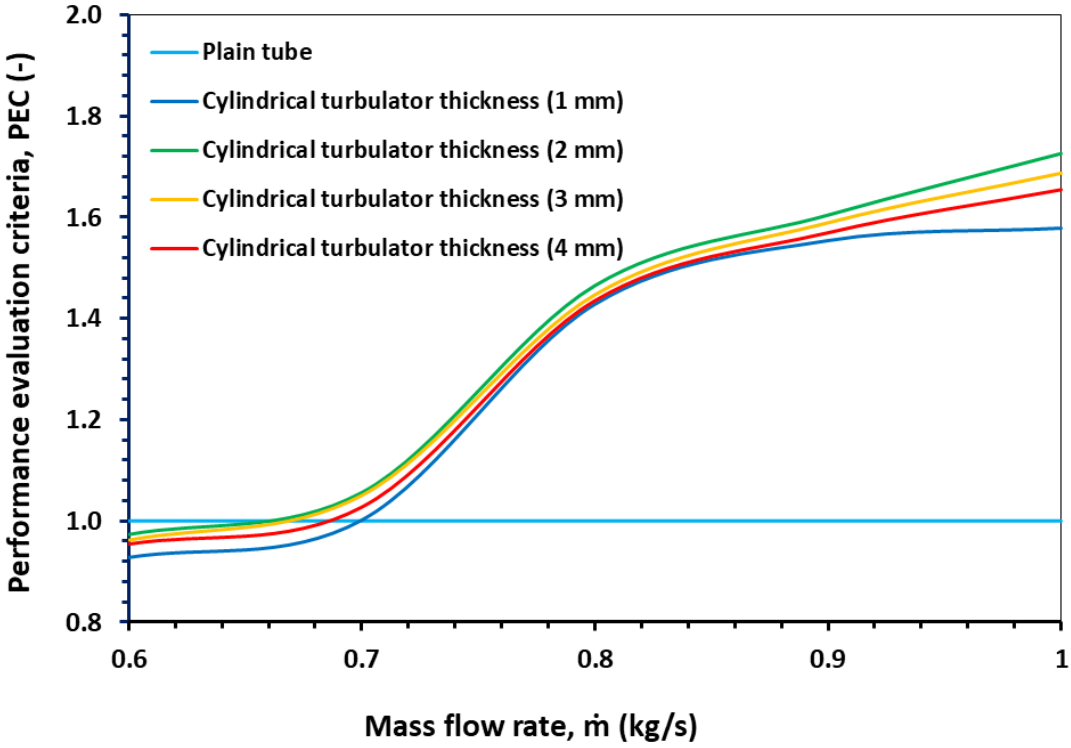

Figure (5-6): PEC with mass flow rates for different cylindrical turbulator thickness with the fixed length (*l* = 40 mm) and the constant number (*N* = 15).

5.2.5 Effect of Cylindrical Turbulators Number

The number of cylindrical turbulators (with the fixed length (*l* = 40 mm) and thickness (*t* = 2 mm)) was varied from 5 to 20 to investigated its effect on the thermo-hydraulic performance inside the PTR.

Figure (5-7) shows the variation of the Nusselt number and friction factor with mass flow rates for different cylindrical turbulators with the fixed length (*l* = 40 mm) and thickness (*t* = 2 mm). According to this figure, at mass flow rate of 1.0 kg/s, the increase in the number of cylindrical turbulators from 5 to 20 leads to a 15.1% improvement in the Nusselt number due to increasing both the heat transfer coefficient and the heat transfer area. Also, it is clear that the increase in the number of cylindrical turbulators inside the PTR from 5 to 20 causes a significant increase in the friction factor value.

Increasing the number of cylindrical turbulators enhances the longitudinal and cross-sectional areas of collisions between the PTR's wall and HTF, leading to an increase in the pressure drop. The average improvement in friction factor is 19.6% when increasing the number from 5 to 20.

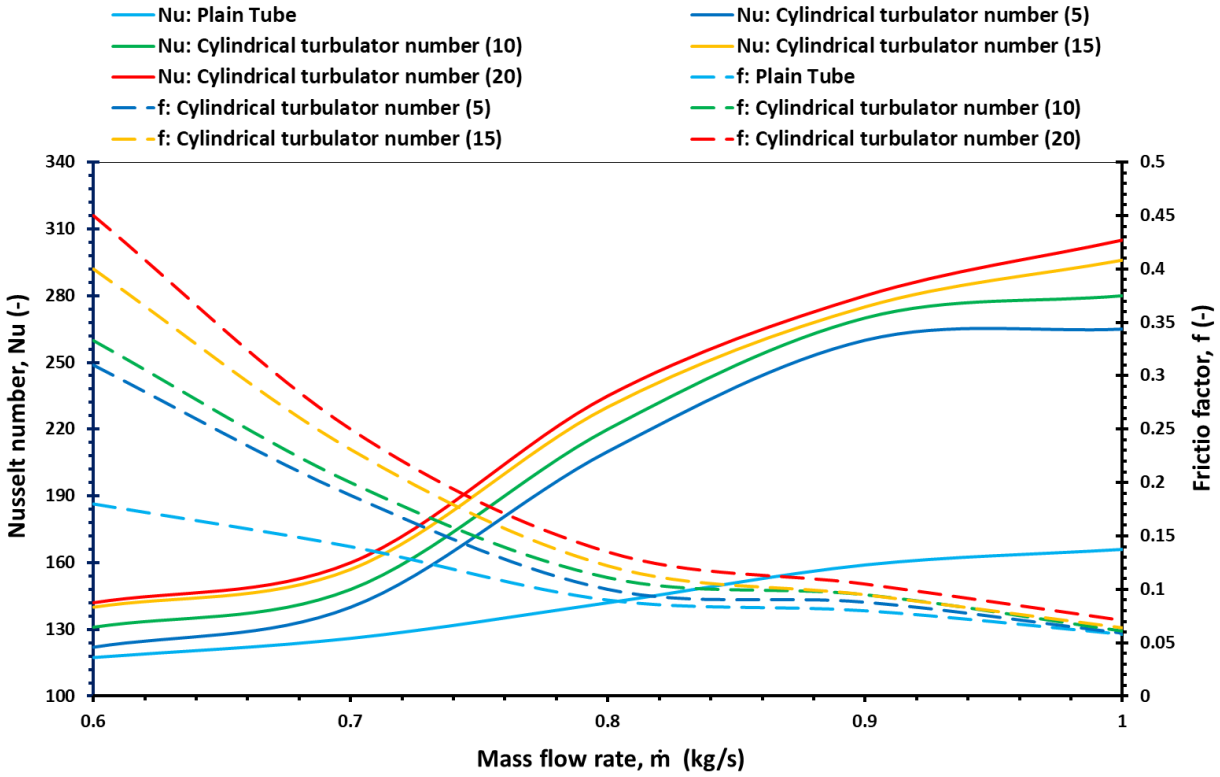

Figure (5-7): Nusselt number and friction factor with mass flow rates for different cylindrical turbulators number with the fixed length (*l* = 40 mm) and thickness (*t* = 2 mm).

Figure (5-8) shows how the PEC value increases with HTF mass flow rate and cylindrical turbulator number with the fixed length (*l* = 40 mm) and thickness (*t* = 2 mm). According to this figure, the values of PEC using the modified PTRs with cylindrical turbulator number of 5, 10, 15, and 20 are 1.59, 1.66, 1.73, and 1.72, respectively. This means that it is not advised to increase the number of cylindrical turbulators to more than 15 inside the modified PTR.

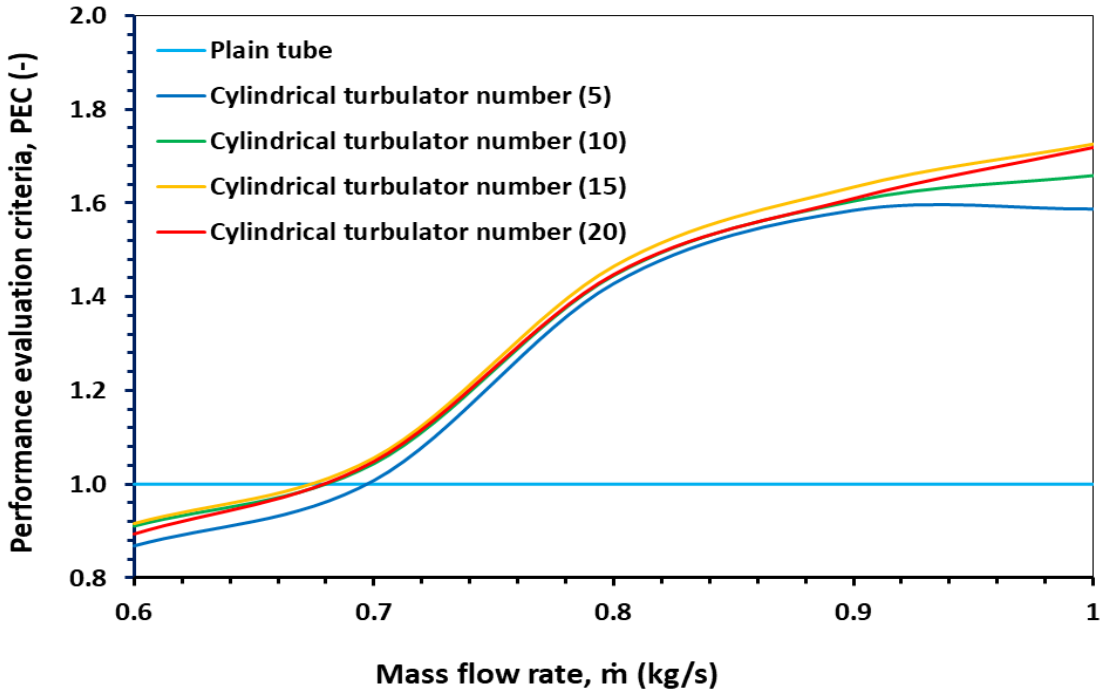

Figure (5-8): PEC with mass flow rates for different cylindrical turbulators number with constant length (*l* = 40 mm) and constant thickness (*t* = 2 mm).

Appendix B listed the results of thermo-hydraulic performance at mass flow rate of 1.0 k/s for all investigated parameters. Finally, a comparison of the PEC values between the present work (cylindrical turbulators) and different types of turbulators is provided in Table (5-3). The comparison shows that the proposed turbulator design has a positive effect on enhancing the thermo-hydraulic performance of the PTR.

Table (5-3): Comparison of the PEC values between the present work and various turbulators inside PTR.

Ref.	Type of turbulators	PEC
[45]	spherical pins	1.25
[34]	twisted tape	1.28
[39]	rectangular longitudinal fins	1.31
[42]	conical strip turbulators	1.33

[47]	porous discs	1.60
[46]	rectangular cross-section fins	1.64
[44]	axially rotating internally finned PTR	1.72
Present work	cylindrical turbulators	1.73

5.2.6 Outlet Temperature Distributions of the HTF

Figure (5-9) displays the CFD result of the temperature contour inside the plain tube. It was noted that the average outlet HTF temperature reaches 325.5 K when the inlet HTF temperature is 300.0 K.

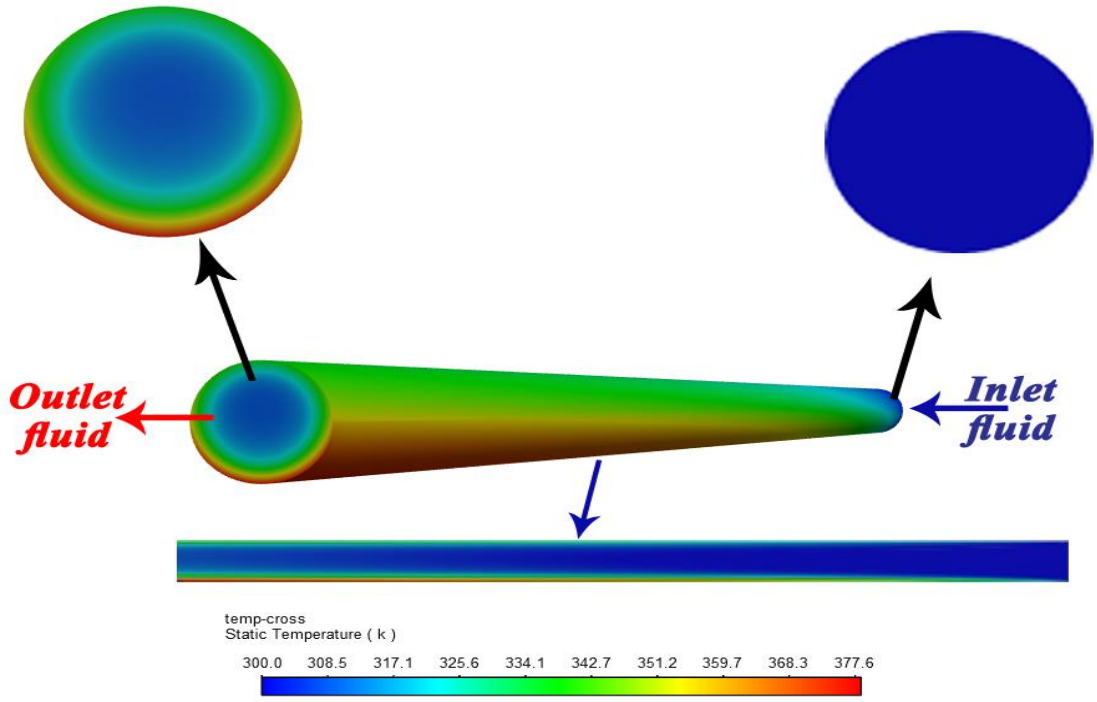

Figure (5-9): CFD result of temperature contour of the plain tube.

As seen, when the HTF flows into the PTR, it will initially begin to heat slowly from the PTR's upper surface due to the beam solar radiation and from the PTR's lower surface due to the concentrated solar radiation, but the HTF temperature is not uniformly distributed. It is observed that the maximum temperature of the HTF outlet surface approaches the wall temperature due to

the absence of any active or passive technology that could enhance heat transfer within the PTR.

Figure (5-10-a) displays the CFD result of the temperature contour inside the modified PTR with l = 40 mm, t = 2 mm, and N = 5. The average outlet HTF temperature from the modified PTR has been observed to be slightly increased compared with the average outlet HTF temperature from the plain tube to record 330.6 K.

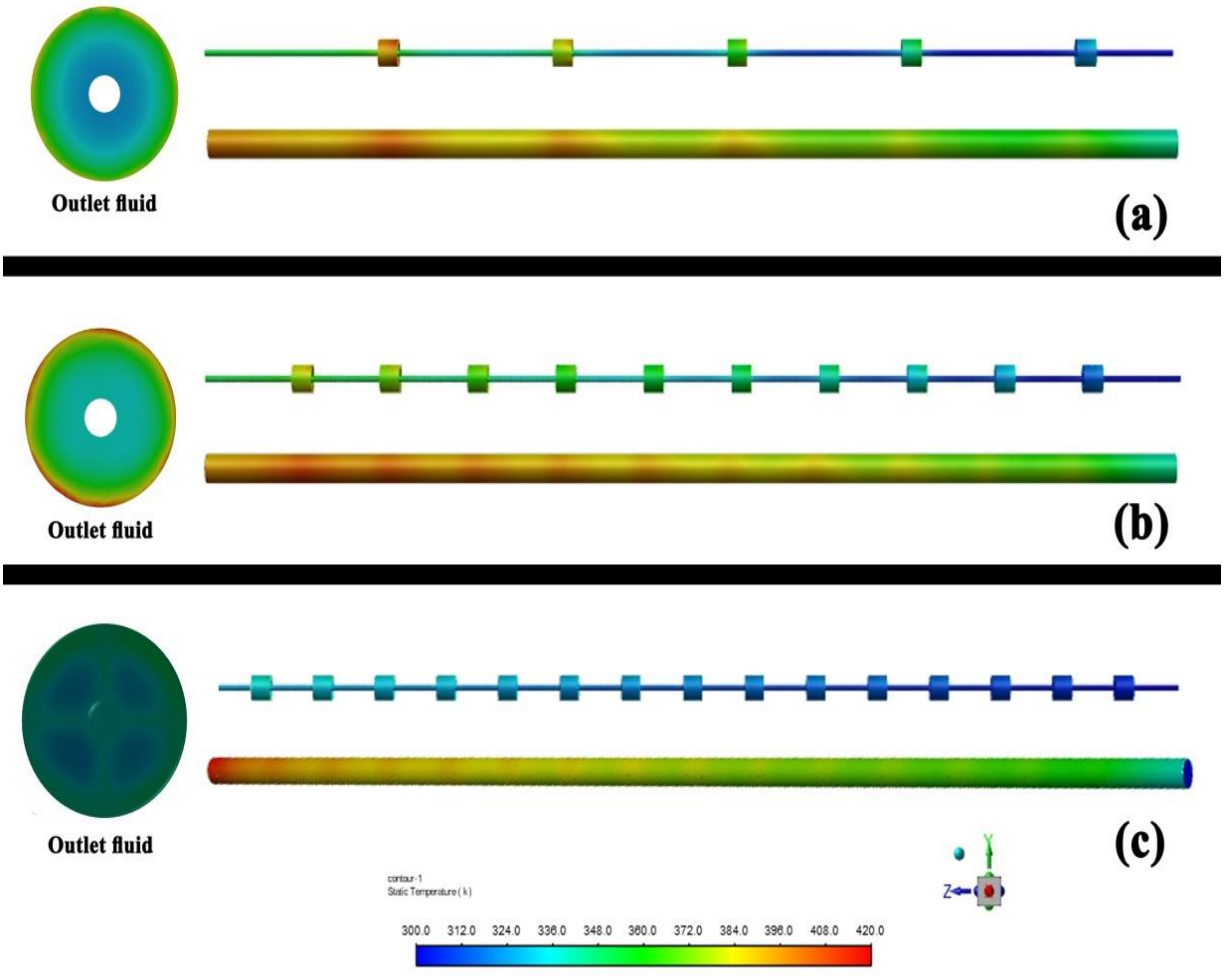

Figure (5-10): CFD results of the temperature contour inside the PTR with the fixed length (l = 40 mm) and thickness (t = 2 mm): (a) N = 5, (b) N = 10, and (c) N = 15.

Figure (5-10-b) shows the CFD result of the temperature contour inside the modified PTR with l = 40 mm, t = 2 mm, and N = 10. The average outlet HTF temperature from the modified PTR increased compared with the average outlet HTF temperature from the previous tubes to reach 337.5 K. Figure (5-10-c) demonstrates the CFD result of the temperature contour inside the modified PTR with l = 40 mm, t = 2 mm, and N = 15. In this modified PTR, the average outlet HTF temperature recorded the highest value at 339.7 K.

5.3 The Experimental Results

5.3.1 The PTR with and without Cylindrical Turbulators

5.3.1.1 The Outlet Temperature

Appendices (C), (D) and (E) present the results of calculated and measured data during selected days during October 2023 to May 2024 at the College of Engineering/Al-Musayab, Babylon (32.77° N, 44.29° W), from 9:00 to 15:00. Appendix (C) displays the calculated data for the angles and values of solar radiation, Appendix (D) shows the experimentally comparison of outlet water temperature from the plain tube and modified PTR, and Appendix (E) lists the theoretically calculated values, such as the useful energy and PTC thermal efficiency. Setting and positioning the PTC manually according to sunlight and running the system for 60 minutes prior to recording the first reading. The time interval between each reading is set to 60 minutes. The inlet and outlet water temperatures are measured using the temperature measurements.

To compare between the experimental and numerical outcomes, the measured data are taken experimentally for both tubes (the plain tube and the

modified PTR (PTR with the optimal parameters of cylindrical turbulators that gated from CFD (l = 40 mm, t = 2 mm, and N = 15))). The measured data encompassed the inlet water temperature, water flow rate, PTR area, reflector area, and time. Then, the model determined the outlet water temperature and useful heat. The modelled results are plotted for each case and compared with the experimental results on May 7, 2024.

Figure (5-11) shows the comparison between the experimental and numerical outlet water temperatures during the test day for the plain tube and modified PTR. In all examined tubes experimental and numerical, at 9:00 a.m., the outlet water temperature recoded 36.0°C. Experimentally, the outlet water temperature from the plain tube gradually rises to reach the maximum value of 57.0°C at 12:00 a.m. and then slowly drops to 34.5°C at 3:00 p.m. due to decreasing the beam solar radiation. The outlet water temperature from the modified PTR recorded the maximum value of 61.5°C at 11:00 a.m. faster than in the plain tube. These turbulators enhance the heat transfer exchange between the PTR's surface and the water by providing a larger surface area for heat transfer and extending the water's residence time to absorb more heat. These advantages enable the PTR to reach higher temperatures quickly, thereby increasing the production of hot water, which is crucial for water desalination processes. By comparing between the average enhancement in outlet water temperature from the plain tube and modified PTR, it was found to be 12%. Additionally, it is observed that as the beam solar radiation decreases, the outlet water temperature decreases. In contrast to the plain tube, the modified PTR shows less temperature drop. The cylindrical turbulators retain the daytime heat and gradually release it to water molecules.

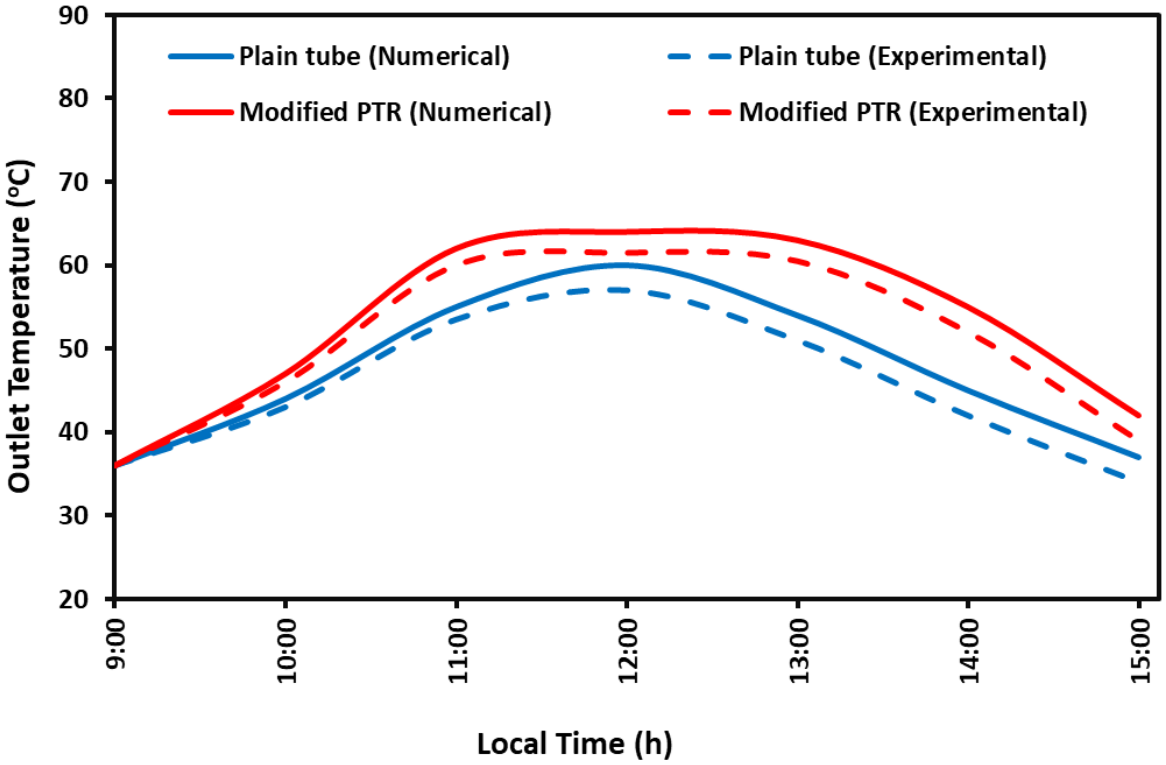

Figure (5-11): Comparison between the experimental and numerical outlet temperatures of the plain tube and modified PTR on 7 May of 2024.

Numerically, the two tubes behave similarly to the experimental observations, albeit with higher outlet water temperatures. The reason for this is that during the simulation period, some inputs remain fixed which are not the cases in the actual experiment. Also, it was found that there was a good agreement between the experimental and numerical results, where there are some discrepancies with an average error of -2.2% and -2.6% for the plain tube and modified PTR, respectively.

5.3.1.2 The Useful Heat

Figure (5-12) shows the comparison between the experimental and numerical useful heats of the water during the test day for the plain tube and modified PTR. According to Eq. (3-24), the useful heat depends on the temperature difference between the outlet and inlet water. Therefore, the

experimental useful heat begins to rise gradually to record its highest value of 1053.4 W in the modified PTR and 903.3 W in the plain tube.

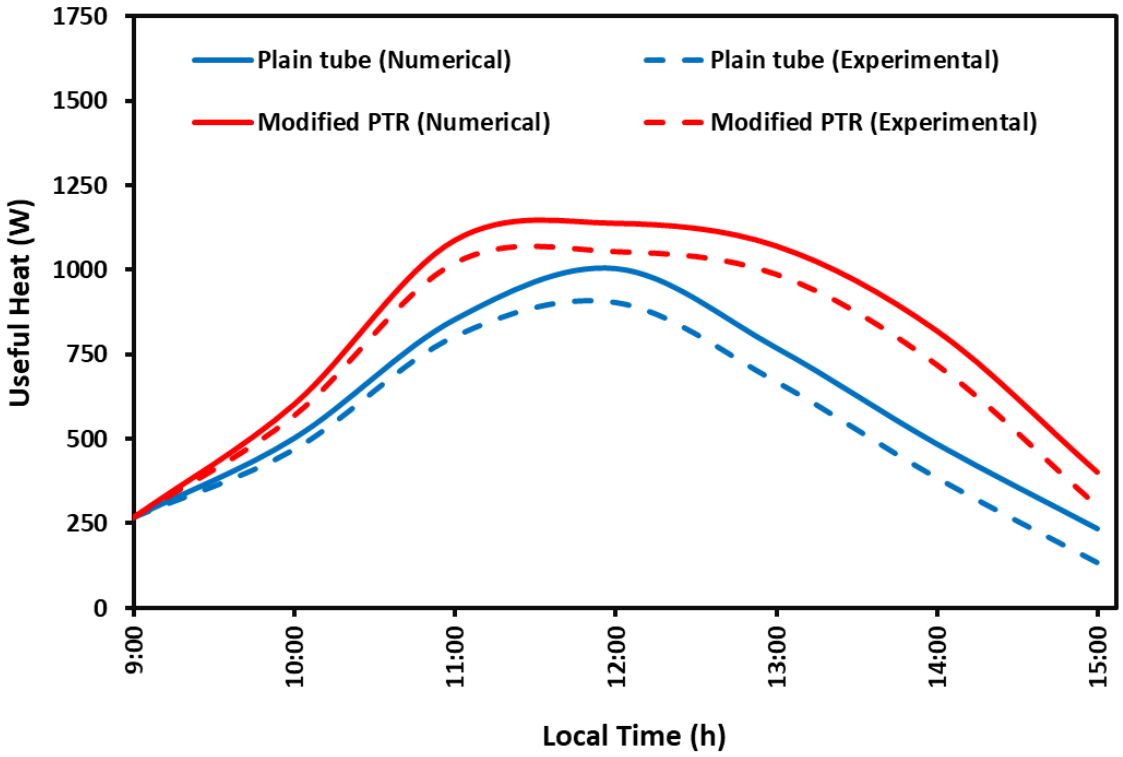

Figure (5-12): Comparison between the experimental and numerical useful heat for the plain tube and modified PTR on 7 May of 2024.

In the modified PTR, the useful heat reaches its maximum value faster (at 11:00 a.m.) than in the plain tube (at 12:00 a.m.). The values of useful heat in the modified PTR remain within the high range for a longer period, unlike in the plain tube. As in the outlet water temperature case (Fig. (5-11)), the drop in the values of useful heat in the modified PTR is gradually less than that for the plain tube. The presence of cylindrical turbulators, which retain heat and begin to lose it when the beam solar radiation values drop, is responsible for all these effects. A convergence between numerical and practical results is observed with some contradictions, with a mean error of -2.6% and -3.7% for the plain tube and modified PTR, respectively.

5.3.2 The PTC Thermal Efficiency

Figure (5-13) illustrates the experimental values of the PTC thermal efficiency using the plain tube and modified PTR with the daylight hours of the selected day (7 May of 2025). The PTC thermal efficiency gradually rose in the early hours of the chosen days, reaching its highest value of 64% at 11:00 a.m. for the modified PTR case and 55% at 12:00 a.m. for the plain tube. Even though the beam solar radiation levels drop after 12:00 a.m., the PTC thermal efficiency using modified PTR stays high, between 60% and 50% due to the cylindrical turbulators which lose heat to water molecules along with the beam solar radiation. This feature shows the benefit of the presence of turbulators inside the PTR.

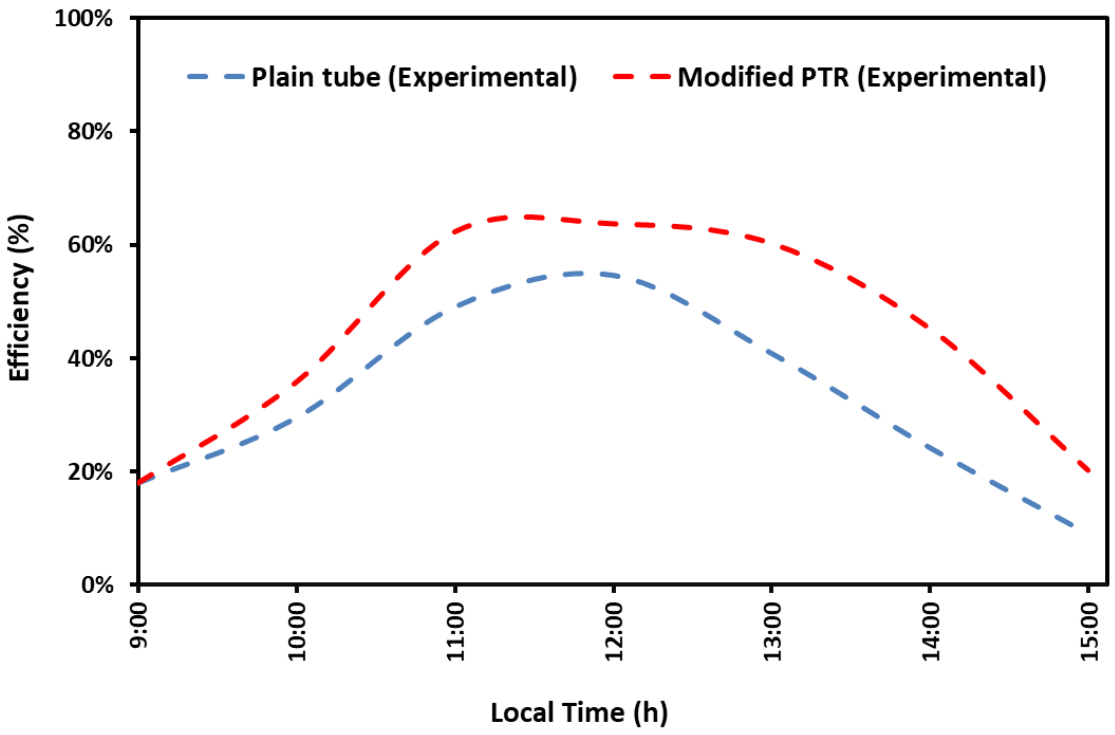

Figure (5-13): Experimental PTC thermal efficiency during selected day (7 May of 2024) of the plain tube and modified PTR.

Also, it was found the daily thermal efficiencies of the PTC with plain tube or modified PTR were 32% and 44%. Despite the inverse relationship

between the thermal efficiency and solar radiation, as demonstrated by Eq. (4-3), we observe an increase in its values even when the solar radiation decreases, particularly in the afternoon. Due to the large increase in useful heat compared to solar radiation.

Generally, there was a good agreement between the experimental and numerical results. However, there are some inconsistencies, which can be attributed to several factors. Firstly, the theoretical calculations in ANSYS assume ideal weather conditions, which can change instantaneously and directly impact the water temperatures inside the PTR and the accuracy of thermo-measurements. Additionally, manufacturing errors in the PTC reflector, the center of the focal point of the PTR, and the tracking of the sun all contribute to the inconsistencies.

5.3.3 The Freshwater Productivity

Figure (5-14) shows the hourly freshwater productivity of the CSS, SDU, and MSDU recorded 40, 110, 120 mL/m^2/h at 9:00 a.m. and 880, 1450, and 1670 kg/m^2/h at 13:00 p.m., respectively, in 7 May of 2024. The results show that the hourly freshwater productivity of SDU is higher than the CSS due to the impact of the PTC that raises the inlet water temperature into the SS's basin. Also, the hourly freshwater productivity of MSDU is higher than the CSS and SDU due to the presence of cylindrical turbulators, which result in increasing the outlet water temperature from the PTC.

5.3.4 Comparison of Current Study with Previous Studies

Many researchers have studied the performance of SDU with different techniques and got variable results [93-96]. In order to compare the results in terms of improving the productivity of freshwater, Fig. (5-15) was prepared to compare the daily productivity of each study.

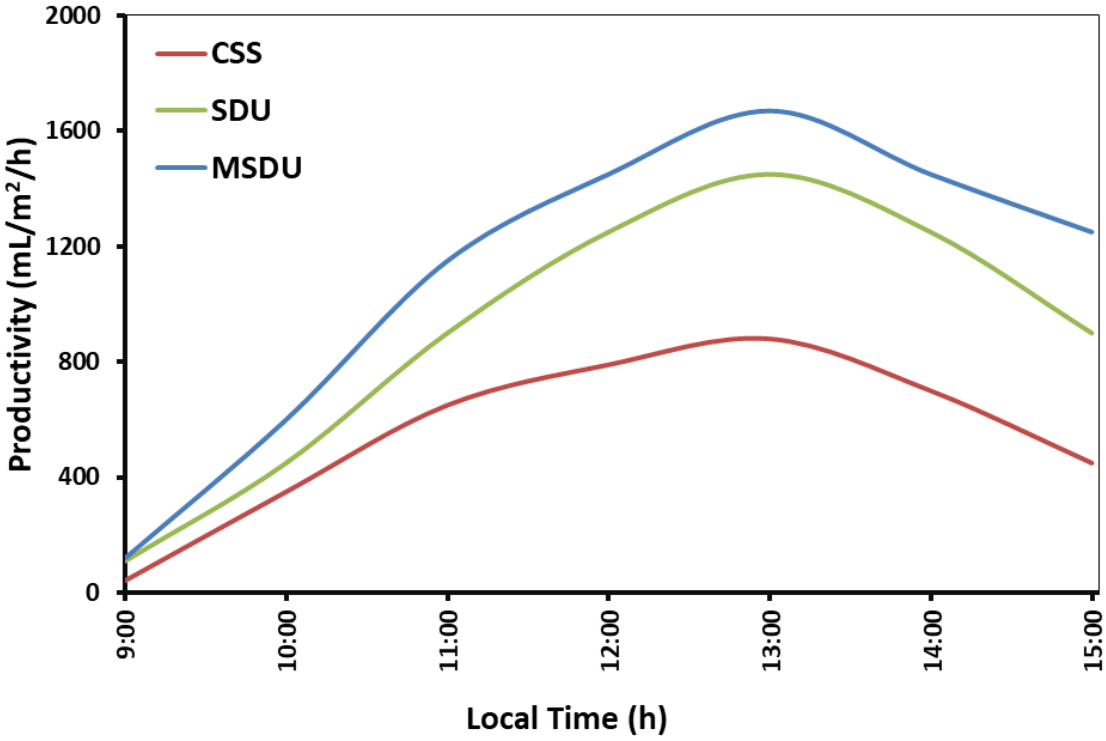

Figure (5-14): Variation of hourly freshwater productivity of CSS, SDU, and MSDU on 7 May of 2024.

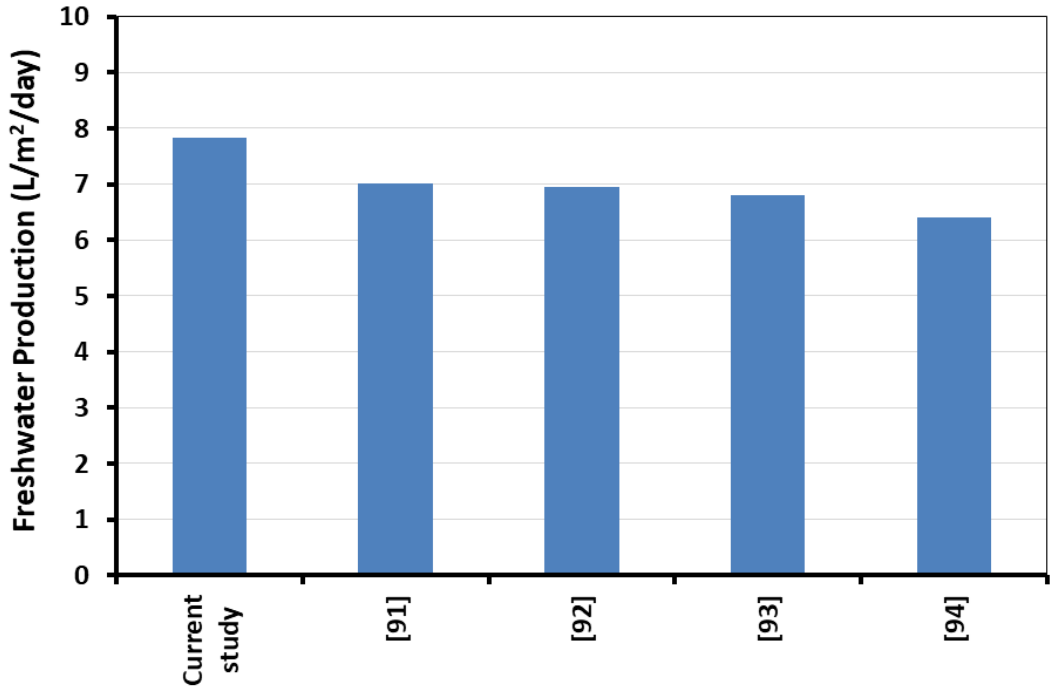

Figure (5-15): Distilled unit comparison of current study with previous studies.

5.3.5 Economic analysis

Table (5-4) lists the values of FC for every unit.

Table (5-4): The values of FC for every unit.

Units	FC ($)
CSS	165
SDU	506
MSDU	612

Consider variable cost *VC* equals 30% from *FC* per year, as stated by Madiouli et al. [17], then:

For CSS, the TC = 165$+(0.3×165$×15) = 907.5$ for 15 years (average solar life span). The average daily production can be calculated by analyzing various experimental data and it finds 0.95 L/day in Babil, Iraq. It is assumed that the sunshine is available for 331 days in a year in Iraq (as listed in Table (1-1)) to calculate the annual cost for 1 L. The overall yield of distilled water during this period (15 years) = 0.95×15×333.6 = 4753.8 L. Thus, the cost of 1 L distilled water obtained from CSS = 907.5/4753.8 = 0.191 $/L.

For SDU, the TC = 506$+(0.3×506$×15) = 2783$. The average yield per year can be taken as 4.25 L/day by assuming that the SDU works for 333.6 days during the year. The whole produce during the life cycle of the SDU = 21267 L. Thus, it can be calculated that the cost of 1 L by SDU is (2783/21267) = 0.131$.

For MSDU, the TC= 612$+(0.3×612$×15) = 3366$. The average yield per year can be taken as 5.23 L/day and the overall yield during the life cycle (15 years) of the MSDU = 5.23×333.6×15=26170.9L. Hence, the cost per 1 L of freshwater produced from MSDU reaches (3366/26170.9) = 0.129 $.

Chapter Six: Conclusions and Future Work

6.1 Conclusions

This study lists numerous techniques that can improve the thermo-hydraulic performance of PTC, which can lead to various benefits:

1) Higher thermal energy production.
2) Reduce thermal losses.
3) Higher PTC thermal efficiency.

When a plain tube is used without any turbulators, it leads to an uneven temperature distribution within the plain tube, which in turn increases thermal loss and heat stress. Changing the turbulator type is a viable approach for studying the corresponding effect on PTC systems' thermo-hydraulic performance. Without a doubt, inserting the turbulator improves heat transfer performance and decreases thermal loss, but it also affects the pressure drop, requiring more pumping power to force the flow through the PTR. Therefore, it should be optimized the geometrical parameters of the turbulator to ensure the effective thermo-hydraulic performance of the PTC.

In the numerical part, all the designed PTRs were performed over a range of Reynolds numbers of 20,000 – 36,000 and uniform heat flux distribution one the upper and lower surfaces of PTR. The main findings of this part are summarized as below:

1) The observed variances from the validation test of the present model with the experimental correlation were found to be negligible; suggesting that the data obtained from the plain tube exhibits a high level of dependability.
2) The mass flow rate has positive effect on the Nusselt number and negative effect on the friction factor.

3) The thermo-hydraulic performance generally increases with the length, thickness, and number of cylindrical turbulators.
4) The variation in thickness of cylindrical turbulators has relatively insignificant effect than variation of other parameters of cylindrical turbulators on the thermo-hydraulic performance.
5) The optimal case of the cylindrical turbulator is 40 mm in length, 2 mm in thickness, and 15 turbulators.
6) In this case, the maximum values of Nusselt number ratio, friction factor ratio, and PEC are 1.790, 1.100, and 1.730, respectively.
7) The comparison of the PEC values between the present work (cylindrical turbulators) and different types of turbulators shows that the proposed turbulator design has a positive effect on enhancing the thermo-hydraulic performance inside the PTR.

In the experimental part, all the examined PTRs were performed over mass flow rate of 0.7 kg/s and non-uniform heat flux distribution on the upper and lower surfaces of PTR. The main findings of this part are summarized:

1) These turbulators enhance heat transfer exchange between the PTR's surface and the water by providing a higher surface area for heat transfer, generating a swirl flow, and increasing the water's residence time to gain more heat.
2) For PTC, there is a good agreement between the experimental and numerical results of outlet water temperature, heat useful, and PTC thermal efficiency.
3) The productivity of distilled water from MSDU increased compared with its for SDU and CSS.

6.2 Recommendations for Future Work:

During the development of this project, different opportunity areas were found and noted. This subsection presents the future work that can follow this line of investigation.

1) The present work used cylindrical turbulators that resulted in enhanced PEC hydraulic performance values. Nevertheless, it is possible that certain turbulators exhibit superior performance compared to others.
2) The use of hybrid nanofluids with turbulators offers good potential since different turbulators could be investigated with numerous types of hybrid nanofluids.
3) By cooling its outer surface, SDU and MSDU can produce more distilled water, and new technologies can enhance the condensation process.

References

[1] M. H. D. A. Farahani, V. Vatanpour, and A. Taheri, *Desalination: challenges and opportunities*, 1 st ed., London, United Kingdom: IntechOpen, 2020.

[2] J. Bundschuh and J. Hoinkis, *Renewable Energy Applications for Freshwater Production*, 2 nd ed., London, UK: CRC Press, 2012.

[3] Y. A. Jebbar, "Theoretical Investigation of Using a Solar Pond for Air Conditioning of Buildings in Karbala City", M.Sc Dissertartion, Department of Physics, University of Kerbala, Karbala, Iraq, 2020.

[4] P. Drożyner, W. Rejmer, P. Starowicz, A. Klasa, and K. A. Skibniewska, "Biomass as a renewable source of energy", *Technical Sciences*, Vol. 16, (3), pp. 211-220, 2013

[5] *Statistical Review of World Energy* (2023, 3/7/2023). Available: https://www.bp.com/en/global/corporate/energy-economics/statistical-review-of-world-energy.html#tab_sr-2021

[6] H. P. Garg, *Solar energy: fundamentals and applications*, 1st ed., New Delhi: Tata McGraw-Hill Education, 2000.

[7] F. A. A. Mutlak, "Design and fabrication of parabolic trough solar collector for thermal energy applications", Ph.D Thesis, Department of Physics, University of Baghdad, Baghdad, Iraq, 2011.

[8] C. Chalkias, A. Faka, and K. Kalogeropoulos, "Assessment of the direct sun-light on rural road network through solar radiation analysis using GIS", *Open Journal of Applied Sciences*, Vol. 3, (2), pp. 224-231, 2013. https://doi.org/10.4236/ojapps.2013.32030

[9] H. B. Tolabi, M. H. Moradi, and S. M. Ayob, "A review on classification and comparison of different models in solar radiation estimation", *International journal of energy research*, Vol. 38, (6), pp. 689-701, 2014. https://doi.org/10.1002/er.3161

[10] M. R. Patel, *Wind and solar power systems: design, analysis, and operation*, 1 st ed., Florida: CRC press, 2005.

[11] *Map of radiation on Iraq* (2019). Available: https://globalsolaratlas.info/download/iraq

[12] NASA. Surface Meteorology and Solar Energy-Available Table [Online]. Available: https://www.academia.edu/4430410/NASA_Surface_meteorology_and_Solar_Energy_Available_Tables

[13] R. K. Singh and P. Chandra, "Parabolic trough solar collector: A review on geometrical interpretation, mathematical model, and thermal performance augmentation", *Engineering Research Express*, Vol. 5, (1), p. 012003, 012003, 2023. https://doi.org/10.1088/2631-8695/acc00a

[14] M. J. Taha, F. B. Kibret, V. Ramayya, and B. A. Zeru, "Design and evaluation of solar parabolic trough collector system integrated with conventional oil boiler", *Archives of Electrical Engineering*, Vol. 70, (3), pp. 657-673, 2021. https://doi.org/10.24425/aee.2021.137580

[15] M. Gharzi, A. M. Kermani, and H. T. Shamsabadi, "Experimental investigation of a parabolic trough collector-thermoelectric generator (PTC-TEG) hybrid solar system with a pressurized heat transfer fluid", *Renewable Energy*, Vol. 202, pp. 270-279, 2023. https://doi.org/10.1016/j.renene.2022.11.110

[16] B. Ghorbani, K. B. Mahyari, M. Mehrpooya, and M.-H. Hamedi, "Introducing a hybrid renewable energy system for production of power and fresh water using parabolic trough solar collectors and LNG cold energy recovery", *Renewable energy*, Vol. 148, pp. 1227-1243, 2020. https://doi.org/10.1016/j.renene.2019.10.063

[17] J. Madiouli, A. Lashin, I. Shigidi, I. A. Badruddin, and A. Kessentini, "Experimental study and evaluation of single slope solar still combined with flat plate collector, parabolic trough and packed bed", *Solar Energy*, Vol. 196, pp. 358-366, 2020. https://doi.org/10.1016/j.solener.2019.12.027

[18] A. Al-Falahi, F. Alobaid, and B. Epple, "Design and Thermo-Economic Comparisons of an absorption air conditioning system based on parabolic trough

and evacuated tube solar collectors", *Energies*, Vol. 13, (12), 3198, 2020. https://doi.org/10.3390/en13123198

[19] C. Philibert, "The present and future use of solar thermal energy as a primary source of energy", *International Energy Agency*, pp. 1-16, 2005. http://philibert.cedric.free.fr/Downloads/solarthermal.pdf

[20] A. Fernández-García, E. Zarza, L. Valenzuela, and M. Pérez, "Parabolic-trough solar collectors and their applications", *Renewable and sustainable energy reviews*, Vol. 14, (7), pp. 1695-1721, 2010. https://doi.org/10.1016/j.rser.2010.03.012

[21] A. A. Shaheed, "Building and Testing a Parabolic Trough Collector to Generate Steam", M.Sc. Dessertartion, Department of Mechanical Engineering, University of Kerbala, Karbala, Iraq, 2017.

[22] A. Sarangi, A. Sarangi, S. S. Sahoo, R. K. Mallik, S. Ray, and S. M. Varghese, "A review of different working fluids used in the receiver tube of parabolic trough solar collector", *Journal of Thermal Analysis and Calorimetry*, Vol. 148, (10), pp. 3929-3954, 2023. https://doi.org/10.1007/s10973-023-11991-y

[23] O. V. Ekechukwu and B. Norton, "Review of solar-energy drying systems II: an overview of solar drying technology", *Energy conversion and management*, Vol. 40, (6), pp. 615-655, 1999. https://doi.org/10.1016/S0196-8904(98)00093-4

[24] M. A. Sharaf, A. S. Nafey, and L. García-Rodríguez, "Exergy and thermo-economic analyses of a combined solar organic cycle with multi effect distillation (MED) desalination process", *Desalination*, Vol. 272, (1-3), pp. 135-147, 2011. https://doi.org/10.1016/j.desal.2011.01.006

[25] S. A. Kalogirou, "Solar thermal collectors and applications", *Progress in energy and combustion science*, Vol. 30, (3), pp. 231-295, 2004. http://dx.doi.org/10.1016/j.pecs.2004.02.001

[26] L. Léal, M. Miscevic, P. Lavieille, M. Amokrane, F. Pigache, F. Topin, B. Nogarède, and L. Tadrist, "An overview of heat transfer enhancement methods and new perspectives: Focus on active methods using electroactive materials", *International Journal of heat and mass transfer*, Vol. 61, pp. 505-524, 2013. https://doi.org/10.1016/j.ijheatmasstransfer.2013.01.083

[27] S. Rashidi, M. Eskandarian, O. Mahian, and S. Poncet, "Combination of nanofluid and inserts for heat transfer enhancement: gaps and challenges", *Journal of Thermal Analysis and Calorimetry*, Vol. 135, (1), pp. 437-460, 2019. https://doi.org/10.1007/s10973-018-7070-9

[28] S. S. Mousavi Ajarostaghi, M. Zaboli, H. Javadi, B. Badenes, and J. F. Urchueguia, "A review of recent passive heat transfer enhancement methods", *Energies*, Vol. 15, (3), p. 986, 2022. https://doi.org/10.3390/en15030986

[29] A. Mwesigye and Z. Huan, "Thermal and thermodynamic performance of a parabolic trough receiver with Syltherm800-Al2O3 nanofluid as the heat transfer fluid", presented at the *7th International Conference on Applied Eergy*, Abu Dhabi, UAE, Energy Procedia, Vol. 75, pp. 394-402, 2015. https://doi.org/10.1016/j.egypro.2015.07.402

[30] A. Mwesigye and J. P. Meyer, "Optimal thermal and thermodynamic performance of a solar parabolic trough receiver with different nanofluids and at different concentration ratios", *Applied Energy*, Vol. 193, pp. 393-413, 2017. https://doi.org/10.1016/j.apenergy.2017.02.064

[31] W. J. Khudhayer, H. Ghanbarpourasi, H. T. Jalel, and H. R. Al-Dayyeni, "Enhanced heat transfer performance of a flat plate solar collector using CuO/water and TiO 2/water nanofluids", *International Journal of Applied Engineering Research*, Vol. 13, (6), pp. 3673-3682, 2018. https://www.ripublication.com/ijaer18/ijaerv13n6_71.pdf

[32] C. Chang, C. Xu, Z. Y. Wu, X. Li, Q. Q. Zhang, and Z. F. Wang, "Heat transfer enhancement and performance of solar thermal absorber tubes with circumferentially non-uniform heat flux", presented at the *International Conference on Concentrating Solar Power and Chemical Energy Systems, SolarPACES 2014*, Beijing, China, Energy Procedia, Vol. 69, pp. 320-327, 2015. https://doi.org/10.1016/j.egypro.2015.03.036

[33] O. Jaramillo, M. Borunda, K. Velazquez-Lucho, and M. Robles, "Parabolic trough solar collector for low enthalpy processes: An analysis of the efficiency

enhancement by using twisted tape inserts", *Renewable energy*, Vol. 93, pp. 125-141, 2016. http://dx.doi.org/10.1016/j.renene.2016.02.046

[34] M. F. Abbas, K. Ibrahim, and A. F. K. Aljanabi, "Modeling and Simulation to Investigate the Thermal Efficiency of a Parabolic Solar Trough Collector with Absorber Tube Inserted Twisted Tape System", *AURUM Journal of Engineering Systems and Architecture*, Vol. 5, (1), pp. 65-88, 2021. https://doi.org/10.53600/ajesa.925830

[35] M. Allam, M. Tawfik, M. Bekheit, and E. El-Negiry, "Experimental Investigation on Performance Enhancement of Parabolic Trough Concentrator with Helical Rotating Shaft Insert", *Sustainability*, Vol. 14, (22), p. 14667, 2022. https://doi.org/10.3390/su142214667

[36] M. Bhargva and A. Yadav, "Factors affecting the performance of a solar still and productivity enhancement methods: a review", *Environmental Science and Pollution Research*, Vol. 28, (39), pp. 54383-54402, 2021. https://doi.org/10.1007/s11356-021-15983-z

[37] S. Ghadirijafarbeigloo, A. Zamzamian, and M. Yaghoubi, "3-D numerical simulation of heat transfer and turbulent flow in a receiver tube of solar parabolic trough concentrator with louvered twisted-tape inserts", presented at the *SolarPACES Conference 2013*, Las Vegas, USA, Energy procedia, Vol. 49, pp. 373-380, 2014. https://doi.org/10.1016/j.egypro.2014.03.040

[38] Z. Zheng, Y. Xu, and Y. He, "Thermal analysis of a solar parabolic trough receiver tube with porous insert optimized by coupling genetic algorithm and CFD", *Science China Technological Sciences*, Vol. 59, (10), pp. 1475-1485, 2016. https://doi.org/10.1007/s11431-016-0373-x

[39] E. Bellos, C. Tzivanidis, and D. Tsimpoukis, "Multi-criteria evaluation of parabolic trough collector with internally finned absorbers", *Applied Energy*, Vol. 205, pp. 540-561, 2017. https://doi.org/10.1016/j.apenergy.2017.07.141

[40] E. Bellos, I. Daniil, and C. Tzivanidis, "Multiple cylindrical inserts for parabolic trough solar collector", *Applied Thermal Engineering*, Vol. 143, pp. 80-89, 2018. https://doi.org/10.1016/j.applthermaleng.2018.07.086

[41] C. Chang, A. Sciacovelli, Z. Wu, X. Li, Y. Li, M. Zhao, J. Deng, Z. Wang, and Y. Ding, "Enhanced heat transfer in a parabolic trough solar receiver by inserting rods and using molten salt as heat transfer fluid", *Applied Energy*, Vol. 220, pp. 337-350, 2018. https://doi.org/10.1016/j.apenergy.2018.03.091

[42] P. Liu, N. Zheng, Z. Liu, and W. Liu, "Thermal-hydraulic performance and entropy generation analysis of a parabolic trough receiver with conical strip inserts", *Energy conversion and management*, Vol. 179, pp. 30-45, 2019. https://doi.org/10.1016/j.enconman.2018.10.057

[43] A. Laaraba and G. Mebarki, "Enhancing thermal performance of a parabolic trough collector with inserting longitudinal fins in the down half of the receiver tube", *Journal of Thermal Science*, Vol. 29, (5), pp. 1309-1321, 2020. https://doi.org/10.1007/s11630-020-1256-8

[44] A. S. Tanious and A. A. Abdel-Rehim, "Numerical investigation of the thermal performance of an axially rotating internally finned receiver tube of a parabolic trough concentrator", *WSEAS Transactions on Power Systems*, Vol. 16, pp. 241-253, 2021. https://doi.org/10.37394/232016.2021.16.25

[45] B. Agagna, O. Behar, and A. Smaili, "Thermal performance enhancement in parabolic trough solar collectors by using an absorber tube with spherical pins", *Energy Sources, Part A: Recovery, Utilization, and Environmental Effects*, Vol. 44, (3), pp. 8161-8183, 2022. https://doi.org/10.1080/15567036.2022.2120578

[46] M. Fatouh, N. Saad, and A. M. Abdala, "Effects of Fins Base Rounding on Heat Transfer Characteristics of Absorber Tube of Parabolic Trough Collector", *Arabian Journal for Science and Engineering*, Vol. 48, (3), pp. 2851–2871, 2022. https://doi.org/10.1007/s13369-022-06948-6

[47] B. Darbari, M. Derikvand, and B. Shabani, "Thermal performance improvement of a LS-2 parabolic trough solar collector using porous disks", *Applied Thermal Engineering*, Vol. 228, 120546, 2023. https://doi.org/10.1016/j.applthermaleng.2023.120546

[48] K. Reddy, K. R. Kumar, and C. Ajay, "Experimental investigation of porous disc enhanced receiver for solar parabolic trough collector", *Renewable Energy*, Vol. 77, pp. 308-319, 2015. https://doi.org/10.1016/j.renene.2014.12.016

[49] B. Kalidasan, R. Shankar, and T. Srinivas, "Absorber tube with internal hinged blades for solar parabolic trough collector", presented at the *5th International Conference on Advances in Energy Research, ICAER 2015*, Mumbai, India, Energy Procedia, Vol. 90, pp. 463-469, 2016. https://doi.org/10.1016/j.egypro.2016.11.213

[50] M. Okour and M. Q. Al-Odat, "Experimental investigation of solar parabolic trough collector with a helical coil receiver under Jordan climate conditions", *International Journal of Engineering &Technology*, Vol. 7, (4), pp. 6415-6420, 2018. https://doi.org/10.14419/ijet.v7i4.20476

[51] S. J. Kutbudeen, M. Arulprakasajothi, N. Beemkumar, and K. Elangovan, "Effect of conical strip inserts in a parabolic trough solar collector under turbulent flow", *Energy Sources, Part A: Recovery, Utilization, and Environmental Effects*, Vol. 44, (1), pp. 2556-2568, 2019. https://doi.org/10.1080/15567036.2019.1650850

[52] R. S. Isravel, M. Raja, S. Saravanan, and V. Vijayan, "Thermal augmentation in parabolic trough collector solar water heater using rings attached twisted tapes", presented at the *International Conference on Recent Trends in Nanomaterials for Energy, Environmental and Engineering Applications*, Materials Today: proceedings, Vol. 21, (1), pp. 127-129, 2020. https://doi.org/10.1016/j.matpr.2019.05.375

[53] S. Naif, S. Mutlag, W. Khalil, and H. Dawooda, "Experimental Study of Parabolic Trough Receiver with Perforated Twisted Tape Insert Using Fuzzy Model Analysis", *Anbar Journal of Engineering Sciences*, Vol. 12, (2), pp. 130-138, 2021. https://doi.org/10.37649/AENGS.2021.171170

[54] S. Thapa, S. Samir, and K. Kumar, "Performance evaluation of solar parabolic trough receiver using multiple twisted tapes with circular perforation and delta winglet", *Proceedings of the Institution of Mechanical Engineers, Part E: Journal*

of Process Mechanical Engineering, Vol. 236, (4), pp. 1296-1307, 2022. https://doi.org/10.1177/09544089211059320

[55] D. M. Muter and M. B. Al-Hadithi, "Numerical Investigation of Heat Transfer Enhancement in Parabolic Trough Solar Collector with Twisted Tape Insert", *Global Scientific Journal of Mechanical Engineering*, Vol. 1, (1), pp. 1-15, 2021. https://www.researchgate.net/profile/Mustafa-Al-Hadithi/publication/349324480

[56] A. N. Özakın, "EXPERIMENTAL AND NUMERICAL INVESTIGATION OF USING SEMICIRCULAR ROTATING TURBULATORS FOR HEAT TRANSFER AUGMENTATION IN THE PARABOLIC TROUGH SOLAR COLLECTOR", *Heat Transfer Research*, Vol. 53, (15), pp. 1-16, 2022. http://dx.doi.org/10.1615/HeatTransRes.2022043218

[57] B. Stanek, J. Ochmann, D. Węcel, and Ł. Bartela, "Study of Twisted Tape Inserts Segmental Application in Low-Concentrated Solar Parabolic Trough Collectors", *Energies*, Vol. 16, (9), p. 3716, 2023. https://doi.org/10.3390/en16093716

[58] D. G. Ullman, *The mechanical design process*, 4th ed., NewYork, USA: McGraw-Hill, 2003.

[59] E. Lüpfert, M. Geyer, W. Schiel, A. Esteban, R. Osuna, E. Zarza, and P. Nava, "Eurotrough design issues and prototype testing at PSA", in *International Solar Energy Conference*, Washington, DC, American Society of Mechanical Engineers, Vol. 16702, pp. 387-391, 2001. https://doi.org/10.1115/SED2001-149

[60] F. Cabrera, A. Fernández-García, R. Silva, and M. Pérez-García, "Use of parabolic trough solar collectors for solar refrigeration and air-conditioning applications", *Renewable and sustainable energy reviews*, Vol. 20, pp. 103-118, 2013. https://doi.org/10.1016/j.rser.2012.11.081

[61] B. Zou, J. Dong, Y. Yao, and Y. Jiang, "An experimental investigation on a small-sized parabolic trough solar collector for water heating in cold areas", *applied energy*, Vol. 163, pp. 396-407, 2016. http://dx.doi.org/10.1016/j.apenergy.2015.10.186

[62] J. Nilsson, H. Håkansson, and B. Karlsson, "Electrical and thermal characterization of a PV-CPC hybrid", *Solar Energy*, Vol. 81, (7), pp. 917-928, 2007. https://doi.org/10.1016/j.solener.2006.11.005

[63] W. Fuqiang, T. Zhexiang, G. Xiangtao, T. Jianyu, H. Huaizhi, and L. Bingxi, "Heat transfer performance enhancement and thermal strain restrain of tube receiver for parabolic trough solar collector by using asymmetric outward convex corrugated tube", *Energy*, Vol. 114, pp. 275-292, 2016. http://dx.doi.org/10.1016/j.energy.2016.08.013

[64] H. M. Şahin, E. Baysal, A. R. Dal, and N. Şahin, "Investigation of heat transfer enhancement in a new type heat exchanger using solar parabolic trough systems", *International journal of hydrogen energy*, Vol. 40, (44), pp. 15254-15266, 2015. https://doi.org/10.1016/j.ijhydene.2015.03.009

[65] J. A. Duffie, W. A. Beckman, and N. Blair, *Solar engineering of thermal processes, photovoltaics and wind*, 5 th ed., New Jersey, USA: John Wiley & Sons, 2020.

[66] J. T. Mahdi and Y. A. Jebbar, "A theoretical investigation of solar radiation and heat transfer in a solar pond in Karbala city", in *AIP Conference Proceedings*, AIP Publishing LLC, Vol. 2144, p. 030019, 2019. https://doi.org/10.1063/1.5123089

[67] D. Y. Goswami, *Principles of solar engineering*, 4th ed., Boca Raton, USA: CRC press, 2022.

[68] P. I. Cooper, "The absorption of radiation in solar stills", *Solar energy*, Vol. 12, (3), pp. 333-346, 1969. https://doi.org/10.1016/0038-092X(69)90047-4

[69] J. E. Braun and J. C. Mitchell, "Solar geometry for fixed and tracking surfaces", *Solar energy*, Vol. 31, (5), pp. 439-444, 1983. https://doi.org/10.1016/0038-092X(83)90046-4

[70] S. García-Cortés, A. Bello-García, and C. Ordóñez, "Estimating intercept factor of a parabolic solar trough collector with new supporting structure using off-the-shelf photogrammetric equipment", *Applied Energy*, Vol. 92, pp. 815-821, 2012. https://doi.org/10.1016/j.apenergy.2011.08.032

[71] A. Kasaeian, S. Daviran, R. D. Azarian, and A. Rashidi, "Performance evaluation and nanofluid using capability study of a solar parabolic trough collector", *Energy*

conversion and management, Vol. 89, pp. 368-375, 2015. http://dx.doi.org/10.1016/j.enconman.2014.09.056

[72] A. Menbari, A. A. Alemrajabi, and A. Rezaei, "Experimental investigation of thermal performance for direct absorption solar parabolic trough collector (DASPTC) based on binary nanofluids", *Experimental Thermal and Fluid Science*, Vol. 80, pp. 218-227, 2017. https://doi.org/10.1016/j.expthermflusci.2016.08.023

[73] B. A. Sup, M. F. Zainudin, T. Z. S. Ali, R. A. Bakar, and G. L. Ming, "Effect of rim angle to the flux distribution diameter in solar parabolic dish collector", *Energy procedia*, Vol. 68, pp. 45-52, 2015. https://doi.org/10.1016/j.egypro.2015.03.231

[74] N. S. Ganesh and T. Srinivas, "Design and modeling of low temperature solar thermal power station", *Applied energy*, Vol. 91, (1), pp. 180-186, 2012. https://doi.org/10.1016/j.apenergy.2011.09.021

[75] A. J. Abdulhamed, N. M. Adam, M. Z. A. Ab-Kadir, and A. A. Hairuddin, "Flow and Thermal Mechanisms in Receiver Tube of Parabolic Trough Collectors with Rings Axially Connected Together and Radially Connected to the Inner Tube Surface", *Journal of Engineering and Applied Sciences*, Vol. 15, (3), pp. 762-772, 2020. https://doi.org/10.36478/jeasci.2020.762.772

[76] B. Shaker, M. Gholinia, M. Pourfallah, and D. Ganji, "CFD analysis of Al2O3-syltherm oil Nanofluid on parabolic trough solar collector with a new flange-shaped turbulator model", *Theoretical and Applied Mechanics Letters*, Vol. 12, (2), p. 100323, 100323, 2022. https://doi.org/10.1016/j.taml.2022.100323

[77] S. Samiezadeh, R. Khodaverdian, M. H. Doranehgard, H. Chehrmonavari, and Q. Xiong, "CFD simulation of thermal performance of hybrid oil-Cu-Al2O3 nanofluid flowing through the porous receiver tube inside a finned parabolic trough solar collector", *Sustainable Energy Technologies and Assessments*, Vol. 50, p. 101888, 2022. https://doi.org/10.1016/j.seta.2021.101888

[78] A. Inc, "ANSYS Fluent User ' s Guide.," 2015.

[79] S. Said, S. Mellouli, T. Alqahtani, S. Algarni, and R. Ajjel, "New Evacuated Tube Solar Collector with Parabolic Trough Collector and Helical Coil Heat Exchanger

for Usage in Domestic Water Heating", *Sustainability*, Vol. 15, (15), p. 11497, 2023. https://doi.org/10.3390/su151511497

[80] M. R. Haddouche, "Numerical investigation of an enhanced PTC absorber tube using cylindrical inserts", *Heat Transfer*, Vol. 52, (6), pp. 3967-3988, 2023. https://doi.org/10.1002/htj.22861

[81] T. Fahim, S. Laouedj, A. Abderrahmane, Z. Driss, E. S. M. Tag-ElDin, K. Guedri, and O. Younis, "Numerical study of perforated obstacles effects on the performance of solar parabolic trough collector", *Frontiers in Chemistry*, Vol. 10, p. 1089080, 2023. https://doi.org/10.3389/fchem.2022.1089080

[82] O. Behar, A. Khellaf, and K. Mohammedi, "A novel parabolic trough solar collector model–Validation with experimental data and comparison to Engineering Equation Solver (EES)", *Energy Conversion and Management*, Vol. 106, pp. 268-281, 2015. https://doi.org/10.1016/j.enconman.2015.09.045

[83] K. A. Ahmed and E. Natarajan, "Thermal performance enhancement in a parabolic trough receiver tube with internal toroidal rings: A numerical investigation", *Applied Thermal Engineering*, Vol. 162, p. 114224, 2019. https://doi.org/10.1016/j.applthermaleng.2019.114224

[84] R. Roohi, A. Arya, M. Akbari, and M. J. Amiri, "Performance Evaluation of an Absorber Tube of a Parabolic Trough Collector Fitted with Helical Screw Tape Inserts Using CuO/Industrial-Oil Nanofluid: A Computational Study", *Sustainability*, Vol. 15, (13), p. 10637, 10637, 2023. https://doi.org/10.3390/su151310637

[85] A. Bejan and A. D. Kraus, *Heat transfer handbook*, 1 st ed., United States of America: John Wiley & Sons, 2003.

[86] S. Kakaç, H. Liu, and A. Pramuanjaroenkij, *Heat exchangers: selection, rating, and thermal design*, 2nd ed., Boca Raton, US: CRC press, 2002.

[87] J. P. Holman, *Heat transfer*: McGraw Hill Higher Education, 2010.

[88] E. Bellos and C. Tzivanidis, "Alternative designs of parabolic trough solar collectors", *Progress in Energy and Combustion Science*, Vol. 71, pp. 81-117, 2019. https://doi.org/10.1016/j.pecs.2018.11.001

[89] F. W. Dittus and L. M. K. Boelter, "Heat transfer in automobile radiators of the tubular type", *International communications in heat and mass transfer,* Vol. 12, (1), pp. 3-22, 1985. https://doi.org/10.1016/0735-1933(85)90003-X

[90] A. Standard, "Methods of testing to determine the thermal performance of solar collectors", *American Society of Heating,* pp. 93-77, 1977

[91] S. M. Jeter, "Optical and Thermal Effects in Linear Solar Concentrating Collectors", Ph.D Thesis, Department of Mechanical Engineering, Georgia Institute of Technology, England, 1979.

[92] S. A. Kalogirou, "A detailed thermal model of a parabolic trough collector receiver", *Energy,* Vol. 48, (1), pp. 298-306, 2012. https://doi.org/10.1016/j.energy.2012.06.023

[93] H. F. A. Hassan, "Experimental study and evaluation of single slope solar still combined with parabolic trough using nanofluid", M.Sc., Mechanical engineering, Al-Furat Al-Awsat Technical University, Iraq, Najaf, 2022.

[94] J. Madiouli, C. A. Saleel, A. Lashin, I. A. Badruddin, and A. Kessentini, "An experimental analysis of single slope solar still integrated with parabolic trough collector and packed layer of glass balls", *Journal of Thermal Analysis and Calorimetry,* Vol. 146, pp. 2655-2665, 2021. https://doi.org/10.1007/s10973-020-10320-x

[95] H. Hassan, M. S. Ahmed, M. Fathy, and M. S. Yousef, "Impact of salty water medium and condenser on the performance of single acting solar still incorporated with parabolic trough collector", *Desalination,* Vol. 480, p. 114324, 2020. https://doi.org/10.1016/j.desal.2020.114324

[96] A. Kabeel and M. Abdelgaied, "Observational study of modified solar still coupled with oil serpentine loop from cylindrical parabolic concentrator and phase changing material under basin", *Solar Energy,* Vol. 144, pp. 71-78, 2017. https://doi.org/10.1016/j.solener.2017.01.007

A. APPENDIX (A): The properties of air at atmosphere pressure

T (K)	ρ (kg/m^3)	c_p (kJ/kg.K)	$\mu\times10^{-5}$ (kg/m.s)	$\nu\times10^{6}$ (m^2/s)	k (W/m.K)	Pr
250	1.4128	1.0053	1.599	11.31	0.02227	0.722
300	1.1774	10.0057	1.8462	15.69	0.02624	0.708
350	0.9980	1.0090	2.075	20.76	0.03003	0.697
400	0.8826	1.0140	2.286	25.9	0.03365	0.689
450	0.7833	1.0207	2.484	31.71	0.03707	0.683
500	0.7048	1.0295	2.671	37.90	0.04038	0.680
550	0.6423	1.0392	2.848	44.34	0.04360	0.680

B. APPENDIX (B): The result of thermo-hydraulic performance for investagted paramperts of cylindrical turbulator PTR at mass flow rate of 1.0 k/s

Case	*l (mm)*	*t (mm)*	*N*	*h* ($W/m^2.K^4$)	*Δp (pas)*	*Nu*	*f*	*ΔNu*	*Δf*	*PEC*
plain tube	0	0	0	1437.73	5737.9	133	0.0502	1	1	1
1	10	1	5	1228.50	6349.3	113.65	0.0525	0.850	1.107	0.82
2	10	1	10	1257.41	6362.0	116.32	0.0527	0.870	1.109	0.84
3	10	1	15	1271.86	6374.8	117.66	0.0528	0.880	1.111	0.85
4	10	1	20	1286.31	6948.6	118.99	0.0529	0.890	1.211	0.84
5	10	2	5	1286.31	6000.7	118.99	0.0530	0.890	1.046	0.88
6	10	2	10	1329.67	6012.7	123.00	0.0531	0.920	1.048	0.91
7	10	2	15	2139.04	6024.8	197.88	0.0532	1.480	1.050	1.46
8	10	2	20	2153.49	9238.0	199.21	0.0533	1.490	1.610	1.27
9	10	3	5	2167.95	9639.6	200.55	0.0534	1.500	1.680	1.26
10	10	3	10	2182.40	10213.4	201.89	0.0535	1.510	1.780	1.25
11	10	3	15	2189.62	10442.9	202.56	0.0536	1.515	1.820	1.24
12	10	3	20	2196.85	10901.9	203.22	0.0537	1.520	1.900	1.23
13	10	4	5	2211.30	11188.8	204.56	0.0538	1.530	1.950	1.23
14	10	4	10	2225.76	11475.7	205.90	0.0539	1.540	2.000	1.23
15	10	4	15	2240.21	12049.5	207.24	0.0540	1.550	2.100	1.21
16	10	4	20	2254.66	12336.4	208.57	0.0541	1.560	2.150	1.21
17	20	1	5	2186.83	9089.1	202.30	0.0543	1.513	1.584	1.30
18	20	1	10	2211.40	9107.4	204.57	0.0544	1.530	1.587	1.31
19	20	1	15	2236.25	9125.6	206.87	0.0545	1.547	1.590	1.33
20	20	1	20	2247.44	10041.3	207.90	0.0546	1.555	1.750	1.29
21	20	2	5	2261.37	9143.9	209.19	0.0547	1.565	1.594	1.34
22	20	2	10	2286.78	9162.2	211.54	0.0548	1.582	1.597	1.36
23	20	2	15	2312.48	9180.6	213.92	0.0549	1.600	1.600	1.37
24	20	2	20	2326.93	9467.5	215.26	0.0550	1.610	1.650	1.36
25	20	3	5	2160.06	6118.0	199.82	0.0551	1.495	1.066	1.46
26	20	3	10	2184.33	6130.3	202.07	0.0552	1.511	1.068	1.48
27	20	3	15	2208.88	6142.6	204.34	0.0554	1.528	1.071	1.49
28	20	3	20	2233.69	6154.9	206.63	0.0555	1.545	1.073	1.51
29	20	4	5	2233.69	6154.9	206.63	0.0556	1.545	1.073	1.51
30	20	4	10	2258.79	6167.2	208.95	0.0557	1.563	1.075	1.53
31	20	4	15	2284.17	6179.6	211.30	0.0558	1.580	1.077	1.54
32	20	4	20	2298.02	6541.2	212.58	0.0559	1.590	1.140	1.52
33	30	1	5	2309.84	6192.0	213.68	0.0560	1.598	1.079	1.56
34	30	1	10	2335.79	6204.4	216.08	0.0561	1.616	1.081	1.57
35	30	1	15	2362.03	6216.8	218.50	0.0562	1.634	1.083	1.59
36	30	1	20	2376.07	6541.2	219.80	0.0564	1.644	1.140	1.57

Case	*l* (mm)	*t* (mm)	*N*	*h* ($W/m^2.K^4$)	*Δp* (pas)	*Nu*	*f*	*ΔNu*	*Δf*	*PEC*
37	30	2	5	2388.57	6229.3	220.96	0.0565	1.653	1.086	1.61
38	30	2	10	2415.41	6241.8	223.44	0.0566	1.671	1.088	1.63
39	30	2	15	2442.55	6254.3	225.95	0.0567	1.690	1.090	1.64
40	30	2	20	2457.00	6541.2	227.29	0.0568	1.700	1.140	1.63
41	30	3	5	2114.74	5816.1	195.63	0.0569	1.463	1.014	1.46
42	30	3	10	2138.50	5827.8	197.83	0.0570	1.480	1.016	1.47
43	30	3	15	2162.53	5839.4	200.05	0.0572	1.496	1.018	1.49
44	30	3	20	2183.84	6082.1	202.02	0.0252	1.511	1.060	1.48
45	30	4	5	2186.83	5851.1	202.30	0.0279	1.513	1.020	1.50
46	30	4	10	2211.40	5862.9	204.57	0.0279	1.530	1.022	1.52
47	30	4	15	2236.25	5874.6	206.87	0.0280	1.547	1.024	1.54
48	30	4	20	2241.66	5967.4	207.37	0.0305	1.551	1.040	1.53
49	40	1	5	2261.37	5886.4	209.19	0.0264	1.565	1.026	1.55
50	40	1	10	2286.78	5898.2	211.54	0.0264	1.582	1.028	1.57
51	40	1	15	2312.48	5910.0	213.92	0.0265	1.600	1.030	1.58
52	40	1	20	2319.70	5967.4	214.59	0.0406	1.605	1.040	1.58
53	40	2	5	2312.48	5852.6	213.92	0.0423	1.600	1.020	1.59
54	40	2	10	2442.55	6024.8	225.95	0.0449	1.690	1.050	1.66
55	40	2	15	2587.08	6311.6	239.32	0.0459	1.790	1.100	1.73
56	40	2	20	2659.35	7000.2	246.01	0.0479	1.840	1.220	1.72
57	40	3	5	2544.04	7057.6	235.34	0.0491	1.760	1.230	1.64
58	40	3	10	2572.63	6928.9	237.99	0.0504	1.780	1.208	1.67
59	40	3	15	2601.53	6942.8	240.66	0.0529	1.800	1.210	1.69
60	40	3	20	2615.99	7172.3	242.00	0.0542	1.810	1.250	1.68
61	40	4	5	2558.18	7057.6	236.65	0.0399	1.770	1.230	1.65
62	40	4	10	2586.92	7387.0	239.31	0.0400	1.790	1.287	1.65
63	40	4	15	2615.99	7401.8	242.00	0.0401	1.810	1.290	1.66
64	40	4	20	2623.21	7631.4	242.67	0.0441	1.815	1.330	1.65
65	50	1	5	2460.18	6532.8	227.58	0.0402	1.702	1.139	1.63
66	50	1	10	2487.82	6545.9	230.14	0.0402	1.721	1.141	1.65
67	50	1	15	2515.78	6559.0	232.73	0.0403	1.741	1.143	1.67
68	50	1	20	2544.04	6828.1	235.34	0.0416	1.760	1.190	1.66
69	50	2	5	2544.04	6572.2	235.34	0.0269	1.760	1.145	1.68
70	50	2	10	2572.63	6585.3	237.99	0.0269	1.780	1.148	1.70
71	50	2	15	2601.53	6598.5	240.66	0.0270	1.800	1.150	1.72
72	50	2	20	2615.99	6770.7	242.00	0.0270	1.810	1.180	1.71
73	50	3	5	2473.85	7057.6	228.85	0.0270	1.712	1.230	1.60
74	50	3	10	2501.64	6585.3	231.42	0.0271	1.731	1.148	1.65
75	50	3	15	2529.75	6598.5	234.02	0.0271	1.750	1.150	1.67
76	50	3	20	2550.95	6885.4	235.98	0.0287	1.765	1.200	1.66
77	50	4	5	2558.18	7057.6	236.65	0.0272	1.770	1.230	1.65
78	50	4	10	2586.92	6585.3	239.31	0.0272	1.790	1.148	1.71
79	50	4	15	2615.99	6598.5	242.00	0.0273	1.800	1.150	1.72

Case	*l* *(mm)*	*t* *(mm)*	*N*	*h* *($W/m^2.K^4$)*	*Δp* *(pas)*	*Nu*	*f*	*ΔNu*	*Δf*	*PEC*
80	50	4	20	2630.44	6885.4	243.33	0.0287	1.820	1.200	1.71

C. APPENDIX (C): The calculated data of solar radiation

Time	ω (degree)	θ_z (degree)	I_b (W/m^2)	I_{bt} (W/m^2)
5 October 2023 (N_d = 278, ϕ = 32.77°, δ = -5.793°, I_0 = 1370.3 W/m^2)				
9:00	-45	57.5	657.4	459
10:00	-30	47.95	733.5	628
11:00	-15	41.1	771.4	737
12:00	0	38.6	782.9	774
13:00	15	41.1	771.4	737
14:00	30	47.95	733.5	628
15:00	45	57.5	657.4	459
6 October 2023 (N_d = 279, ϕ = 32.77°, δ = -6.18°, I_0 = 1371 W/m^2)				
9:00	-45	58	655	457
10:00	-30	50.2	732	626
11:00	-15	41	770	735
12:00	0	39	782	772
13:00	15	41	770	735
14:00	30	50.2	732	626
15:00	45	58	655	457
18 October 2023 (N_d = 291, ϕ = 32.77°, δ = -10.69°, I_0 = 1380.2 W/m^2)				
9:00	-45	61.1	642.3	428
10:00	-30	52.0	710.0	597
11:00	-15	45.8	752.3	706
12:00	0	43.5	765.1	744
13:00	15	45.8	752.3	706
14:00	30	52.0	710.0	597
15:00	45	61.1	674.1	428
19 October 2023 (N_d = 292, ϕ = 32.77°, δ = -11.50°, I_0 = 1380.9 W/m^2)				
9:00	-45	61.3	621.6	425
10:00	-30	52.3	708.1	595
11:00	-15	46.1	750.7	704
12:00	0	43.8	763.6	742
13:00	15	46.1	760.4	704
14:00	30	52.3	708.1	595
15:00	45	61.3	621.6	425
16 January 2024 (N_d = 16, ϕ = 32.77°, δ = -21.10°, I_0 = 1410.4 W/m^2)				
9:00	-45	68.9	525.1	337
10:00	-30	61.0	638.6	504
11:00	-15	55.7	693.9	613
12:00	0	53.9	710.6	650
13:00	15	55.7	693.9	613
14:00	30	61.0	638.6	504
15:00	45	68.9	525.1	337

Time	ω (degree)	θ_z (degree)	I_b (W/m^2)	I_{bt} (W/m^2)
17 January 2024 (N_d = 17, ϕ = 32.77º, δ = -20.92º, I_0 = 1410.2 W/m^2)				
9:00	-45	68.6	527.4	339
10:00	-30	60.9	640.3	506
11:00	-15	55.6	695.4	615
12:00	0	53.7	712.0	652
13:00	15	55.6	697.4	615
14:00	30	60.9	640.3	506
15:00	45	68.6	527.4	339
25 March 2024 (N_d = 85, ϕ = 32.77º, δ = 1.61º, I_0 = 1371.8 W/m^2)				
9:00	-45	52.4	702.6	497
10:00	-30	42.0	767.9	665
11:00	-15	34.2	800.9	773
12:00	0	31.2	810.9	811
13:00	15	34.2	800.9	773
14:00	30	42.0	767.9	665
15:00	45	52.4	702.6	497
26 March 2024 (N_d = 86, ϕ = 32.77º, δ = 2.02º, I_0 = 1371.1 W/m^2)				
9:00	-45	52.2	704.3	498
10:00	-30	41.7	769.0	666
11:00	-15	33.8	801.7	774
12:00	0	30.8	811.7	812
13:00	15	33.8	801.7	774
14:00	30	41.7	769.0	666
15:00	45	52.2	704.3	498
27 March 2024 (N_d = 86, ϕ = 32.77º, δ = 2.42º, I_0 = 1370.3 W/m^2)				
9:00	-45	51.9	705.9	499
10:00	-30	41.4	770.1	667
11:00	-15	33.5	802.5	775
12:00	0	30.4	812.5	813
13:00	15	33.5	802.5	775
14:00	30	41.4	770.1	667
15:00	45	51.9	705.9	499
15 April 2024 (N_d = 106, ϕ = 32.77º, δ = 9.78º, I_0 = 1355.7 W/m^2)				
9:00	-45	47.3	729	514
10:00	-30	35.9	785	676
11:00	-15	26.8	813	780
12:00	0	23.0	822	816
13:00	15	26.8	813	780
14:00	30	35.9	785	676
15:00	45	47.3	729	514
16 April 2024 (N_d = 107, ϕ = 32.77º, δ = 10.15º, I_0 = 1354.9 W/m^2)				
9:00	-45	47.1	731	514

Time	ω (degree)	θ_z (degree)	I_b (W/m^2)	I_{bt} (W/m^2)
10:00	-30	36	786	676
11:00	-15	27	814	780
12:00	0	23	822	816
13:00	15	27	814	780
14:00	30	36	786	676
15:00	45	47	731	514
17 April 2024 (N_d = 108, ϕ = 32.77º, δ = 10.51º, I_0 = 1354.0 W/m^2)				
9:00	-45	47	732	515
10:00	-30	35	787	677
11:00	-15	26	815	781
12:00	0	22	823	817
13:00	15	26	815	781
14:00	30	35	787	677
15:00	45	47	732	515
5 May 2024 (N_d = 126, ϕ = 32.77º, δ = 10.51º, I_0 = 1354.0 W/m^2)				
9:00	-45	44	743	513
10:00	-30	32	792	668
11:00	-15	21	817	767
12:00	0	16	825	802
13:00	15	21	817	767
14:00	30	32	792	668
15:00	45	44	743	513
6 May 2024 (N_d = 127, ϕ = 32.77º, δ = 16.7º, I_0 = 1341.0 W/m^2)				
9:00	-45	43	744	514
10:00	-30	31	794	670
11:00	-15	20	818	768
12:00	0	15	826	803
13:00	15	20	818	768
14:00	30	31	794	670
15:00	45	43	744	514
7 May 2024 (N_d = 128, ϕ = 32.77º, δ = 16.97º, I_0 = 1340.0 W/m^2)				
9:00	-45	42	745	515
10:00	-30	30	795	671
11:00	-15	19	819	769
12:00	0	14	827	804
13:00	15	19	819	769
14:00	30	30	795	671
15:00	45	42	745	515

D. APPENDIX (D): The outlet water temperature from CFD and experimental work

Time	Numericaly		Experimentaly	
	T_{fo} (ºC)			
	Plain tube	Modified PTR	Plain tube	Modified PTR
5 October 2023				
9:00	34.0	34.0	34.0	34.0
10:00	37.0	39.4	36.5	39.5
11:00	41.0	55	40.5	52
12:00	45	56	44	54
13:00	42	56	41	54
14:00	39	55	37	52
15:00	36	44	35.5	42
6 October 2023				
9:00	33	33	33	33
10:00	36.4	40	35.5	39.2
11:00	40.5	52.5	39	50
12:00	42	53	41.5	51
13:00	42	52	40	50
14:00	39	48	37	45
15:00	36	43	35	42
18 October 2023				
9:00	32.0	32.0	32.0	32.0
10:00	38.0	49.2	36.5	48.0
11:00	41	52	40.0	51
12:00	48	58.8	46	57.0
13:00	46.0	57.5	44	56
14:00	45	56	43	55
15:00	40	50	39.2	48.8
19 October 2023				
9:00	32	32	32	32
10:00	37.5	48.7	36.0	47.5
11:00	40.5	54	39	52
12:00	43.0	54	40.5	52.0
13:00	42	50	40	47.5
14:00	38	48	36	45
15:00	35	46	34	44
16 Junaury 2024				
9:00	18	18	18	18
10:00	23.5	28.7	23	28.0
11:00	30	42	28	40.5
12:00	34	46	32	44

Time	Numericaly		Experimentaly	
	T_{fo} (ºC)			
	Plain tube	Modified PTR	Plain tube	Modified PTR
13:00	38	45	36	42.5
14:00	33	40	31	38
15:00	30	38.8	29	37.2
17 January 2024				
9:00	18	18	18	18
10:00	23.5	28.7	22.5	28.0
11:00	27.5	40.5	26	39
12:00	31.0	41	30	39.5
13:00	31	41	30	39.5
14:00	28	39	27	37
15:00	27	38	26	36
25 March 2024				
9:00	28	35	27	33.4
10:00	35	45.5	34	44.0
11:00	40	52	39	51.2
12:00	42	55	41	52.3
13:00	41	54	40	53
14:00	39	52	38	50.1
15:00	37	49	36	47
26 March 2024				
9:00	29	29	29	29
10:00	35	40	34	38.4
11:00	41	54	40	52.5
12:00	45	56	44	54
13:00	42	55	41	53.5
14:00	39	51	37.8	49.7
15:00	36	45	35	43.7
27 March 2024				
9:00	29.5	29.5	29.5	29.5
10:00	35.5	40.5	34.5	39
11:00	41.5	56	40.5	54
12:00	45.5	56.5	44.1	55.8
13:00	41	54	40	52
14:00	38	50.5	37	48.2
15:00	35	46	34	42
15 April 2024				
9:00	32	32	32	32
10:00	41.5	43.5	41	42
11:00	50.5	56.5	50	55
12:00	55.5	58	54	57

Time	Numericaly		Experimentaly	
	T_{fo} (ºC)			
	Plain tube	Modified PTR	Plain tube	Modified PTR
13:00	49.5	57.5	49	55
14:00	40	50.5	39	49.5
15:00	33.5	37.5	33	36
16 April 2024				
9:00	32.5	32.5	32.5	32.5
10:00	42	44	41	43
11:00	51	57	50	54
12:00	56	58.8	54.5	58
13:00	50	58	49	56
14:00	41	51	40	49
15:00	34	38	33.2	36
17 April 2024				
9:00	33	33	33	33
10:00	42.5	45	41	43.5
11:00	51.5	58	50	57
12:00	57	60	56	59
13:00	51	60	50	58
14:00	42	51.5	41	50
15:00	35	38.5	34.5	37
5 May 2024				
9:00	34	34	34	34
10:00	43	45.5	42	44
11:00	53	60	52	58.8
12:00	57.8	61.5	56.5	59.5
13:00	51.2	60.4	50.2	58.7
14:00	42.5	53	42	52
15:00	35.5	39	35	37.8
6 May 2024				
9:00	35.5	35.5	35.5	35.5
10:00	43.2	46	42.5	44.5
11:00	53.8	61	53	59
12:00	58	62	57	60
13:00	52	61	50	59
14:00	43	54	42	52.0
15:00	36	40	35	38
7 May 2024				
9:00	36.0	36	36	36.0
10:00	44.0	47	43	46.0
11:00	55.0	62	53.5	60.0
12:00	60.0	64	57	61.5

Time	Numericaly		Experimentaly	
	T_{fo} (ºC)			
	Plain tube	Modified PTR	Plain tube	Modified PTR
13:00	54.0	63	51	60.5
14:00	45.0	55	42	52.0
15:00	37.0	42	35.8	39.0

E. APPENDIX (E): The calculated values

Time	Numericaly				Experimentaly			
	Q_{use} (W)		η (%)		Q_{use} (W)		η (%)	
	Plain tube	Modified PTR	Plain tube	Modified PTR	Plain tube	Modified PTR	Plain tube	Modified PTR
5 October 2023								
9:00	409.8	409.8	31%	31%	409.8	409.8	31%	31%
10:00	468.4	538.6	32%	37%	468.4	541.6	32%	37%
11:00	556.2	966.0	36%	63%	556.2	878.2	36%	57%
12:00	585.5	907.5	37%	58%	585.5	848.9	37%	54%
13:00	526.9	936.8	34%	61%	526.9	878.2	34%	57%
14:00	497.7	966.0	34%	66%	497.7	878.2	34%	60%
15:00	468.4	702.6	36%	53%	468.4	644.0	36%	49%
6 October 2023								
9:00	380.6	380.6	29%	29%	380.6	380.6	29%	29%
10:00	450.8	556.2	31%	38%	424.5	532.8	29%	36%
11:00	541.6	892.9	35%	58%	497.7	819.7	32%	53%
12:00	497.7	819.7	32%	52%	483.0	761.1	31%	49%
13:00	526.9	819.7	34%	53%	468.4	761.1	30%	49%
14:00	497.7	761.1	34%	52%	439.1	673.3	30%	46%
15:00	468.4	673.3	36%	51%	439.1	644.0	34%	49%
18 October 2023								
9:00	276.0	276.0	26%	26%	276.0	276.0	26%	26%
10:00	401.5	682.5	31%	53%	363.8	652.4	28%	51%
11:00	451.7	727.7	33%	52%	426.6	702.6	31%	51%
12:00	627.3	898.3	44%	63%	577.1	853.1	41%	60%
13:00	602.2	890.8	43%	64%	552.0	853.1	40%	61%
14:00	577.1	853.1	45%	67%	526.9	828.0	41%	65%
15:00	476.7	727.7	45%	69%	456.7	697.6	43%	66%
19 October 2023								
9:00	276.0	276.0	26%	26%	276.0	276.0	26%	26%
10:00	388.9	670.0	30%	52%	351.3	639.8	27%	50%
11:00	439.1	777.9	32%	56%	401.5	727.7	29%	52%
12:00	501.8	777.9	35%	55%	439.1	727.7	31%	51%
13:00	501.8	702.6	36%	50%	451.7	639.8	32%	46%
14:00	401.5	652.4	31%	51%	351.3	577.1	27%	45%
15:00	351.3	627.3	33%	59%	326.2	577.1	31%	55%
16 Janury 2024								
9:00	25.1	25.1	2%	2%	25.1	25.1	2%	2%
10:00	150.6	281.0	12%	22%	138.0	263.5	11%	21%
11:00	301.1	602.2	22%	43%	250.9	564.6	18%	41%

Time	Numericaly				Experimentaly			
	Q_{use} (W)		η (%)		Q_{use} (W)		η (%)	
	Plain tube	Modified PTR	Plain tube	Modified PTR	Plain tube	Modified PTR	Plain tube	Modified PTR
12:00	401.5	702.6	28%	49%	351.3	652.4	25%	46%
13:00	501.8	677.5	36%	49%	451.7	614.8	33%	44%
14:00	426.6	602.2	33%	47%	376.4	552.0	29%	43%
15:00	363.8	584.6	35%	56%	338.7	544.5	32%	52%
17 Januay 2024								
9:00	50.2	50.2	5%	5%	50.2	50.2	5%	5%
10:00	163.1	293.6	13%	23%	138.0	276.0	11%	22%
11:00	250.9	577.1	18%	41%	213.3	539.5	15%	39%
12:00	326.2	577.1	23%	41%	301.1	539.5	21%	38%
13:00	326.2	577.1	23%	41%	301.1	539.5	22%	39%
14:00	276.0	552.0	22%	43%	250.9	501.8	20%	39%
15:00	276.0	552.0	26%	52%	250.9	501.8	24%	48%
25 March 2024								
9:00	250.9	426.6	18%	30%	225.8	386.4	16%	27%
10:00	401.5	664.9	26%	43%	376.4	627.3	25%	41%
11:00	526.9	828.0	33%	52%	432.7	808.0	31%	50%
12:00	552.0	878.2	34%	54%	526.9	810.5	32%	50%
13:00	526.9	853.1	33%	53%	501.8	828.0	31%	52%
14:00	501.8	828.0	33%	54%	476.7	780.4	31%	51%
15:00	476.7	777.9	34%	55%	451.7	727.7	32%	52%
26 March 2024								
9:00	288.6	288.6	20%	20%	288.6	288.6	20%	20%
10:00	414.0	539.5	27%	35%	388.9	499.3	25%	32%
11:00	564.6	890.8	35%	56%	539.5	853.1	34%	53%
12:00	652.4	928.4	40%	57%	627.3	878.2	39%	54%
13:00	577.1	903.3	36%	56%	552.0	865.7	34%	54%
14:00	526.9	828.0	34%	54%	496.8	795.4	32%	52%
15:00	464.2	690.0	33%	49%	439.1	657.4	31%	47%
27 March 2024								
9:00	288.6	288.6	20%	20%	288.6	288.6	20%	20%
10:00	426.6	552.0	28%	36%	401.5	514.4	26%	33%
11:00	564.6	928.4	35%	58%	539.5	878.2	34%	55%
12:00	652.4	928.4	40%	57%	617.3	910.8	38%	56%
13:00	526.9	853.1	33%	53%	501.8	802.9	31%	50%
14:00	476.7	790.4	31%	51%	451.7	732.7	29%	48%
15:00	414.0	690.0	29%	49%	388.9	589.7	28%	42%
15April 2024								
9:00	380.6	380.6	26%	26%	380.6	380.6	26%	26%
10:00	644.0	702.6	41%	45%	629.4	658.7	40%	42%

Time	Numericaly				Experimentaly			
	Q_{use} (W)		η (%)		Q_{use} (W)		η (%)	
	Plain tube	Modified PTR	Plain tube	Modified PTR	Plain tube	Modified PTR	Plain tube	Modified PTR
11:00	892.9	1068.5	55%	66%	878.2	1024.6	54%	63%
12:00	1024.6	1097.8	62%	67%	980.7	1068.5	60%	65%
13:00	863.6	1097.8	53%	68%	848.9	1024.6	52%	63%
14:00	600.1	907.5	38%	58%	570.8	878.2	36%	56%
15:00	424.5	541.6	29%	37%	409.8	497.7	28%	34%
16April 2024								
9:00	395.2	395.2	27%	27%	395.2	395.2	27%	27%
10:00	658.7	717.2	42%	46%	629.4	687.9	40%	44%
11:00	907.5	1083.1	56%	67%	878.2	995.3	54%	61%
12:00	1039.2	1121.2	63%	68%	995.3	1097.8	61%	67%
13:00	878.2	1112.4	54%	68%	848.9	1053.9	52%	65%
14:00	629.4	922.1	40%	59%	600.1	863.6	38%	55%
15:00	439.1	556.2	30%	38%	415.7	497.7	28%	34%
17April 2024								
9:00	395.2	395.2	27%	27%	395.2	395.2	27%	27%
10:00	673.3	746.5	43%	47%	629.4	702.6	40%	45%
11:00	922.1	1112.4	57%	68%	878.2	1083.1	54%	66%
12:00	1068.5	1156.3	65%	70%	1039.2	1127.0	63%	68%
13:00	878.2	1141.7	54%	70%	848.9	1083.1	52%	66%
14:00	644.0	922.1	41%	59%	614.8	878.2	39%	56%
15:00	468.4	570.8	32%	39%	453.7	526.9	31%	36%
5 May 2024								
9:00	234.2	234.2	16%	16%	234.2	234.2	16%	16%
10:00	501.8	585.5	32%	37%	468.4	535.3	30%	34%
11:00	819.7	1053.9	50%	64%	786.2	1013.7	48%	62%
12:00	963.5	1087.3	58%	66%	920.0	1020.4	56%	62%
13:00	709.3	1017.1	43%	62%	675.8	960.2	41%	59%
14:00	451.7	802.9	29%	51%	434.9	769.5	27%	49%
15:00	217.5	334.6	15%	23%	200.7	294.4	14%	20%
6 May 2024								
9:00	284.4	284.4	19%	19%	284.4	284.4	19%	19%
10:00	508.5	602.2	32%	38%	485.1	552.0	31%	35%
11:00	829.7	1070.6	51%	65%	802.9	1003.7	49%	61%
12:00	953.5	1087.3	58%	66%	920.0	1020.4	56%	62%
13:00	736.0	1037.1	45%	63%	669.1	970.2	41%	59%
14:00	451.7	819.7	28%	52%	418.2	752.8	26%	47%
15:00	234.2	368.0	16%	25%	200.7	301.1	13%	20%
7 May 2024								
9:00	267.6	267.6	18%	18%	267.6	267.6	18%	18%

Time	Numericaly				Experimentaly			
	Q_{use} (W)		η (%)		Q_{use} (W)		η (%)	
	Plain tube	Modified PTR	Plain tube	Modified PTR	Plain tube	Modified PTR	Plain tube	Modified PTR
10:00	501.8	602.2	32%	38%	468.4	568.8	29%	36%
11:00	853.1	1087.3	52%	66%	802.9	1020.4	49%	62%
12:00	1003.7	1137.5	61%	69%	903.3	1053.9	55%	64%
13:00	769.5	1070.6	47%	65%	669.1	987.0	41%	60%
14:00	485.1	819.7	31%	52%	384.7	719.3	24%	45%
15:00	234.2	401.5	16%	27%	133.8	301.1	9%	20%

F. APPENDIX (F): Published papers

International Journal of Heat and Technology
Vol. 42, No. 3, June, 2024, pp. 924-932
Journal homepage: http://iieta.org/journals/ijht

Improvement of Heat Transfer in a Parabolic Trough Collector Receiver Tube with Hollow Cylindrical Inserts: A CFD Study

Yasser Abidnoor Jebbar[1,2*], Fadhil Khaddam Fluiful[2], Wisam J. Khudhayer[3], Nasser Ali Hasson[1], Ali Jaber Abdulhamed[3]

[1] Department of Electrical Techniques, Al-Mussaib Technical Institute, Al-Furat Al-Awsat Technical University, Babil 51007, Iraq
[2] Department of Physics, College of Science, University of Kerbala, Karbala 56001, Iraq
[3] Department of Energy Engineering, Collage of Engineering, Al-Musayab, University of Babylon, Babil 51007, Iraq

Corresponding Author Email: yasser.jebbar.ims@atu.edu.iq

https://doi.org/10.18280/ijht.420321

Received: 21 March 2024
Revised: 27 May 2024
Accepted: 13 June 2024
Available online: 27 June 2024

Keywords:
inserts, parabolic trough collector, heat exchanges, heat transfer enhancement, CFD

ABSTRACT

The thermal performance of a parabolic trough receiver (PTR) with hollow cylindrical inserts (HCIs) is numerically investigated. The HCIs are coupled in an axial manner and also radially joined to the interior of the PTR. Totally, eleven different internally hollow cylindrical receivers are examined and compared with the plain tube (PT). The lengths, thicknesses, and numbers of HCIs are tested at varied values, and all these tubes are examined under a constant inlet temperature of 300 K and mass flow rates in the range of 0.6-1.0 kg/s. ANSYS Fluent is the simulation software in this work. The developed model is validated with experimental correlations for PT case. The simulation findings demonstrated that the addition of HCIs may greatly enhance the uniformity of the temperature gradient between the wall of the PTR and the water. The optimum case of the HCIs has a length of 40 mm, a thickness of 2 mm, and a number of 15 inserts. This model recoded the higher ranges of Nusselt number (132-296), fraction factor (0.301-0.064), and thermal efficiency (41-79%). Also, the outlet temperatures of the PT and modified tube are increased from 300 K to 325.5 K and 339.7 K, respectively. As a result, this approach provides advantages over the utilization of interior fins, as it can be applied on the parabolic trough collector (PTC) without requiring any modifications to the PTR, which are associated with numerous operational challenges.

1. INTRODUCTION

Improving the thermal conductivity between a heat transfer fluid (HTF) and a parabolic trough receiver (PTR) is important for many uses, such as making energy [1], desalination [2], cooling [3], and more. Generally, three techniques are used to improve heat transfer between the HTF and the PTR: active, passive, and compound techniques (active and passive). Furthermore, these techniques are designed to minimize the temperature variation inside the PTR to mitigate thermal stresses and, subsequently, decrease the likelihood of failure. An active technique is needed for an external energy source to enhance heat transfer in a PTR. In contrast, a passive technique involves altering the configuration of thermal systems in order to enhance their thermal performance without requiring the use of external energy sources. The compound techniques mix two first techniques: active-active, active-passive, or passive-passive [4].

Broadly, passive techniques are the most commonly used techniques for enhancing the heat transfer rate (Nusselt number) and pressure drop (fraction factor) inside the PTR. Therefore, numerous researchers have extensively studied these techniques to comprehend their mechanisms.

Several experts have conducted numerical studies on the twisted-tape inserts. Ghadirijafarbeigloo et al. [5] investigated the effect of introducing louvered twisted-tape inside a PTR. The results revealed that, in comparison to the plain tube (PT) case, the Nusselt number (Nu) and friction factor (f) factors are 3.5 and 4.1, respectively, while the thermal enhancement factor (TEF) reaches 2.26. Chang et al. [6] analyzed the effect of varying clearness ratios and twisted ratios of twisted-tapes on (Nu) and (f) inside the PTR. The results showed that the maximum factors of the Nu and f can be 2.9 and 2.5 times greater than in the PT. Abbas et al. [7] used twisted-tapes with six different inclination angles inside the PTR. They found the thermal performance increased, especially when the inclination angle was 50°.

Also, a wide group of researchers has also studied the use of the fins inside the PTR to enhance thermal performance. Bellos et al. [8] examined how the length and thickness of longitudinal fins affect the increase of Nu and f within the PTR. In the optimal case, the thermal efficiency reached 68.8%, and the enhancements in Nu and f are 1.652 and 2.00, respectively, compared with the PT case. Laaraba and Mebraki [9] carried out a numerical calculation to ascertain the optimal number, length, and thickness of fins attached to the lower half of the

Fluid Dynamics &
Materials Processing

Tech Science Press

DOI: 10.32604/fdmp.2024.050753

ARTICLE

Heat Transfer Enhancement of the Absorber Tube in a Parabolic Trough Solar Collector through the Insertion of Novel Cylindrical Turbulators

Yasser Jebbar[1,2,*], Fadhil Fluiful[2] and Wisam Khudhayer[3]

[1]Department of Electrical Techniques, Al-Mussaib Technical Institute, Al-Furat Al-Awsat Technical University, Babil, Iraq

[2]Department of Physics, Collage of Science, University of Kerbala, Karbala, Iraq

[3]Department of Energy Engineering, Collage of Engineering/Al-Musayab, University of Babylon, Babil, Iraq

[*]Corresponding Author: Yasser Jebbar. Email: yasser.jebbar.ims@atu.edu.iq

Received: 16 February 2024 Accepted: 30 April 2024 Published: 27 June 2024

ABSTRACT

This study includes an experimental and numerical analysis of the performances of a parabolic trough collector (PTC) with and without cylindrical turbulators. The PTC is designed with dimensions of 2.00 m in length and 1.00 m in width. The related reflector is made of lined sheets of aluminum, and the tubes are made of stainless steel used for the absorption of heat. They have an outer diameter of 0.051 m and a wall thickness of 0.002 m. Water, used as a heat transfer fluid (HTF), flows through the absorber tube at a mass flow rate of 0.7 kg/s. The dimensions of cylindrical turbulators are 0.04 m in length and 0.047 m in diameter. Simulations are performed using the ANSYS Fluent 2020 R2 software. The PTC performance is evaluated by comparing the experimental and numerical outcomes, namely, the outlet temperature, useful heat, and thermal efficiency for a modified tube (MT) (tube with novel cylindrical turbulators) and a plain tube (PT) (tube without novel cylindrical turbulators). According to the results, the experimental outlet temperatures recorded 63.2°C and 50.5°C for the MT and PT, respectively. The heat gain reaches 1137.5 W in the MT and 685.8 W in the PT. Compared to the PT collector, the PTC exhibited a (1.64 times) higher efficiency.

KEYWORDS

Parabolic trough collector; turbulators; absorber tube; ANSYS; thermal efficiency

Nomenclature

A_a	Area of reflector (m^2)
A_L	The altitude of location above mean sea level (km)
a_0	Constant
a_1	Constant
c_p	Specific heat capacity of fluid (J/Kg.°C)
D_{S-E}	The mean distance between the sun and earth (m)
d_o	Outer diameter of the tube (m)
f_L	Focal length of receiver tube (m)
I_0	Extraterrestrial solar radiation (W/m^2)
I_b	Beam radiation (W/m^2)

الخلاصة

الماء ضروري لبقاء الإنسان؛ إذ يستهلك الأفراد (10-30 لتراً) من الماء النظيف يوميًا للشرب والطهي والأنشطة المنزلية الأخرى. فالمياه الملوثة ليست غير صحية فحسب، بل إنها أيضًا خطيرة على صحة الإنسان. الهدف الرئيسي من هذه الدراسة هو التحقيق في هذه المشكلة وتحسين إنتاجية المياه العذبة من خلال تطوير وحدة تقطير الطاقة الشمسية (SDU) التي تحتوي على جهاز تقطير الطاقة الشمسية (SS) والجامع الشمسي ذي الحوض المكافئ (PTC) الذي له التأثير الإيجابي على الإنتاجية التراكمية. ان تحسين معامل انتقال الحرارة لـ PTC هو النقطة الأساسية في هذه الدراسة، والتي يتم إجراؤها عن طريق إدخال معرقلات أسطوانية مجوفة جديدة التصميم داخل انبوب الاستقبال لمنظومة العاكس الشمسي ذي القطع المكافئ (PTR). من المتوقع أن تعمل المعرقلات الأسطوانية المصممة داخل الـPTR على تحسين معامل انتقال الحرارة ومنطقة انتقال الحرارة بين الـPTR والماء كسائل لنقل الحرارة (HTF) مقارنة بالمعرقلات الأخرى المذكورة في الدراسات السابقة (مثل الشريط الملتوي، و القضبان، و الزعانف، إلخ). تم تنفيذ العمل عددياً وتجريبياً في ظل الظروف المناخية لمدينة بابل (32.77 درجة شمالاً، 44.29 درجة غرباً) في كلية الهندسة / المسيب من الساعة 9:00 إلى 15:00 من أكتوبر 2023 إلى مايو 2024.

عددياً، تم اختيار أفضل تصميم للسطح العاكس لمنظومة الـPTC بواسطة برنامج (Parabola Calculator software) وتم ادخال التصميم في برنامج (ANSYS FLUENT R-2 20.0) لإجراء المحاكاة. تم تصميم ومحاكاة نظام الـ (PTC) والمعرقلات الأسطوانية باستخدام أدوات الـ (Solidworks) وديناميكيات الموائع الحسابية (CFD) على التوالي. صمم الـ (PTC) بأبعاد (2.00 م) طولاً و (1.00 م) عرضًا. السطح العاكس صنع من صفائح مبطنة من الألومنيوم، والأنابيب مصنوعة من الفولاذ المقاوم للصدأ المستخدم لامتصاص الحرارة. يبلغ القطر الخارجي للأنبوب (0.051 م) وسمكه (0.002 م). اتصلت المعرقلات الأسطوانية محوريًا وقطريًا أيضًا بالجزء الداخلي من PTR. ثمانون انبوب استقبال أسطواني مختلف تم تصميمها ومقارنتها بالأنبوب العادي. كان طول ، و سمك، وعدد المعرقلات بقيم مختلفة، وفحصت جميع هذه الأنابيب تحت درجة حرارة دخول ثابتة تبلغ (300 كلفن) ومعدلات تدفق كتلة تتراوح بين (0.6-1.0 كجم / ثانية). كما و تم التحقق من صحة نموذج الانبوب العادي من خلال مقارنة نتائجة مع النتائج التجريبية للأنبوب العادي من الدراسات السابقة. أظهرت نتائج المحاكاة أن إضافة تلك المعرقلات الأسطوانية المجوفة عززت و بشكل كبير من توحيد التدرج في درجة الحرارة بين جدار PTR والماء. كان اختيار النموذج الأمثل للمعرقلات

الأسطوانية لتكون: بطول (0.004 م) ، بسمك (0.002 م)، وبعدد (15 إدخالاً). سجل هذا النموذج نسبة رقم نسلت (1.79)، نسبة معامل كسر (1.100)، و اعلى قيمة للاداء الهيدرو-حراري (1.73). وعلاوة على ذلك، تمت زيادة درجات حرارة مخرج الأنبوب العادي والأنبوب المعدل من (300 كلفن) إلى (325.5 كلفن) و (339.7 كلفن) على التوالي. واستنادًا إلى النتائج العددية، تم اعتبار النموذج الأمثل للمعرقلات الأسطوانية المجوفة للعمل التجريبي.

عملياً فأن اعلى نتائج تجربية سجلت يوم 7 ايار 2024، حيث كانت درجات حرارة خروج الماء (61.5 درجة مئوية) و (57.0 درجة مئوية) في حالة الانبوب المعدل (انبوب الاستقبال الذي يحتوي على المعرقلات الأسطوانية) و في حالة الأنبوب العادي (انبوب الاستقبال الخالي من اي معرقلات اسطوانية) على التوالي. الحرارة المفيدة وصلت قيمتها الى (1053.9 واط) في حالة الانبوب المعدل و (903.3 واط) في حالة الانبوب العادي. بالمقارنة مع PTC ذو الانبوب العادي، أظهر PTC ذو الانبوب المعدل زيادة بالكفاءة الحرارية وصلت الى 38% . لوحظ ايضا ان هناك توافق جيد بين النتائج العملية و النتائج العددية، حيث تم تقييم أداء (PTC) من خلال مقارنة النتائج العملية والعددية: درجة حرارة الماء الخارج والحرارة المفيدة والكفاءة الحرارية في حالتي الانبوب المعدل و الانبوب العادي. أخيرًا، لوحظ ان انتاجية المياه العذبة من SDU المعدلة (MSDU) (SS + PTC + المعرقلات الأسطوانية داخل انبوب الاستقبال) تحسنت بنسبة 89٪ و 15٪ مقارنة بـ SS و SDU التقليدتين على التوالي.

جمهورية العراق
وزارة التعليم العالي والبحث العلمي
جامعة كربلاء
كلية العلوم
قسم الفيزياء

تحسين الأداء الحراري للمجمع الشمسي ذي القطع المكافئ باستخدام معرقلات اسطوانية لتحلية المياه

اطروحة مقدمة إلى مجلس كلية العلوم / جامعة كربلاء وهي جزء من متطلبات نيل درجة الدكتوراه في علوم الفيزياء

الطالب
ياسر عبد نور جبار

بأشراف
أ.د فاضل خدام فليفل
أ.م.د وسام جليل خضير

1446 هـ

2025م